QC
911.8
.G62
1961

TIROS II RADIATION DATA

USERS' MANUAL

GODDARD SPACE FLIGHT CENTER
GREENBELT, MARYLAND

~~115 152~~

73 6285

TIROS II RADIATION DATA
USERS' MANUAL

QC
911.8
.G62
1961

By
Staff Members
of the
Aeronomy and Meteorology Division
U.S. Goddard Space Flight Center, Greenbelt, Md.
National Aeronautics and Space Administration
and the
Meteorological Satellite Laboratory
United States Weather Bureau
Department of U. S. Commerce

TD 6285

LIBRARY
AUG 10 2009
Atmospheric Sciences Division

August 15, 1961

National Oceanic and Atmospheric Administration
TIROS Satellites and Satellite Meteorology

ERRATA NOTICE

One or more conditions of the original document may affect the quality of the image, such as:

Discolored pages
Faded or light ink
Binding intrudes into the text

This has been a co-operative project between the NOAA Central Library and the Climate Database Modernization Program, National Climate Data Center (NCDC). To view the original document contact the NOAA Central Library in Silver Spring, MD at (301) 713-2607 x124 or Library.Reference@noaa.gov.

HOV Services
Imaging Contractor
12200 Kiln Court
Beltsville, MD 20704-1387
January 26, 2009

Blank page retained for pagination

FOREWORD

Many members of the staffs of both the Aeronomy and Meteorology Division, Goddard Space Flight Center, and the Meteorological Satellite Laboratory contributed to the success of the TIROS II satellite. However, the following persons contributed in large measure to the production of this manual and its companion volume, the "TIROS II Radiation Data Catalogue," and their efforts are hereby acknowledged:

GSFC	*MSL*
Mr. B. Conrath	Mr. R. T. Hite
Mr. W. R. Bandeen	Mr. C. L. Bristor
Dr. R. A. Hanel	Mr. G. E. Martin
Miss I. Persano	Dr. D. Q. Wark

ABSTRACT

The NASA TIROS II Meteorological Satellite contains a five-channel medium resolution scanning radiometer. Two of the channels of this instrument are sensitive to reflected solar radiation and the remaining three respond to emitted terrestrial radiation. In the original design concept, the radiometer output signal was supposed to be proportional to the difference in energy flux viewed by the bi-directional optics. In addition to a primary calibration, which employed two targets of known radiant emittance, auxiliary measurements were made to determine optical balance, thermal stability, and electronics temperature correction factors. The calibration data, along with orbital and attitude data and the infrared data from the satellite, were incorporated in a computer program for an IBM–7090 which was used to produce the "Final Meteorological Radiation Tape (Binary)."

After launch, the radiometer displayed characteristics which had not been previously suspected. These characteristics, which indicate a departure from the concept on which the calibration was based, result in some uncertainties in the absolute values of the data. These characteristics and other possible sources of error are discussed. Before serious work with the TIROS II radiation data is attempted, and understanding of the radiometer, its calibration, and the problems encountered in the experiment is essential. The instrumentation design, development work, and the calibrations herein described were performed by the Goddard Space Flight Center staff, whereas the computer and programming effort was carried out by the Meteorological Satellite Laboratory Staff for the most part.

Blank page retained for pagination

TABLE OF CONTENTS

	Page
Abstract	iii
List of Common Symbols	vi
I. Introduction	1
1.1 The TIROS II Program	1
1.2 Limitations of Data Utilization	1
1.3 Description of the Principle of the Radiometer	1
II. Calibration	1
2.1 Effective Spectral Response	1
2.1.1 Definition	1
2.1.2 Discussion	2
2.2 Effective Radiant Emittance	2
2.2.1 Definition	2
2.2.2 Computation of $\overline{W}$ vs. T_{BB}	2
2.3 Flow Sequence	2
2.4 Electronics Temperature Correction, Δ vs. D_0	3
2.5 Balance (α) and Stability (β) Factors	3
2.6 Target Effective Radiant Emittance, $\overline{W}$ vs. Digital Number D	4
2.6.1 Thermal Channels, 1, 2, and 4	4
2.6.2 Visible Channels, 3 and 5	4
2.7 Summary of the Calibration	4
III. Data Processing	5
3.1 Information Flow in the Satellite	5
3.2 Information Flow at the Command and Data Acquisition Station	6
3.3 Information Flow at the Data Reduction Center	6
IV. Format of the Final Meteorological Radiation Tape (Binary)	6
V. IBM-7090 Computer Flow Diagram	8
VI. Post-launch Observations and Developments	9
VII. Conclusions	9
VIII. Bibliography	10

LIST OF FIGURES

Figure	
1. Block Diagram of the Scanning Radiometer	12
2. ϕ_λ vs. λ, Channel 1	13
3. ϕ_λ vs. λ, Channel 2	14
4. ϕ_λ vs. λ, Channel 3	15
5. ϕ_λ vs. λ, Channel 4	16
6. ϕ_λ vs. λ, Channel 5	17
7. $\overline{W}$ vs. T_{BB}, Channel 1	18
8. $\overline{W}$ vs. T_{BB}, Channel 2	19
9. $\overline{W}$ vs. T_{BB}, Channel 4	20
10. Calibration Flow Diagram	21
11. Calibration Flow Diagram	22
12. Calibration Flow Diagram	23
13. Calibration Flow Diagram	24
14. Δ vs. D_0, Channel 1	25
15. Δ vs. D_0, Channel 2	26
16. Δ vs. D_0, Channel 3	27
17. Δ vs. D_0, Channel 4	28
18. Δ vs. D_0, Channel 5	29
19. α vs. T_C, Channel 1	30
20. α vs. T_C, Channel 2	31
21. α vs. T_C, Channel 3	32
22. α vs. T_C, Channel 4	33
23. α vs. T_C, Channel 5	34
24. β vs. T_C, Channel 1	35
25. β vs. T_C, Channel 2	36
26. β vs. T_C, Channel 3	37
27. β vs. T_C, Channel 4	38
28. β vs. T_C, Channel 5	39
29. $\overline{W}$ vs. D ("Normalized Case"), Channel 1	40
30. $\overline{W}$ vs. D ("Normalized Case"), Channel 2	41
31. $\overline{W}$ vs. D ("Normalized Case"), Channel 3	42
32. $\overline{W}$ vs. D ("Normalized Case"), Channel 4	43
33. $\overline{W}$ vs. D ("Normalized Case"), Channel 5	44
34. Block Diagram of the Radiation Experiment	45
35. Block Diagram of a Data Acquisition Station	46

Figure		Page
36.	Block Diagram of the Data Reduction Center	47
37.	IBM-7090 Computer Flow Diagram	48
38.	Time History of the Space Viewed Digital Number, Channel 1	51
39.	Time History of the Space Viewed Digital Number, Channel 2	52
40.	Time History of the Space Viewed Digital Number, Channel 3	53
41.	Time History of the Space Viewed Digital Number, Channel 4	54
42.	Time History of the Space Viewed Digital Number, Channel 5	55
43.	Variation in T_E and T_C Over a Two-Orbit Period	56
44.	Time History of the Characteristic Analog Signals	57

LIST OF TABLES

Table		
I.	Mean Orbital Characteristics of TIROS II	1
II.	Filter and Lens Materials	10
III.	Effective Spectral Response, Channel 1	11
IV.	Effective Spectral Response, Channel 2	11
V.	Effective Spectral Response, Channel 3	11
VI.	Effective Spectral Response, Channel 4	11
VII.	Effective Spectral Response, Channel 5	11
VIII.	T_{BB} vs. $\overline{W}$, Channel 1	11
IX.	T_{BB} vs. $\overline{W}$, Channel 2	11
X.	T_{BB} vs. $\overline{W}$, Channel 4	11

LIST OF COMMON SYMBOLS

A_λ Spectral absorptivity of the thermistor detector
D Digital number: scale 0 to 127
D_o Uncorrected digital number
D_1 Digital number corrected for electronics temperature, but not for side or radiometer housing temperature.
F Number of cycles-per-second above the base frequency of a given 50 c.p.s. subcarrier band
F_{sc} Output frequency of the voltage controlled oscillator
J_λ Spectral radiant intensity of standard lamp (watts/steradian)
K'' Value which an assumed linear transfer function of V_{rad} vs. $\overline{W}$ intercepts on the $\overline{W}$ axis
R_λ^b Spectral reflectivity of the black half of the chopper disk
R_λ^m Spectral reflectivity of the aluminized half of the chopper disk
R_λ^p Spectral reflectivity of the radiometer prism
R_λ The ratio $\frac{R_b}{R^m}$
R Distance from the filament of the standard lamp to the center of the diffuse reflector
T_{BB} Equivalent blackbody temperature (degrees Kelvin)
T_C Radiometer housing temperature
T_E Satellite electronics temperature
T_1 Temperature of the ambient reference honeycomb target
T_2 Temperature of the hot honeycomb target
V_w Output voltage of the radiometer with radiation entering the wall side only
V_f Output voltage of the radiometer with radiation entering the floor side only
V_w^* Defined by eq. (9)
V_f^* Defined by eq. (10)
$W_\lambda(T)$ Spectral radiant emittance (the Planck function) for a blackbody of temperature T (watts/meter^2/micron).
$\overline{W}$ Effective radiant emittance defined by eq. (3) (watts/meter^2)
$\overline{W}_1$ Effective radiant emittance of the ambient reference honeycomb target
$\overline{W}_2$ Effective radiant emittance of the hot honeycomb target
$\overline{W}'$ Defined by eq. (21)
$\overline{W}^*$ Effective radiant emittance of a diffuse reflector of albedo 1.0 exposed to solar radiation at normal incidence above the atmosphere as defined by eq. (22).
V_{rad} Output voltage of the radiometer with radiation entering the wall side only
f_λ Spectral transmission of the filter-lens combinations in the radiometer
$k_w(T_C)$, $k_f(T_C)$ Proportionality factors which are functions of radiometer housing temperature and are defined by eqs. (5) and (6) respectively.
r_λ Spectral reflectivity of the diffuse reflector employed in the calibration of the visible channels
Δ Term added to the uncorrected digital number to correct for electronics temperature
Ω Solid angle of the sun as viewed from the earth
α Balance correction factor defined by eq. (7)
β Thermal stability correction factor defined by eq. (8)
$\overline{\alpha}$ Defined by eq. (9)
$\overline{\beta}$ Defined by eq. (10)
δ Incidence angle of radiation from standard lamp on diffuse reflector employed in the calibration of the visible channels.
ϵ_λ Spectral emissivity of the honeycomb targets used in the primary calibration
$\epsilon_{\lambda 1}$ Spectral emissivity of the ambient reference used in the balance and stability measurements
$\epsilon_{\lambda 2}$ Spectral emissivity of the hot target used in the balance and stability measurements
λ Wavelength in microns
ϕ_λ Effective spectral response of the radiometer defined by eq. (1)

I. INTRODUCTION

1.1 *The TIROS II Program* [1, 2, 3, 4]

The NASA TIROS II meteoroligical satellite was injected into orbit on November 23, 1960. Its mean orbital characteristics are listed in Table I.

TABLE I

Perigee Altitude	385.6 st. mi.
Apogee Altitude	454.4 st. mi.
Inclination	48.53 deg.
Anomalistic Period	98.27 min.

The instrumentation flown in the satellite includes two television cameras and two radiometers. The radiometers measure emitted and reflected solar radiation from the earth and its atmosphere. One is a wide field non-scanning instrument with two detectors, one white and the other black. This manual is concerned only with the second radiation measuring device, the five-channel medium resolution scanning radiometer.

1.2 *Limitations of Data Utilization*

Before attempting to interpret the data contained on the "Final Meteorological Radiation Tape (Binary)," careful consideration should be given to all points discussed in this manual. For an understanding of the significance of the radiant emittance values or equivalent blackbody temperatures a familiarity with the principle of the radiometer, its peculiarities, and the method of calibration is essential.

Care should be exercised in the use of the correlation of the radiation data with geographic location, such as in attempted comparisons with synoptic situations. Uncertainties in attitude determination lead to an estimated standard error of 2° to 3° in great circle arc. At a nadir angle of 0°, a 3° error would result in a position error on the surface of the earth of less than about 20 miles. At a nadir angle of 60°, a 3° error corresponds to an error of less than 200 miles. It should be emphasized that such errors result in distortion as well as translation, and a simple linear shift of the data is in general not sufficient for correction. [5, 6, 7, 8, 9]

In addition to attitude errors, time errors also contribute to difficulties in geographic correlation. The principal sources of time errors are mistakes at the ground station in transmission of the end-of-tape pulse, erroneous sensing by the analog-to-digital converter of the end-of-tape pulse, and the necessity of counting through noise on the relative satellite clock frequency. These errors may at times amount to as much as one to two minutes. Time errors also result in distortion as well as translation.

1.3 *Description of the Principle of the Radiometer* [1, 2]

The principle of the radiometer is illustrated in Fig. 1, where the components of a single channel are pictured. The fields of view of the channels are approximately coincident, each being about five degrees wide at the half-power points of the response. The optical axis of each channel is bi-directional 180° apart. As the half-aluminized, half-black chopper disk rotates, radiation from first one direction and then the other reaches the detector. This results in a chopped output which is amplified and rectified, giving a DC signal proportional to the difference in energy flux viewed in the two directions.

The radiometer is mounted in the satellite such that the optical axes are inclined 45° to the satellite spin axis. The viewing directions are designated "wall" and "floor" according to their orientation in the satellite. While one optic views the earth, the other views outer space. Thus, the outer space radiation level (assumed to be zero) can be used as a reference. As the satellite rotates on its axis, the radiometer scan pattern on the surface of the earth is defined by the intersection of a 45° half-angle cone and a sphere. This pattern ranges from a circle when the spin vector is parallel to the orbital radius vector, to two hyperbola-like branches when the spin vector is perpendicular to the radius vector. The orbital motion of the satellite provides the scan advance. Variations in the amplitude of the radiometer signal are converted into subcarrier frequency deviations and stored by means of a minature magnetic tape recorder. When the satellite is interrogated while passing over a Command and Data Acquisition Station, the information is telemetered back to earth where it is recorded on magnetic tape. The further processing of these magnetic tapes is discussed in Section III of this Manual.

II. CALIBRATION

Before considering the calibration flow sequence, it is necessary to define and discuss two quantities which are fundamental to the calibration. These are the effective spectral response and the effective radiant emittance.

2.1 *Effective Spectral Response*

2.1.1 *Definition.* The effective spectral response ϕ_λ is defined as

$$\phi_\lambda = R_\lambda^p (R_\lambda^m - R_\lambda^b) f_\lambda A_\lambda. \tag{1}$$

In the actual computation of ϕ_λ the expression

$$\phi_\lambda = (1 - R_\lambda) f_\lambda \tag{2}$$

was used. The use of the factor $(1-R_\lambda)$ assumes that the aluminized half of the chopper disk is independent of wavelength. It is also assumed that the detector absorptivity and the prism reflectivity are wavelength independent.

The materials used in the lens and filter of each channel are given in Table II. The effective spectral response for each channel is given in Figs. 2, 3, 4, 5, and 6, and in Tables III, IV, V, VI, and VII.

2.1.2 *Discussion.* The ratio R_λ was taken from measurements performed at the Meteorological Satellite Laboratory of the Weather Bureau, using a Beckman IR-7 spectrophotometer. The determinations were made on two different chopper disks taken from a radiometer similar to that flown in TIROS II. An average or the two was taken and used for channels 1, 2, and 4. No measurements were available in the spectral ranges covered by channels 3 and 5, so R_λ was assumed to be independent of wavelength.

A discussion of the final values of ϕ_λ derived for each channel follows.

CHANNEL 1

The function f_λ was taken from Barnes Engineering Company measurements made on the channel 1 filter of the TIROS II radiometer in combination with plane samples of the lens material having thichnesses equivalent to the mean thicknesses of the lens elements. An immersion detector is used in this channel. The hemispherical germanium immersion lens was assumed to have a transmission independent of wavelength.

CHANNEL 2

In the spectral region 7.2μ to 16μ f_λ was taken from measurements by Barnes similar to those already described in the discussion of channel 1.

In the 16μ to 22μ region no direct measurements of f_λ for the TIROS II radiometer were available. Transmission measurements of a similar filter were made by the Meteorological Satellite Laboratory of the Weather Bureau. The transmission of the germanium doublet lens was calculated theoretically by MSL from transmission curves of germanium specimens supplied by Barnes. In addition, direct measurements of f_λ were made by the University of Michigan, using a filter-lens combination taken from a radiometer similar to the one employed in TIROS II. An average of the two methods was adopted for the final value of f_λ in this region.

CHANNEL 3

Barnes measurements of the type described in the channel 2 discussion were used for f_λ throughout the entire range covered.

CHANNEL 4

In the region 7.2μ to 16μ f_λ was taken from Barnes measurements performed on the TIROS II radiometer.

From 16μ to 32.6μ no direct measurements were available. The transmission of a sample InSb filter was measured by Eastman Kodak Company. The transmission of the KRS-5 lens was assumed to be constant throughout the entire 7.2μ to 32μ range. This constant value was obtained by taking the ratio of the area under the Barnes transmission curve from 7.2μ to 16μ to the area under the Kodak curve over the same wavelength range. The product of the Kodak curve and the constant obtained for the KRS-5 lens was adopted for f_λ in the 16μ to 32.6μ region.

CHANNEL 5

From $.45\mu$ to 1.2μ f_λ was taken from Barnes measurements on the flight radiometer. In the 1.2μ to 3.35μ region, University of Michigan measurements on a filter-lens combination from a radiometer similar to that flown in TIROS II were used for f_λ.

2.2 *Effective Radiant Emittance*

2.2.1 *Definition.* The effective radiant emittance of a target $\overline{W}$ is defined as that portion of blackbody radiant emittance which would be detected by a sensor with a spectral response ϕ_λ when the field of view is completely filled. This may be written as

$$\overline{W}=\int_0^\infty W_\lambda(T)\phi_\lambda d\lambda. \tag{3}$$

2.2.2 $\overline{W}$ vs. T_{BB}. The $\overline{W}$ vs. T_{BB} functions in Tables VIII, IX, and X and Figs. 7, 8, and 9 were obtained using the equation defining $\overline{W}$. The integration necessary in the computation of each point was carried out using an LGP-30 electronic computer. These transfer functions are provided in order that values of $\overline{W}$ may be converted to equivalent blackbody temperature T_{BB}.

2.3 *Flow Sequence*

The radiation data flow sequence is shown in Figs. 10 through 13. The sequence from statellite through ground station is illustrated in Fig. 10(a). When an effective radiant emittance $\overline{W}$ is viewed by one side of the radiometer while the other side views outer space and with a radiometer housing temperature T_C, a radiometer output voltage V_{rad} is obtained. This signal is fed into a voltage controlled oscillator which produces an output frequency F_{sc} when the oscillator electronics temperature is T_E.

At the ground station the frequency F_{sc}, now increased by a factor of 30, is fed into a demodulator, the output of which enters an analog-to-digital converter. The resulting digital number D_0,

and the temperatures T_E and T_C which are also telemetered from the satellite, are used to obtain the value of $\overline{W}$ from the calibration data as indicated below.

2.4 *Correction for Electronics Temperature*

The realtion between the radiometer output voltage V_{rad} and the frequency output of the voltage controlled oscillator F_{sc} depends on the electronics temperature T_E as shown schematically in Fig. 10(c). Algebraically, the relation may be expressed as

$$F_{sc}=f(V_{rad},\ T_E). \tag{4}$$

A "normalized" case was established for $T_E=25°$ C, in terms of which all data are to be expressed. Therefore, a correction Δ must be added to the "uncorrected" digital number D_0, yielding a digital number D_1 corrected for T_E only as shown in Fig. 10(d).

Using graphs similar to those shown in Fig. 10(c), the correction Δ can be found as a function of D_0 and T_E as shown schematically in Fig. 11(a). The Δ functions for each channel are given in Figs. 14, 15, 16, 17, and 18.

2.5 *Balance (α) and Stability (β) Factors*

Initially, it was assumed that the response of the radiometer depended on the particular optic viewing the target and on radiometer housing temperature T_C, as shown in Fig. 10(b). Accordingly, the radiometer output signal when the wall optic is viewing the target and no radiation is entering the floor side can be expressed as

$$V_w=k_w(T_C)[W-K''] \tag{5}$$

Similarly, when the floor side is viewing the target, the expression is

$$V_f=k_f(T_C)[W-K''] \tag{6}$$

In practice, the values K'' were found to be very small compared to other uncertainties in the calibration measurements and, hence, were neglected in all calculations involving second order corrections to the normalized calibration data.

If the radiometer optics were in perfect balance, then $k_w(T_C)=k_f(T_C)$. However, this in general is not the case. Hence, it is necessary to reduce all data to a set of standard conditions. It was decided, arbitrarily, to express all measurements in terms of the wall optic at a housing temperature of 25° C. Accordingly, two correction factors were defined:

$$\begin{cases} \alpha(T_C)=\dfrac{k_w(T_C)}{k_f(T_C)} & \text{(floor side)} \\ \alpha=1 & \text{(wall side)} \end{cases} \tag{7}$$

$$\beta(T_C)=\frac{k_w(25°\text{ C})}{k_w(T_C)} \tag{8}$$

To facilitate the determination of these factors, a series of measurements were made. The radiometer was placed in a thermal chamber with the optics in line with ports in either side. A black painted sheet metal box filled with water at room temperature T_1 was placed in front of one port. At the other port was a Barnes Engineering blackbody source, model RS–12, set for a temperature T_2 such that a signal of convenient magnitude was obtained from the radiometer. When the radiometer housing reached thermal equilibrium with the chamber, a reading of the radiometer output voltage was obtained. The positions of the targets were then reversed and another reading taken. This procedure was repeated for a number of housing temperatures, covering the range expected under operating conditions.

The output signals obtained in this way can be expressed as (neglecting K'')

$$V_w^*=|k_w(T_C)\overline{W}_2-k_f(T_C)\overline{W}_1| \tag{9}$$

$$V_f^*=|k_f(T_C)\overline{W}_2-k_w(T_C)\overline{W}_1| \tag{10}$$

where

$$\overline{W}_1=\int_0^\infty W_\lambda(T_1)\,\epsilon_{\lambda 1}\,\phi_\lambda\,d_\lambda+\int_0^\infty W_\lambda(T_C)\,(1-\epsilon_{\lambda 1})\,\phi_\lambda\,d\lambda \tag{11}$$

$$\overline{W}_2=\int_0^\infty W_\lambda(T_2)\,\epsilon_{\lambda 2}\,\phi_\lambda\,d_\lambda+\int_0^\infty W_\lambda(T_C)\,(1-\epsilon_{\lambda 2})\,\phi_\lambda\,d\lambda \tag{12}$$

In the above relations it is assumed that all radiation reflected from the targets originates inside the thermal chamber.

The desired correction factors may be written in the form

$$\alpha(TC)=\frac{\overline{W}_2\,\alpha(T_C)+\overline{W}_1}{\overline{W}_1\,\alpha(T_C)+\overline{W}_2} \tag{13}$$

$$\beta(T_C)=\left[\frac{\overline{W}_2+\overline{W}_1\dfrac{1}{\alpha(25°\text{ C})}}{\overline{W}_2+\overline{W}_1\dfrac{1}{\alpha(T_C)}}\right]\cdot\beta(T_C) \tag{14}$$

where

$$\overline{\alpha}(T_C)=\frac{V_w^*(T_C)}{V_f^*(T_C)} \tag{15}$$

$$\overline{\beta}(T_C)=\frac{V_w^*(25°\text{ C})}{V_w^*(T_C)} \tag{16}$$

In making the final calculations, it was assumed that $\epsilon_{\lambda 1}=\epsilon_{\lambda 2}=1$.

The α and β functions are shown schematically in Figs. 11(c) and 12 respectively. The functions are given for each channel in Figs. 19 to 28 inclusive.

2.6 *Target Effective Radiant Emittance, $\overline{W}$ vs. Digital Number, D*

2.6.1 Thermal Channels 1, 2, and 4. The radiometer was originally calibrated using a target at liquid nitrogen temperature on the floor side and a warm target on the wall side. Since it was not possible to calibrate the radiometer and its electronics data storage package as a system, the radiometer was calibrated alone, with a resistive load substituted for the package. When auxiliary calibrations were later performed on the entire system, it was found that the electronics matching caused considerable shift in the measurements. Hence, it has become necessary to rely entirely on the auxiliary measurements in constructing the final $\overline{W}$ vs. D curves.

The auxiliary calibration measurements were carried out using two honeycomb targets, one at room temperature and the other at higher temperatures. Each honeycomb consisted of a flat brass plate to which were soldered, perpendicularly, two inch lengths of one-fourth inch I.D. copper tubing. The ends of the tubes were countersunk, presenting thin edges. The surfaces were coated with black India ink. The temperature of each target was recorded by means of thermocouples. In the hot target there was found to be a temperature difference of about two degrees between the brass plate and the exposed ends of the tubes. The plate temperature was assumed to be the effective blackbody temperature.

The resulting output signal of the radiometer can be expressed in the form

$$V=\beta\cdot k_w\left[\overline{W}(T_2)-\frac{1}{\alpha}\overline{W}(T_1)\right] \tag{17}$$

where T_1 is room temperature, T_2 is the warm target temperature, and the wall side is facing the warm target. The radiant emittance for each target can be calculated using:

$$\overline{W}(T_1)=\int_0^\infty W_\lambda(T_1)\phi_\lambda d\lambda \tag{18}$$

$$\overline{W}(T_2)=\int_0^\infty W_\lambda(T_2)\epsilon_\lambda\phi_\lambda d\lambda+\int_0^\infty W_\lambda(T_1)(1-\epsilon_\lambda)\phi_\lambda d\lambda. \tag{19}$$

Measurements of the emissivities of the targets showed them to be very near to one; hence, in the final evaluation, it was assumed that ϵ_λ was unity.

A curve of V vs. $\beta\cdot\left[\overline{W}(T_2)-\frac{1}{\alpha}\overline{W}(T_1)\right]$ was plotted from the calibration data. This is assumed to be equivalent to a curve of V vs. $\overline{W}$ "normalized" with $T_C=25°$ C, viewing a target through the wall side with no radiation entering the floor side.

Using a V_{rad} vs. frequency curve and converting from frequency to digital number with the formula

$$D=\frac{127}{50}F \tag{20}$$

a normalized $\overline{W}$ vs. D curve was constructed of the type shown in Fig. 11(b). The $\overline{W}$ vs. D curves for each channel are given in Figs. 29 to 33 inclusive.

2.6.2 *Visible Channels 3 and 5.* The original source used to calibrate channels 3 and 5 consisted of a projection lamp placed behind a piece of opal glass. It was later found that the opal glass was partially transparent from the red end of the visible into the infrared. This caused the gain of both channels to be set lower than was originally desired. Since this difficulty was not discovered until after launch, it was necessary to work with another radiometer in recalibrating. Radiometer 105A was employed for this purpose, its gain setting being approximately the same as the gain setting of 106A.

A tungsten filament lamp calibrated by the Bureau of Standards was used in the recalibration procedure. Radiation from the lamp was diffusely reflected from a piece of white paper of known spectral reflectivity. The output signal of each channel was read with the illuminated paper completely filling the field of view of the radiometer. The effective radiant emittance was computed using

$$\overline{W}'=\frac{\cos\gamma}{R^2}\int_0^\infty J_\lambda\cdot r_\lambda\cdot\phi_\lambda d\lambda \tag{21}$$

This measurement gives one point on a voltage vs. $\overline{W}$ curve. Taking the noise level as the $W=0$ point and assuming a linear relationship, a calibration curve can be constructed. The accuracy of this calibration suffers due to the small radiometer signals obtainable with the diffusely reflecting arrangement. Only 0.48v out of 12v was obtainable with channel 5 and 1.6v out of 12v with channel 3.

The maximum signal obtainable with albedo 1.0 and solar radiation at normal incidence is only 2.40 volts for channel 5 and 4.44 volts for channel 3. These figures are based on calculations using

$$\overline{W}^*=\frac{\Omega}{\pi}\int_0^\infty W_\lambda(T)\phi_\lambda d\lambda \tag{22}$$

taking the sun as a 5800° blackbody for channel 3 and a 6000° blackbody for channel 5.

2.7 *Summary of the Calibration*

When a certain value of effective radiant emittance $\overline{W}_0$ is viewed by the radiometer through a given side with a given radiometer housing temperature T_C, an output signal V_0 results. This is shown diagrammatically in Fig. 10(b) where the case is taken when the radiation enters the floor

side. If the signal $V_0=V_1$ is used with the "normalized" case (wall side, $T_C=25°$), an effective radiant emittance W_1 is obtained. When the Δ correction is applied to the corresponding uncorrected digital number D_0, (shown in Fig. 11(a) for a case when $T_E=60°$ C) and the resulting digital number D_1 is used with the normalized $\overline{W}$ vs. D curve (Fig. 11(b)), the same radiant emittance $\overline{W}_1$ is obtained, as can be seen from Figs. 10(c) and 10(d). Thus, $\overline{W}_1$ is corrected for T_E but not for side or T_C.

It was assumed that in the normalized case the function $V_{rad}=f(\overline{W})$ was linear and could be expressed as

$$V_{rad}=k_w(T_C=25° \text{ C})[\overline{W}-K''] \tag{23}$$

There is now some doubt as to whether this assumption is correct. From the definitions of V_1, V_2, and V_3 given in Fig. 11(c), it follows that $V_3=\alpha\beta V_1$ and from the linearity relation

$$V_3=\alpha\beta k_w(25° \text{ C})[\overline{W}_1-K'']=k_w(25° \text{ C}))[\overline{W}_3-K''] \tag{24}$$

is obtained. Solving for $\overline{W}_3$ gives

$$\overline{W}_3=\alpha\beta[\overline{W}_1-K'']+K'' \tag{25}$$

Since $\overline{W}_3=\overline{W}_0$ this is the final effective radiant emittance value desired.

In summary, in order to obtain an effective radiant emittance value it is necessary to know D_0, T_C, and T_E. With T_E using the curve D_0 vs. Δ, the electronic correction Δ is obtained. The digital number D_1 corrected for T_E is computed from

$$D_1=D_0+\Delta$$

Using D_1 with the D vs. $\overline{W}$ curve, $\overline{W}_1$ is obtained. With T_C the α and β factors are obtained from the α vs. T_C and β vs. T_C curves respectively. Finally $\overline{W}_3$ is computed using

$$\overline{W}_3=\alpha\beta[\overline{W}_1-K'']+K''$$

III. DATA PROCESSING

3.1 *Information Flow in the Satellite*

The radiation experiment instrumentation is independent of the television camera system except for power, command, certain timing signals and antennas (Fig. 34).[1] The output of the five medium resolution radiometer channels is fed to five subcarrier oscillators. These voltage controlled oscillators are of the phase shift type with symmetric amplifiers in the feedback loops, the gains of which are controlled by the balanced input signal. A sixth channel is provided for telemetry of the wide angle low resolution sensor data, environmental temperatures, instrumentation canister pressure, and calibration. A mechanical commutator switches resistive sensors in one branch of a phase shift oscillator. The seventh channel, a tuning fork oscillator, serves as a reference frequency and timing signal. The outputs from these seven different channels are summed and the resultant composite signal equalized in a record amplifier which drives the head of a miniature tape recorder. An oscillator provides an alternating current bias to the record head and the signal required for the erase head. For convenience, erase of the magnetic tape occurs immediately before recording. The record spectrum extends from 100 cps to 550 cps. The tape recorder is an endless-loop, two-speed design running at 0.4 ips record and 12 ips playback speed. The endless loop records continuously, day and night, except during a playback sequence. A hysteresis synchronous motor generates torque in the record mode through a mylar belt speed reduction. The fourth subharmonic of the tuning fork oscillator generated by flip flops drives the motor. The record motor also drives a cam shaft which activates a bank of micro switches connected to the five commutated sub-channels of the time-sharing sixth channel. Each is sampled six seconds and the fifth includes a group of seven to be sub-commutated.

Playback is initiated upon command by applying power to a direct current motor. A magnetized flywheel generates a frequency proportional to the motor speed. A frequency discriminator feeds the error signal to the stabilized power supply of the motor and closes the servo loop. Playback speed is essentially constant from 0° to 50° C. A low flutter and wow of 2.5% peak-to-peak measured without frequency limitations is achieved by using precision bearings and ground-in-place shafts having tolerances of better than 50 parts per million. A command pulse activates the playback motor, the playback amplifier, and the 238 Mc FM telemetry transmitter feeding the duplexer and antenna.

In order to permit comparison of the low resolution measurements with TV pictures, each TV shutter action generates a 1.5 second pulse which is recorded as an amplitude modulation of the channel seven timing signal. There are nine solar cells mounted behind narrow slits for north angle determination. These slits have an opening angle of close to 180° in planes through the spin axis. The sun illumination generates pulses as long as illumination parallel to the spin axis is avoided. One of these sensors generates a 0.5 second pulse in addition to the north indicator code so that spin rate information and a measure of relative sun position is available. Again, this pulse is recorded as an amplitude modulation of channel seven. Reconstruction of the radiation information vitally depends on its correlation with absolute time. An accurate but relative timing signal is provided by the tuning fork oscillator and a crude one by the sun pulses except when the satellite is in the earth's umbra. Absolute time is transmitted to the satellite and recorded on the

tape as a one second dropout of channel seven. The occurrence of this pulse is known within milliseconds of absolute time.

3.2 *Information Flow at the Command and Data Acquisition Station*

Upon interrogation, the 238 Mc carrier is received by a 60-foot parabolic antenna, and the composite signal is recorded on magnetic tape and, simultaneously, fed to a "Quick-Look" demodulator (Fig. 35a). At the same time, the envelope of channel 7 and the clipped signal of channel 4 are graphically recorded. The 8–30 micron "events" on the graphic record show alternately the earth and sky scan intervals as the satellite spins and progresses along the orbit, and the channel 7 envelope shows the three distinctive types of AM pulses impressed on the clock frequency during the record; namely, the sun sensor pulses, the TV camera pulses, and the "end-of-tape" pulse. Auxiliary uses of the radiation data include determination of the spin axis attitude in space and the times when television pictures were taken and recorded in the satellite, to be read out later over a ground station (Figs. 35b and 35c).

The magnetic tapes are routinely mailed every day to the Aeronomy and Meteorology Division, GSFC, in Washington. The master tape containing the composite radiation signal is demultiplexed, demodulated and fed to an analog-to-digital converter (Fig. 36). The pressure is read separately. The analog-to-digital converter produces a magnetic "Radiation Data Tape" made up of 36 bit words suitable for an IBM–7090 computer.

3.3 *Information Flow at the Data Reduction Center*

The IBM–7090 computer program of the Meteorological Satellite Laboratory, U.S. Weather Bureau, requires inputs from four sources to produce the "Final Meteorological Radiation Tape (FMR Tape)". One source is the Radiation Data Tape containing satellite environmental parameters in digital form. Another source is the calibration for converting digital information to meaningful physical units. The "Orbital Tape" from the NASA Space Computing Center is used for satellite position and attitude data. In addition, it is possible to insert attitude data taken from other sources on punched cards. In practice, this is the method generally used. The FMR Tape (in binary form) then is the basic repository of data from the medium resolution scanning radiometer. Simultaneously with its publication, a radiation map of sample data from each channel is produced. In order to study and utilize the scanning radiometer data, appropriate computer programs must be written to "talk" to the Final Meteorological Radiation Tape and provide for printing out data, punching cards, or producing maps. The make-up of the IBM–7090 computer program and the format of the Final Meteorological Radiation Tape are discussed in detail in Sections IV and V.

IV. FORMAT OF FINAL METEOROLOGICAL RADIATION TAPE

TIROS II radiation data will be available on low density, binary tapes prepared on an IBM–7090 computer. This FMR tape is the product of a computer program whose input is the orbital data, digitized radiation data, TIROS II radiometer calibration package, and satellite attitude. In addition to the calibrated radiation measurements, the final meteorological radiation tape also contains geographical locations associated with the radiation measurements, orbital data, solar ephemeris, and satellite temperature. The exact format of these data is described below, and the purpose of this section is to emphasize certain features that will aid programmers in utilizing these data.

Each orbit of radiation data is treated as a file which contains a documentation record plus data records that represent one minute intervals of time. The documentation record is the first record of each file and contains 14 data words whose format is described below. Dref was defined as the number of days between zero hour of September 1, 1957, and zero hour of launch day. Julian time counts zero time as zero hour at Greenwich on the day of launch, thus launch time is given in GMT and launch day is zero day, with succeeding days numbered sequentially. However, if the satellite life extends beyond about 100 days, the value of dref is redefined by adding approximately 100, while the Julian day is decreased by the same amount.

Each record of data covers approximately one minute of time, and the data are found in the decrement (D) and address (A) of each data word. The record terminates with the end of swath in progress at 60.0 seconds past the minute specified in words 1D, 1A, and 2D. In the case of satellite-earth orientation such that the radiometer continuously scans the earth for more than one rotation of the satellite, the record will terminate with the end of the revolution in progress at 60.0 seconds past the minute specified in words 1D, 1A, and 2D. The End of File will be duplicated at the end of the last file on each Final Meteorological Radiation Tape.

The Greenwich Hour Angle and Declination of the sun are computed for each even minute and these values agree with the Air Almanac within a small fraction of a degree. The declination of the sun does not carry a sign to indicate north or south direction. In the case of TIROS II data, this value is south declination from time of launch to the Vernal Equinox which occurred at 2032 hours GMT, 20 March 1961. TIROS II radiation data extends from time of launch to orbit 2071 which occurred on April 13, 1961. All orbits after number 1721 occurred after the Vernal Equinox;

hence, the value of the solar declination for these orbits is positive (or north).

For each earth viewing swath, the radiation measured from each of the five channels in the medium resolution radiometer is reported in watts/meter^2. For each fifth measurement in a swath, the point on earth being "viewed" by the radiometer is defined in terms of latitude and longitude. These computations are based on the best estimate of satellite attitude.

In order that the user may distinguish between data from the wall and floor sides of the satellite, the data words which contain energy expressed as watts/meter^2 are labeled with a 1 in position 19 when the wall side of the satellite is viewing the earth. When the observed swath size exceeds the calculated theoretical size, the remaining earth viewing responses are retained with a negative sign. The user should realize that if the signal from the satellite becomes noisy, the swath sizes are abnormal, and the data can be labeled and located incorrectly.

At the end of each earth viewing swath, two additional data words contain the end of swath code, the minimum nadir angle of the radiation optic axis occurring in this swath, and the latitude and longitude of the point on earth being "viewed" by the radiometer when the minimum nadir angle occurred.

The block of data from words 6D to 24A will be repeated, thus defining every fifth measurement in a swath. The address of the third word in the last response of a swath will contain 010101010101010 to signal end of record. However, since the End of Tape signal can occur at any point, the last data record in any file may terminate at any point. Thus, when the End of Tape occurs, words N and $N+1$ are inserted without the minimum nadir angle computation and the special End of File code word is added as the last word appearing on tape.

Occasionally dropouts are encountered and the corresponding data records contain no radiation data. In such cases the radiation data record contains only five words (1D to 5A) which document the record with respect to time. In such records the datum in address of the third word (T_C) is destroyed by the End of Record code.

FORMAT OF FINAL METEOROLOGICAL RADIATION TAPE

Documentation Record

Word No.	Quantity	Units	Scaling	Remarks
1=(*DOC*)	Dref		$B=35$	Number of days between zero hour of Sept. 1, 1957, and zero hour of launch day.
2=(*DOC*+1)	Date			Date of Interrogation expressed as a packed word, i.e. Sept. 2, 1960 would be $(090260)_{10}$ or $(110274)_8$. These numbers are shifted to extreme right side of data word.
3=(*DOC*+2)	Day	Julian day	$B=35$	Start time of this file of radiation data.
4=(*DOC*+3)	Hour	Z hour	$B=35$	
5=(*DOC*+4)	Minute	Z minute	$B=35$	
6=(*DOC*+5)	Seconds	Z seconds	$B=26$	
7=(*DOC*+6)	Day	Julian day	$B=35$	Time of Interrogation, i.e. end time of this file of radiation data.
8=(*DOC*+7)	Hour	Z hour	$B=35$	
9=(*DOC*+8)	Minute	Z minute	$B=35$	
10=(*DOC*+9)	Seconds	Z seconds	$B=26$	
11=(*DOC*+10)	Satellite Spin Rate	Deg/Sec	$B=26$	Satellite spin rate (accuracy about 0.01 deg/sec).
12=(*DOC*+11)	Frequency	36, 72, 144	$B=35$	Data sampling frequency (cycles of a 550 KC tuning fork).
13=(*DOC*+12)	Orbit No.		$B=35$	Orbit No. at time of Interrogation.
14=(*DOC*+13)	Station Code		$B=35$	Code defining ground station ("1" for Fort Monmouth, New Jersey; "2" for San Nicolas Island, California).

Format of FMR Tape—N^{th} Record

1D	Day		$B=17$	Julian Day.
1A	Hour		$B=35$	Z time in day specified in word 1D.
2D	Minute		$B=17$	
2A	GHA	Degrees	$B=29$	Greenwich hour angle and declination of the sun at time specified in words 1D, 1A and 2D. Sign of the declination is not stored.
3D	Decl	Degrees	$B=11$	
3A	T_C	Degrees K	$B=35$	Reference temperature of the medium resolution radiometer.
4D	T_R	Degrees K	$B=17$	Reference temperature of the maindeck electronics.
4A	Height	Kilometers	$B=35$	Height of satellite at time specified in words 1D, 1A, 2D.
5D	Latitude	Degrees	$B=11$	Latitude of subsatellite point at time specified in words 1D, 1A, 2D. 90 degrees are added to all latitudes to yield positive numbers.
5A	Longitude	Degrees	$B=29$	Longitude of subsatellite point at time specified in words 1D, 1A, 2D. Longitudes are reported as 0 to 360 degrees, with west being positive.
6D	Seconds		$B=8$	Seconds past time specified in words 1D, 1A, 2D when first earth viewing response is detected, and every fifth response thereafter.
6A	Latitude	Degrees	$B=29$	Latitude of subsatellite point at time specified in words 1D, 1A, 2D, 6D. 90 degrees are added to all latitudes to yield positive numbers.
7D	Longitude	Degrees	$B=11$	Longitude of subsatellite point at time specified in words 1D, 1A, 2D, 6D. Longitudes are reported as 0 to 360 degrees, with west being positive.
7A	Latitude	Degrees	$B=29$	Latitude of point on earth being "viewed" by radiometer at time specified in words 1D, 1A, 2D, 6D. 90 degrees are added to all latitudes to yield positive numbers.
8D	Longitude	Degrees	$B=11$	Longitude of point on earth being "viewed" by radiometer at time specified in words 1D, 1A, 2D, 6D. Longitudes are reported as 0 to 360 degrees, with west being positive.
8A	Nadir Angle	Degrees	$B=29$	Nadir Angle of optic axis from radiometer to point specified in words 7A, 8D.

FORMAT OF FINAL METEOROLOGICAL RADIATION TAPE—Continued

Format of FMR Tape—N^{th} Record—Continued

Word No.	Quantity	Units	Scaling	Remarks
9D	Azimuth Angle	Degrees	$B=11$	Azimuth angle of optic axis from radiometer to point specified in words 7A, 8D. This angle is measured clockwise and expressed as a positive number.
9A	Zero			
10D	W (Ch. 1)	Watts/meter^2	$B=14$	Energy measured by each of the five medium resolution channels at time specified in 1D, 1A, 2D, 6D when radiometer is "viewing" point on earth described in 7A, 8D.
10A	W (Ch. 2)	Watts/meter^2	$B=32$	
11D	W (Ch. 3)	Watts/meter^2	$B=14$	
11A	W (Ch. 4)	Watts/meter^2	$B=32$	
12D	W (Ch. 5)	Watts/meter^2	$B=14$	
12A	Zero			
13D	W (Ch. 1)	Watts/meter^2	$B=14$	The data sample immediately following the measurement recorded in words 10D–12A.
13A	W (Ch. 2)	Watts/meter^2	$B=32$	
14D	W (Ch. 3)	Watts/meter^2	$B=14$	
14A	W (Ch. 4)	Watts/meter^2	$B=32$	
15D	W (Ch. 5)	Watts/meter^2	$B=14$	
15A	Zero			
16D	W (Ch. 1)	Watts/meter^2	$B=14$	The data sample immediately following the measurement recorded in words 13D to 15A.
16A	W (Ch. 2)	Watts/meter^2	$B=32$	
17D	W (Ch. 3)	Watts/meter^2	$B=14$	
17A	W (Ch. 4)	Watts/meter^2	$B=32$	
18D	W (Ch. 5)	Watts/meter^2	$B=14$	
18A	Zero			
19D	W (Ch. 1)	Watts/meter^2	$B=14$	The data sample immediately following the measurement recorded in words 16D to 18A.
19A	W (Ch. 2)	Watts/meter^2	$B=32$	
20D	W (Ch. 3)	Watts/meter^2	$B=14$	
20A	W (Ch. 4)	Watts/meter^2	$B=32$	
21D	W (Ch. 5)	Watts/meter^2	$B=14$	
21A	Zero			
22D	W (Ch. 1)	Watts/meter^2	$B=14$	The data sample immediately following the measurement recorded in words 19D to 21A.
22A	W (Ch. 2)	Watts/meter^2	$B=32$	
23D	W (Ch. 3)	Watts/meter^2	$B=14$	
23A	W (Ch. 4)	Watts/meter^2	$B=32$	
24D	W (Ch. 5)	Watts/meter^2	$B=14$	
24A	Zero			

The block of data from words 6D to 24A will be repeated, thus defining every fifth point in a swath. The address of the third word in the last response of a particular swath will contain 010101010101010 to signal the end of record. Each time the swath terminates, two words (N and $N+1$) will follow the last "earth-viewing" response with the following format. When the EOT is encountered, an additional word ($N+2$) is inserted to indicate End of File.

Word No.	Quantity	Units	Scaling	Remarks
ND	Code	111111111111111		Code indicating end of swath.
NA	Nadir Angle	Degrees	$B=29$	The minimum nadir angle that occurred in the previously defined swath.
$(N+1)D$	Latitude	Degrees	$B=11$	Latitude of point on earth being "viewed" by radiometer when the minumum nadir angle occurred. 90 degrees are added to all latitudes to yield positive numbers.
$(N+1)A$	Longitude	Degrees	$B=29$	Longitude of point on earth being "viewed" by radiometer when minumum nadir angle occurred. Longitudes are reported as 0 to 360 degrees with west being positive.
$N+2$	Code	11001100 etc.		Code word indicating end of file. Occurs only in the last record of a file.

V. IBM–7090 COMPUTER FLOW DIAGRAM

The final meteorological radiation tape, described in the previous section, is prepared with an IBM–7090 computer program whose input consists of orbital data, digital radiation data, TIROS II radiometer calibration package, and satellite attitude. The flow chart shown in Fig. 37 outlines the logical steps in this program and thus gives some insight into the mechanics of preparing these tapes. The flow chart has been greatly condensed since it is impossible to present a detailed flow chart within the space limitations of this publication.

The first phase of this program sets up the documentation data, and then reads the entire file of radiation data to compute the start time from the End of Tape time and data sampling frequency. Given the starting and ending times, the program then searches the orbital tape to find orbital data (subsatellite point, height, nadir angle, right ascension and declination) covering the same time interval. These data are then arranged in tables as a function of time so that interpolation subroutines can be used in the second phase to obtain values of the orbital characteristics for any specified time.

At this point, an optional feature allows the program to accept the attitude data from the orbital tape, or an alternate estimate of the attitude from a second documentation card. If the alternate attitude is accepted, the nadir angles are recomputed.

The second phase of the program reduces the digitized radiation data into useful meteorological data. This begins with a detailed examination

of the radiation data to distinguish between earth and space viewed data. This distinction is based on an arbitrarily defined threshold value applied to channel 4 up to orbit 649, and channel 2 from orbit 650 to orbit 2071. Both sensors are assumed to be viewing space when the measured radiation falls below the threshold value, and one sensor is viewing the earth when the measured radiation exceeds the threshold value.

For each earth-viewing swath the program proceeds to determine which sensor is viewing the earth, computes the latitude and longitude of the point on the earth being "viewed" by the radiometer for each fifth measurement in the swath, and converts the digitized data into radiant emittance units for each measurement in the swath. The data words containing radiation measurements contain a 1 in position 19 when the wall sensor is viewing the earth. When the swath size exceeds the theoretically computed number of responses, the remaining earth-viewing measurements are retained with a negative sign.

Each record on the final meteorological radiation tape covers approximately one minute of time and terminates with the end of swath in progress at 60.0 seconds past the minute. When the End of Tape is encountered, the program writes the last data record and reinitializes in preparation for the next orbit of radiation data.

VI. POST-LAUNCH OBSERVATIONS AND DEVELOPMENTS

The formulation of the data processing procedures was based on the original concepts of the way in which the radiometer was supposed to perform. Since that time further experience with the radiometer has indicated characteristics which depart from these basic concepts. Because of the effects of these characteristics on the accuracy of the experiment, it is necessary to give them some consideration.

The calibration described in Section II indicates the function $V_{rad}=f(\overline{W})$ departs somewhat from linearity in the three thermal channels. The greatest departure occurs for small values of $\overline{W}$. Channel 1 shows the largest non-linearity and channel 2 the least.

The radiometer output was measured in the laboratory prior to launch with both targets at room temperature. Since the difference in radiation between the wall side and floor side was zero, this was taken to be the zero radiation level. It was assumed this level would be the same when both optics were viewing outer space. However, shortly after launch it became apparent that the space viewed levels of the three thermal channels were higher than the zero levels measured in the laboratory. The levels varied somewhat as time progressed. Figs. 38 through 42 show the time histories of the space-viewed levels compared with the time history of the radiometer housing temperature. The housing temperature shown for a given orbit represents an average taken over that orbit. The variations in housing temperature and electronics temperature over a sample orbit are shown in Fig. 43. There appears to be correlation between housing temperature and space viewed level in channel 1 and to a lesser extent in channel 4.

Other symptoms developed in the radiometer output as time progressed. From about orbit 600 on, channel 1 displayed an extremely high space viewed level with the signal going in a negative sense from this level when the wall optic scanned the earth. The signal remained positive with respect to the space viewed level when the floor side scanned the earth.

Channel 4 displayed a small negative going signal at the beginning of the earth scan on the wall side, but the signal returned positive and became apparently normal as the scan progressed. The floor side did not display this characteristic. The effect appeared slightly from the beginning, but did not become pronounced until after orbit 650. From this time on, the performance of channel 4 decayed steadily. An imbalance between wall and floor side became noticeable, with the wall displaying consistently lower signals than the floor. The history of these effects is shown in Fig. 44.

The wall optic was exposed to direct sunlight during the orbits 115 to 220, 752 to 772 and 1025 to 1046. It is probable that some type of damage incurred during these periods resulted in the effects observed in channel 1 and contributed to those seen in channel 4. Possibly the transmission of the wall half of the filter was altered, leading to radiation components originating internally, producing the effects observed in channel 1.

Radiation components originating within the radiometer and having phase angles different from the external radiation are possibly responsible for the high space viewed levels observed. The analysis of such a situation turns out to be rather complex and no satisfactory model has been found which would lead to a possible method of correcting the data for this effect. An investigation of the problem is now under way and will continue.

The formulation of the α and β corrections is probably no longer rigorously correct, due to non-linearity of the response and lack of symmetry between wall and floor side. However, in general these corrections are relatively small and do not contribute greatly to the overall accuracy.

VII. CONCLUSIONS

The accuracy of the absolute values of the measurements suffers somewhat due to the several sources of uncertainty involved. These include the problems associated with the determination of the effective spectral response, the assumptions involved in the α and β correction formulation, and the space viewed level problem.

The greatest uncertainty is due to the apparent shift in the zero radiation level. The error introduced by not correcting for this effect is probably largest at low equivalent blackbody temperatures, becoming smaller with increasing temperature. The significance of the data is doubtful beyond orbit 600 for channel 1 and orbit 650 for channel 4 due to the degradations which developed in the output of these channels.

Rather than withhold publication of the data until a study of the space viewed level problem is completed, it was thought desirable to make the data available to the scientific community at this time. As the study progresses, inquiries and/or ideas concerning this problem are invited.

VIII. REFERENCES AND BIBLIOGRAPHY

1. Bandeen, W. R., R. A. Hanel, John Licht, R. A. Stampfl, and W. G. Stroud: "Infrared and Reflected Solar Radiation Measurements from the TIROS II Meteorological Satellite." (To be published in the *J. of Geophys. Res.*, October 1961.)
2. Hanel, R. A. and W. G. Stroud: "Infrared Imaging from Satellites." *J. of the SMPTE, 69*(1), 25–26, January 1960.
3. Sternberg, Sidney and William G. Stroud: "TIROS I: Meteorological Satellite." *Astronautics, 5*(6), 32–34 and 84–86, June 1960.
4. Stroud, W. G.: "Initial Results of the TIROS I Meteorological Satellite." *J. of Geophys. Res., 65*, 1643–1644, May 1960.
5. Bandeen, William R. and Warren P. Manger: "Angular Motion of the TIROS I Meteorological Satellite due to Magnetic and Gravitational Torques." *J. of Geophys. Res., 65*, 2992–2995, September 1960.
6. Doolittle, R. C., L. Miller and I. Ruff: "Geographic Locations of Cloud Features." Appendix I of "Some Meteorological Results from TIROS I," by Staff, Meteorological Satellite Laboratory, U.S. Weather Bureau, in a report by NASA. (In press.)
7. Bristor, C. L., E. G. Albert, and J. B. Jones: "Problems in Mapping Data from Meteorological Satellites." Proceedings of COSPAR meeting, Florence, Italy, April 1961. (In press.)
8. Hubert, L. F.: "TIROS I: Camera Attitude Data, Analysis of Location Errors, and Derivation of Correction for Calibration." MSL Report #5 to NASA.
9. Dean, C.: "Attitude Determination from Picture Data," "TIROS I: An Operational Evaluation of a New Meteorological Tool," Second Semi-Annual Technical Summary Report, Contract AF 19(604)–5581, Allied Research Associates, Inc., June 30, 1960.
10. Davis, J., R. Hanel, R. Stampfl, M. Strange, and M. Townsend: "Telemetering IR Data from the TIROS II Meteorological Satellite." (To be published in the Proceedings of the I.R.E. National Symposium on Space Electronics and Telemetry to be held in Albuquerque, N.M., in September 1961.)
11. Astheimer, R. W., D. DeWaard, and E. A. Jackson: "Infrared Radiometric Instrumentation on TIROS II." Presented at OSA meeting, Pittsburgh, Pa., March 3, 1961. (To be published in the *J. Opt. Soc. Am.*)
12. Greenfield, S. M. and W. W. Kellogg: "Calculations of Atmospheric Infrared Radiation as seen from a Meteorological Satellite." *J. of Meteor.*, 17, 283–289, June 1960.
13. Hanel, R., J. Licht, W. Nordberg, R. Stampfl, and W. G. Stroud: "The Satellite Vanguard II: Cloud Cover Experiment." *IRE Transactions on Mil. Electronics*, MIL–4 (2 and 3), 245–247, April–July 1960.
14. Hanel, R. A. and D. Q. Wark: "TIROS II Radiation Experiment and Its Physical Significance." Paper presented at the March 1961 meeting of the Optical Society of America, Pittsburg, Pa.
15. Wark, D. Q.: "On Indirect Temperature Soundings of the Stratosphere from Satellites." *J. of Geophys. Research, 66*, 77–82, January 1961.
16. Wark, D. Q. and G. Yamamoto: "Methods of Transforming Terrestrial Infrared Radiation Measurements Made from Satellites." Unpublished paper presented at the 41st Annual Meeting of the Am. Met. Soc., New York City, January 23–26, 1961.
17. Wexler, R.: "Satellite Observations of Infrared Radiation." First Semi-annual Technical Summary Report (Allied Research Assoc., Inc., Boston, Mass.), Contract No. AF 19-(604)-5968, ARCRC. December 24, 1959.

TABLE II.—*Filter and lens materials*

	Channel 1	Channel 2	Channel 3	Channel 4	Channel 5
Lens 1	Germanium with two sides anti-reflection coated	Germanium with two sides anti-reflection coated	Sapphire (Al_2O_3)	KRS-5 (Thallium-bromo-iodide)	Sapphire (Al_2O_3)
Lens 2	Germanium with two sides anti-reflection coated	Germanium with two sides anti-reflection coated	Barium Floride (BaF_2)	None	Silicon Dioxide (SiO_2)
Lens 3	Germanium immersion lens at detector	None	None	None	None
Filter 1	Band pass interference type centered at 6.3 microns	Indium Antimonide (InSb)	None	Indium Antimonide anti-reflection coated	Infrared Industries Type 2,590,115B
Filter 2	None	Arsenic Trisulfide (As_2S_3)	None	None	Infrared Industries Type 259,011,608
Filter 3	None	None	None	None	One-eighth inch thick Chance Glass

TABLE III.—*Effective spectral response, channel 1*

λ (microns)	ϕ_λ	λ (microns)	ϕ_λ	λ (microns)	ϕ_λ
5.72	0.007	6.16	0.376	6.60	0.131
5.76	.012	6.20	.385	6.64	.086
5.80	.019	6.24	.395	6.68	.054
5.84	.032	6.28	.409	6.72	.027
5.88	.049	6.32	.416	6.76	.014
5.92	.079	6.36	.422	6.80	.010
5.96	.166	6.40	.423	6.84	.008
6.00	.245	6.44	.400	6.88	.006
6.04	.286	6.48	.364	6.92	.004
6.08	.354	6.52	.272	6.96	.002
6.12	.372	6.56	.189	7.00	0

TABLE IV.—*Effective spectral response, channel 2*

λ (microns)	ϕ_λ	λ (microns)	ϕ_λ	λ (microns)	ϕ_λ
7.18	0	10.4	0.462	15.0	0.006
7.2	.010	10.6	.473	15.5	.018
7.4	.122	10.8	.462	16.0	.034
7.6	.240	11.0	.444	16.5	.039
7.8	.309	11.2	.435	17.0	.040
8.0	.322	11.4	.478	17.5	.035
8.2	.328	11.6	.413	18.0	.031
8.4	.356	11.8	.380	18.5	.028
8.6	.384	12.0	.319	19.0	.018
8.8	.404	12.2	.264	19.5	.013
9.0	.431	12.4	.203	20.0	.009
9.2	.460	12.6	.142	20.5	.007
9.4	.468	12.8	.133	21.0	.004
9.6	.472	13.0	.121	21.5	.003
9.8	.475	13.5	.043	22.0	.001
10.0	.464	14.0	.010	22.2	0
10.2	.454	14.5	0		

TABLE V.—*Effective spectral response, channel 3*

λ (microns)	ϕ_λ	λ (microns)	ϕ_λ	λ (microns)	ϕ_λ
0.26	0.560	2.54	0.824	4.70	0.820
.38	.723	2.66	.828	4.82	.808
.50	.757	2.78	.828	4.94	.800
.62	.778	2.90	.828	5.06	.788
.74	.785	3.02	.824	5.18	.768
.86	.790	3.14	.833	5.30	.756
.98	.791	3.26	.828	5.42	.727
1.10	.795	3.38	.828	5.54	.697
1.22	.798	3.50	.828	5.66	.677
1.34	.797	3.62	.828	5.78	.653
1.46	.799	3.74	.836	5.90	.612
1.58	.805	3.86	.838	6.02	.571
1.70	.811	3.98	.838	6.14	.483
1.82	.817	4.10	.838	6.26	.418
1.94	.818	4.22	.838	6.50	.296
2.06	.818	4.34	.839	7.00	.056
2.18	.820	4.46	.838	7.20	.056
2.30	.820	4.58	.838	7.60	0
2.42	.820				

TABLE VI.—*Effective spectral response, channel 4*

λ (microns)	ϕ_λ	λ (microns)	ϕ_λ	λ (microns)	ϕ_λ
7.2	0	11.6	0.337	16.0	0.191
7.4	.075	11.8	.348	16.2	.197
7.6	.170	12.0	.336	16.4	.201
7.8	.231	12.2	.315	16.6	.202
8.0	.259	12.4	.274	16.8	.204
8.2	.266	12.6	.269	17.0	.204
8.4	.283	12.8	.249	18.0	.194
8.6	.301	13.0	.246	19.0	.198
8.8	.308	13.2	.262	20.0	.209
9.0	.300	13.4	.290	21.0	.218
9.2	.310	13.6	.245	22.0	.209
9.4	.308	13.8	.265	23.0	.194
9.6	.309	14.0	.299	24.0	.186
9.8	.309	14.2	.274	25.0	.195
10.0	.305	14.4	.216	26.0	.192
10.2	.310	14.6	.195	27.0	.171
10.4	.306	14.8	.178	28.0	.113
10.6	.305	15.0	.167	29.0	.107
10.8	.297	15.2	.165	30.0	.092
11.0	.285	15.4	.170	31.0	.070
11.2	.294	15.6	.180	32.0	.038
11.4	.354	15.8	.187	32.6	0

TABLE VII.—*Effective spectral response, channel 5*

λ (microns)	ϕ_λ	λ (microns)	ϕ_λ	λ (microns)	ϕ_λ
0.365	0	0.815	0	1.75	0.058
.395	.002	.845	0	1.85	.063
.425	.002	.875	0	1.95	.078
.455	.003	.905	0	2.05	.122
.485	.020	.935	0	2.15	.134
.515	.170	.965	0	2.25	.136
.545	.560	.995	0	2.35	.124
.575	.522	1.025	0	2.45	.124
.605	.420	1.055	0	2.55	.138
.635	.510	1.085	0	2.65	.118
.665	.540	1.115	.005	2.75	.056
.695	.400	1.145	.023	2.85	.018
.710	.350	1.175	.020	2.95	.010
.725	.400	1.205	.015	3.05	.007
.733	.430	1.45	.020	3.15	.003
.755	.220	1.55	.038	3.25	.001
.775	.023	1.65	.051	3.35	0
.785	.010				

TABLE VIII.—T_{BB} vs. $\overline{W}$, Channel 1

T_{BB} (° K.)	$\overline{W}$ (watts/m^2)
180	0.028
200	.100
220	.282
230	.442
240	.668
250	.978
260	1.389
280	2.602
300	4.486
320	7.227
340	11.010

TABLE IX.—T_{BB} vs. $\overline{W}$, Channel 2

T_{BB} (° K.)	$\overline{W}$ (watts/m^2)
140	0.42
160	1.26
180	3.09
200	6.45
220	11.93
240	20.11
260	31.50
280	46.77
300	65.71
320	88.90
340	116.39

TABLE X.—T_{BB} vs. $\overline{W}$, Channel 4

T_{BB} (° K.)	$\overline{W}$ (watts/m^2)
200	14.63
240	34.60
260	49.04
280	67.20
300	88.49
320	112.81
340	142.68

605807 O - 61 - 2

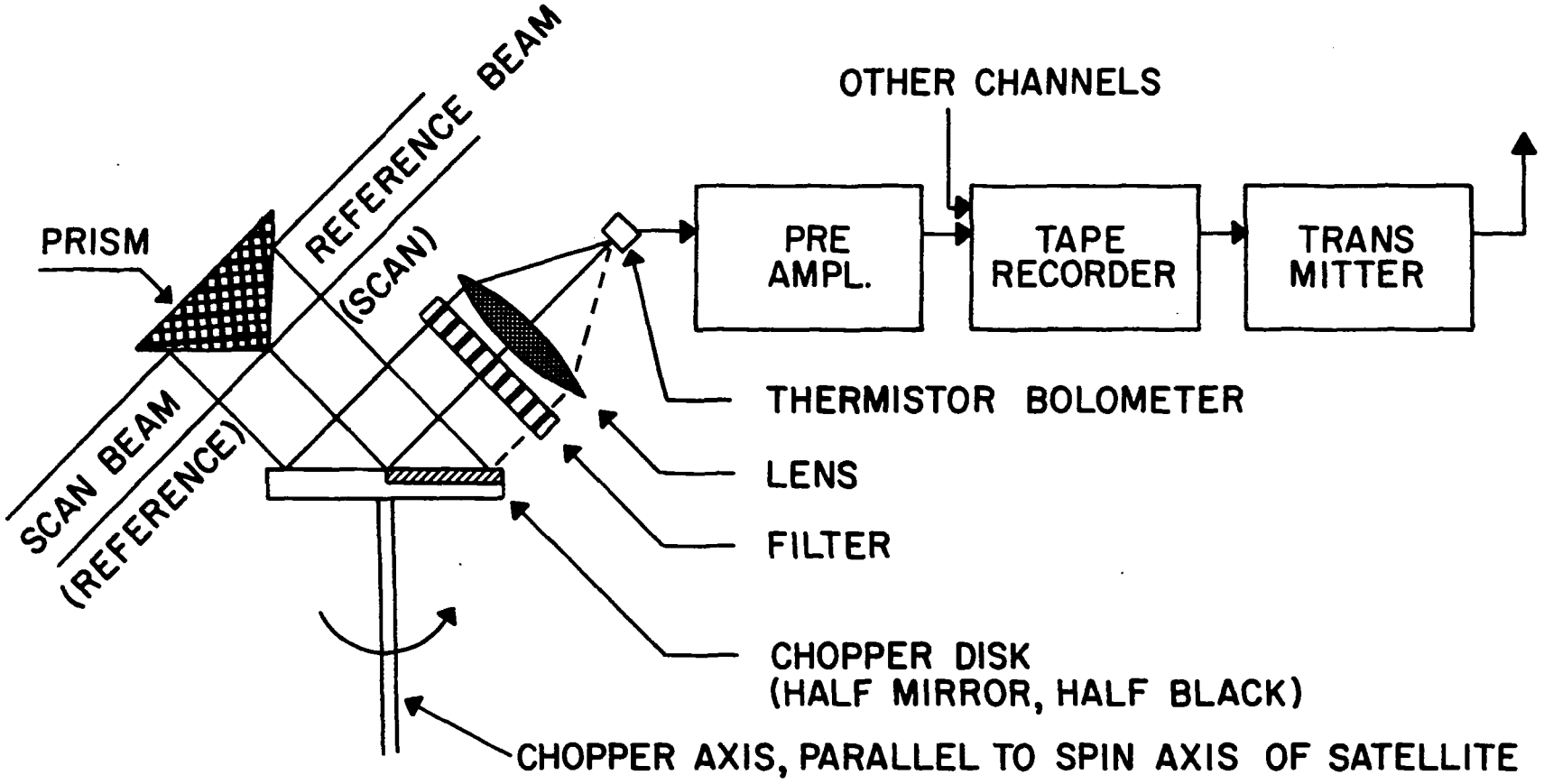

Figure 1—Block diagram of one channel of the medium resolution scanning radiometer.

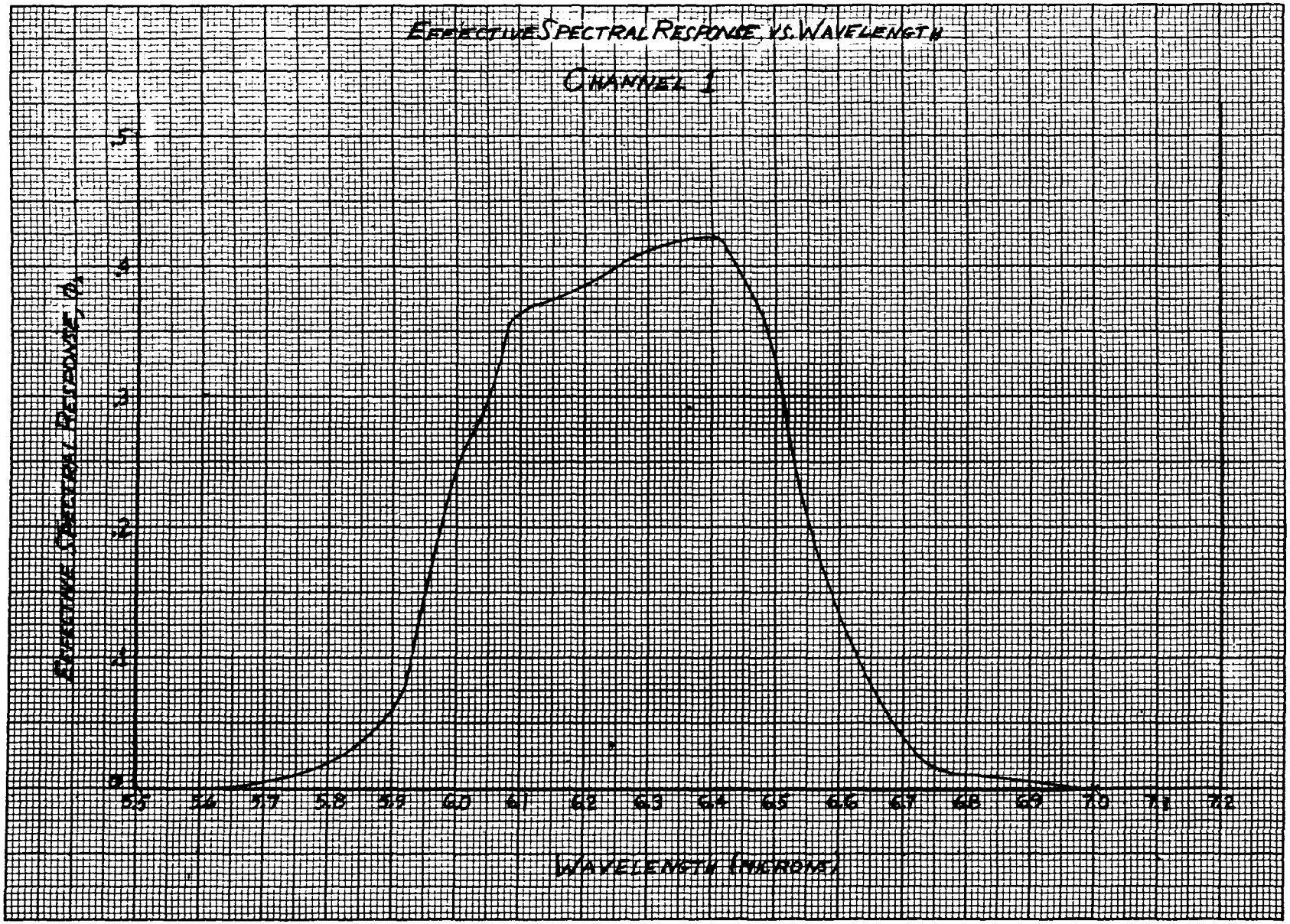

Figure 2—The effective spectral response of channel 1 versus wavelength.

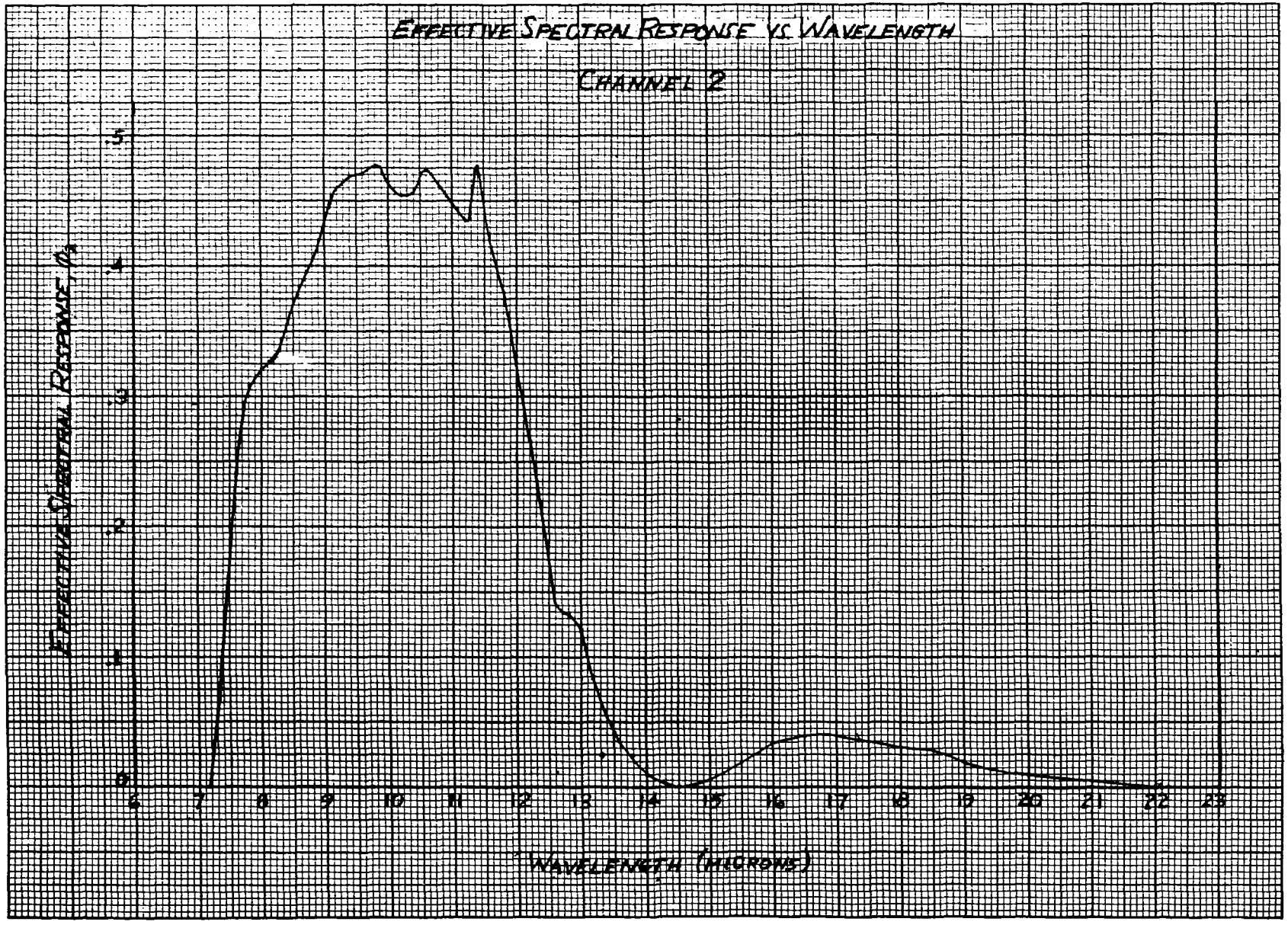

Figure 3—The effective spectral response of channel 2 versus wavelength.

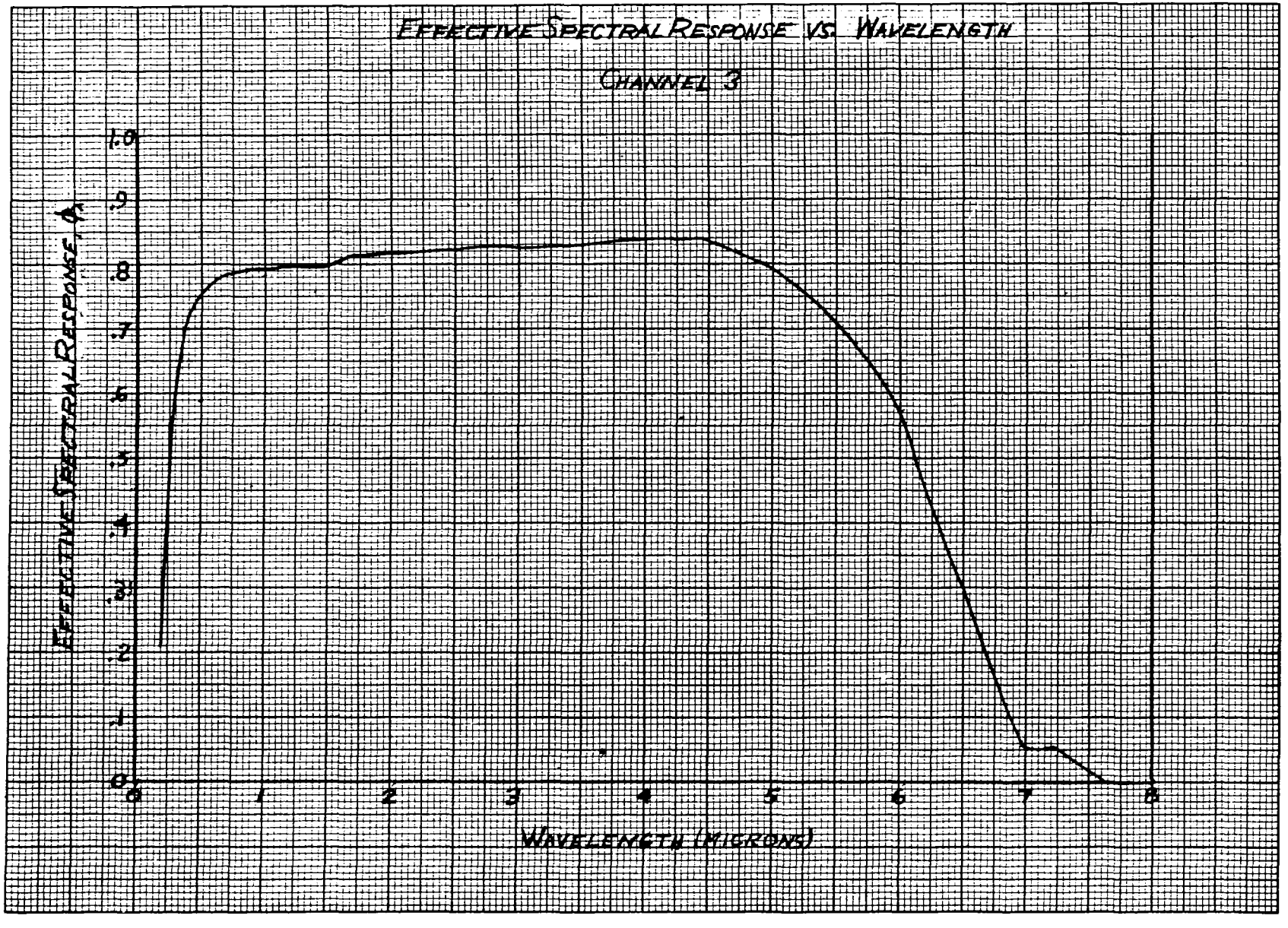

Figure 4—The effective spectral response of channel 3 versus wavelength.

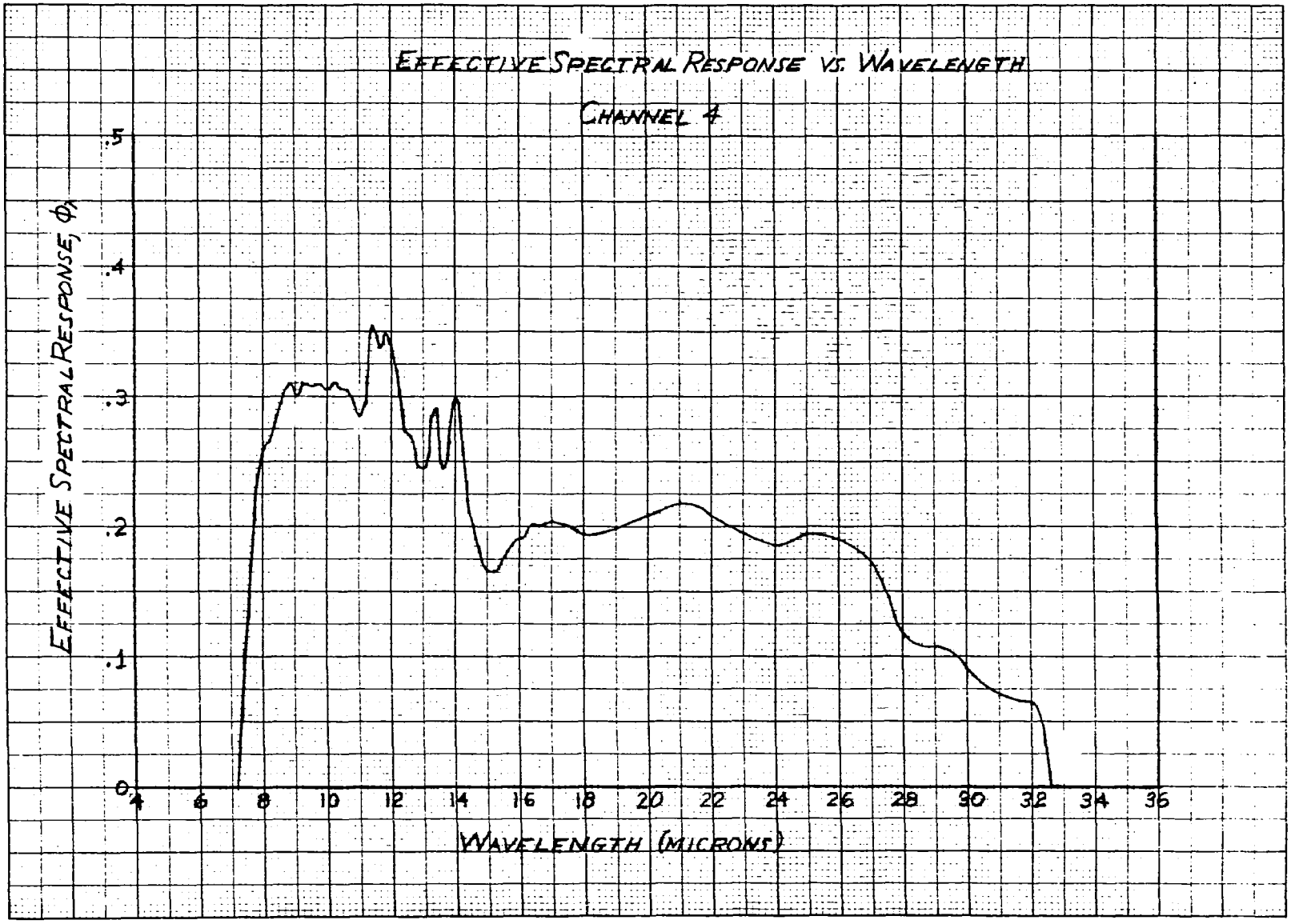

Figure 5—The effective spectral response of channel 4 versus wavelength.

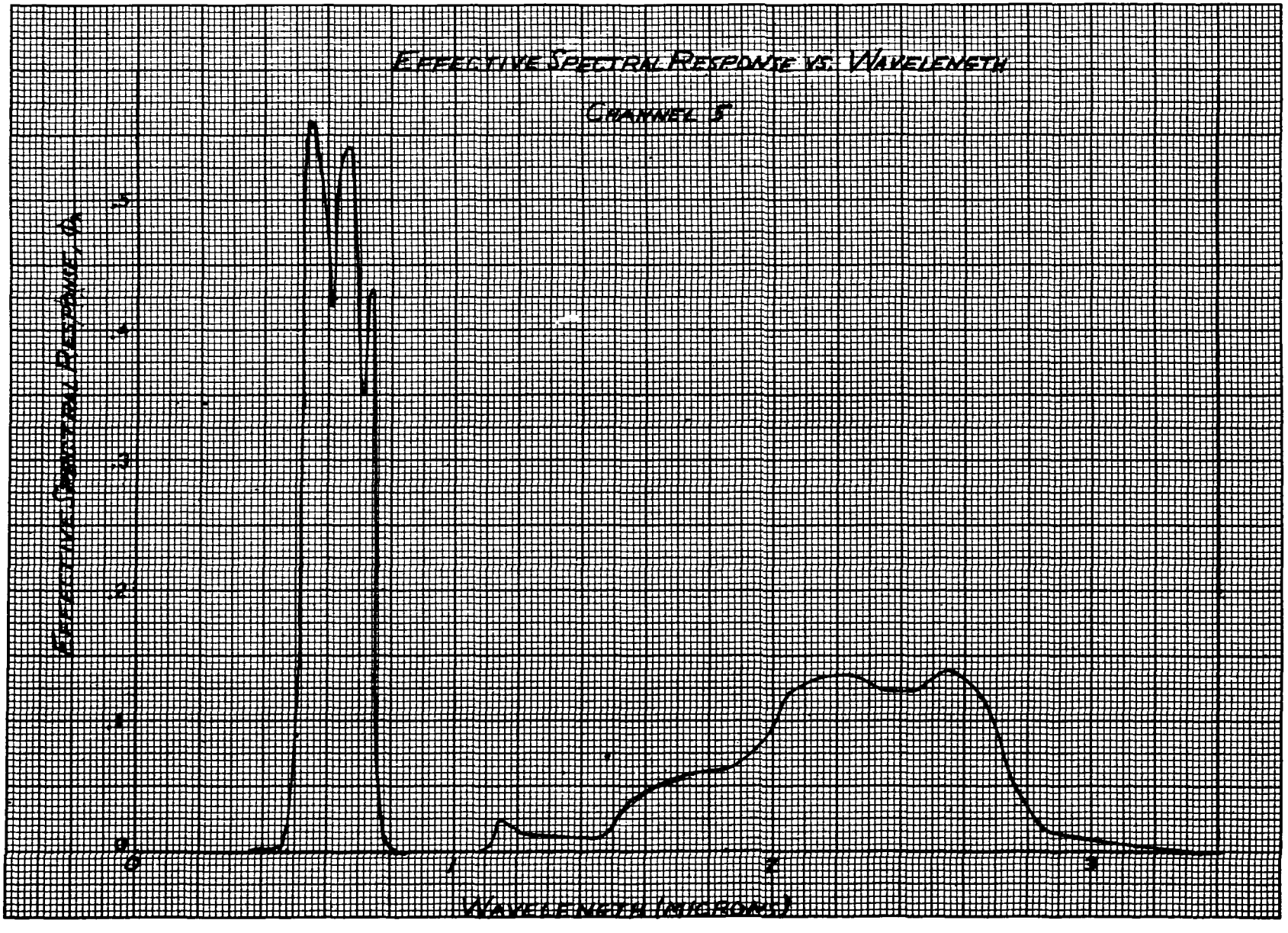

Figure 6—The effective spectral response of channel 5 versus wavelength.

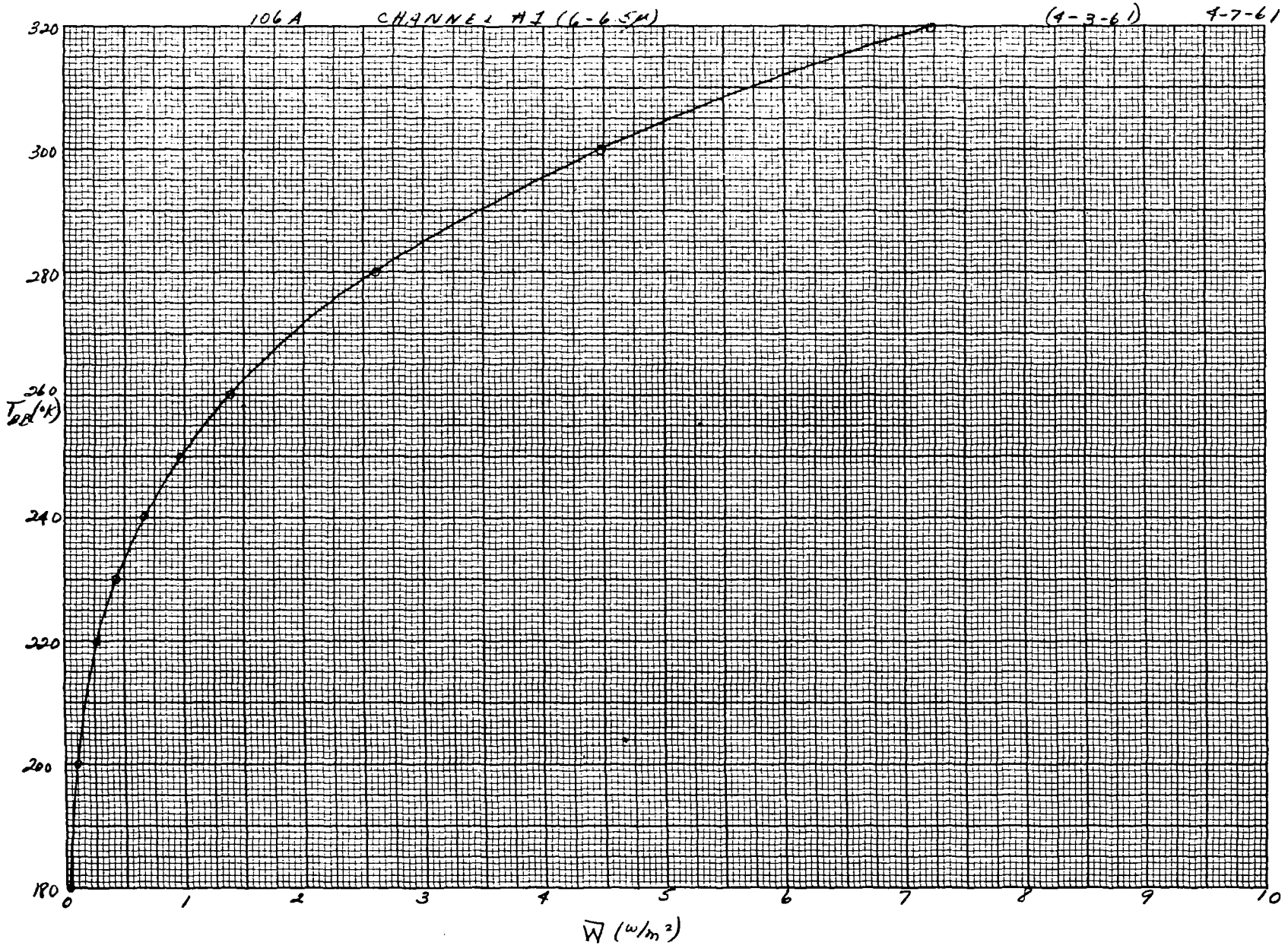

Figure 7—The effective radiant emittance $\overline{W}$ of channel 1 versus equivalent blackbody temperature T_{BB}. The curve was computed using the integral defining $\overline{W}$.

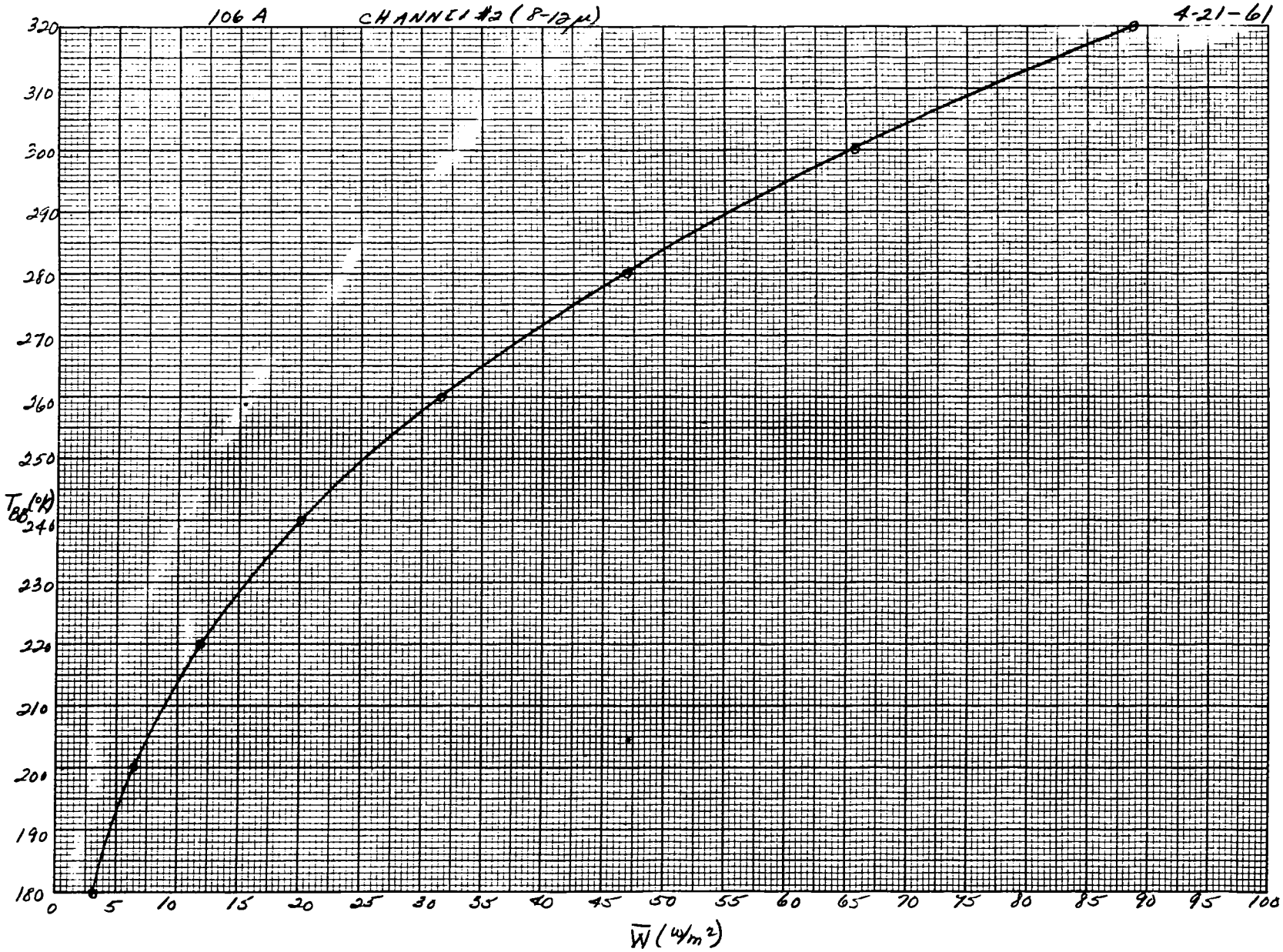

Figure 8—The effective radiant emittance of channel 2 versus equivalent blackbody temperature.

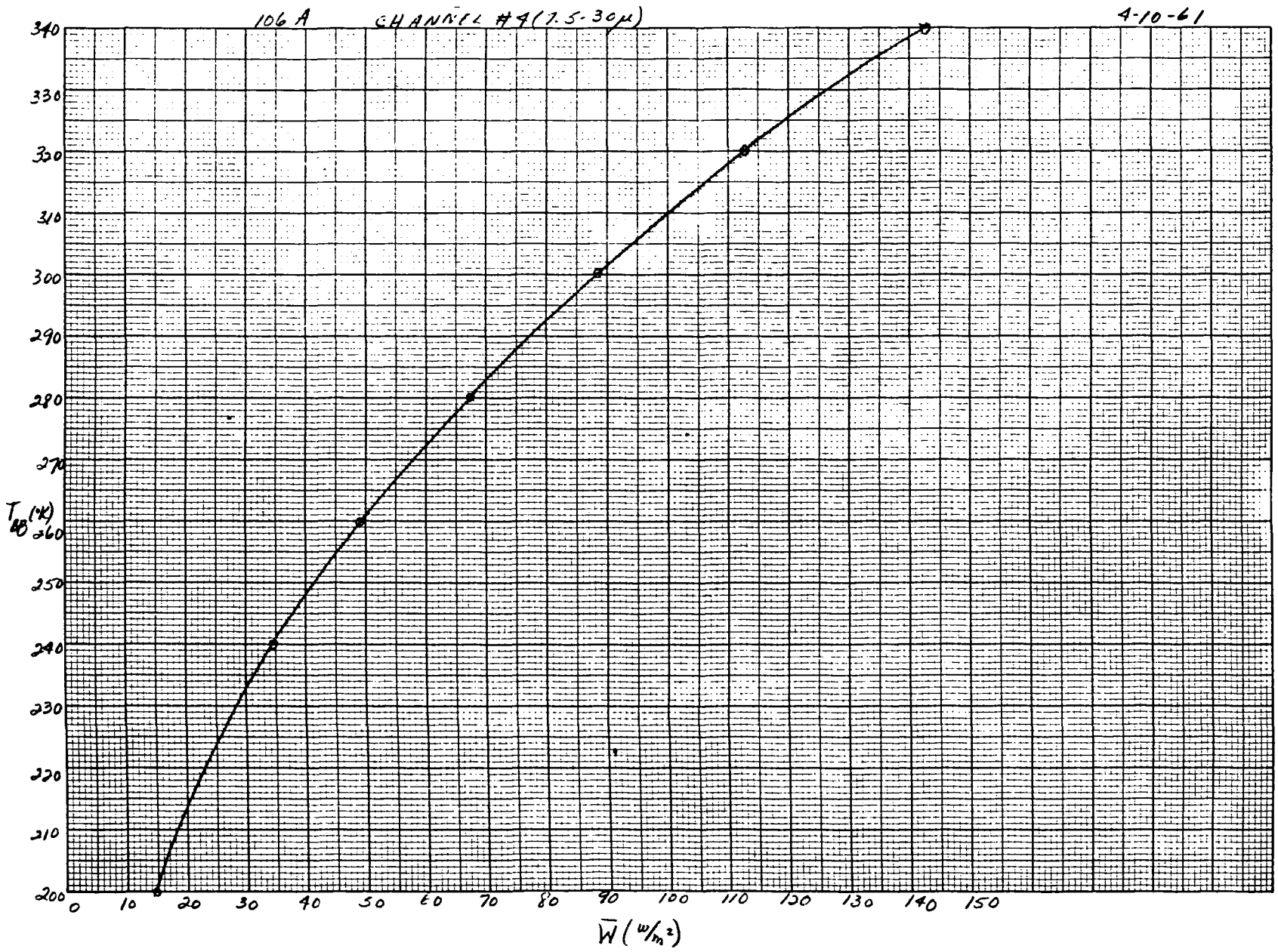

Figure 9—The effective radiant emittance of channel 4 versus equivalent blackbody temperature.

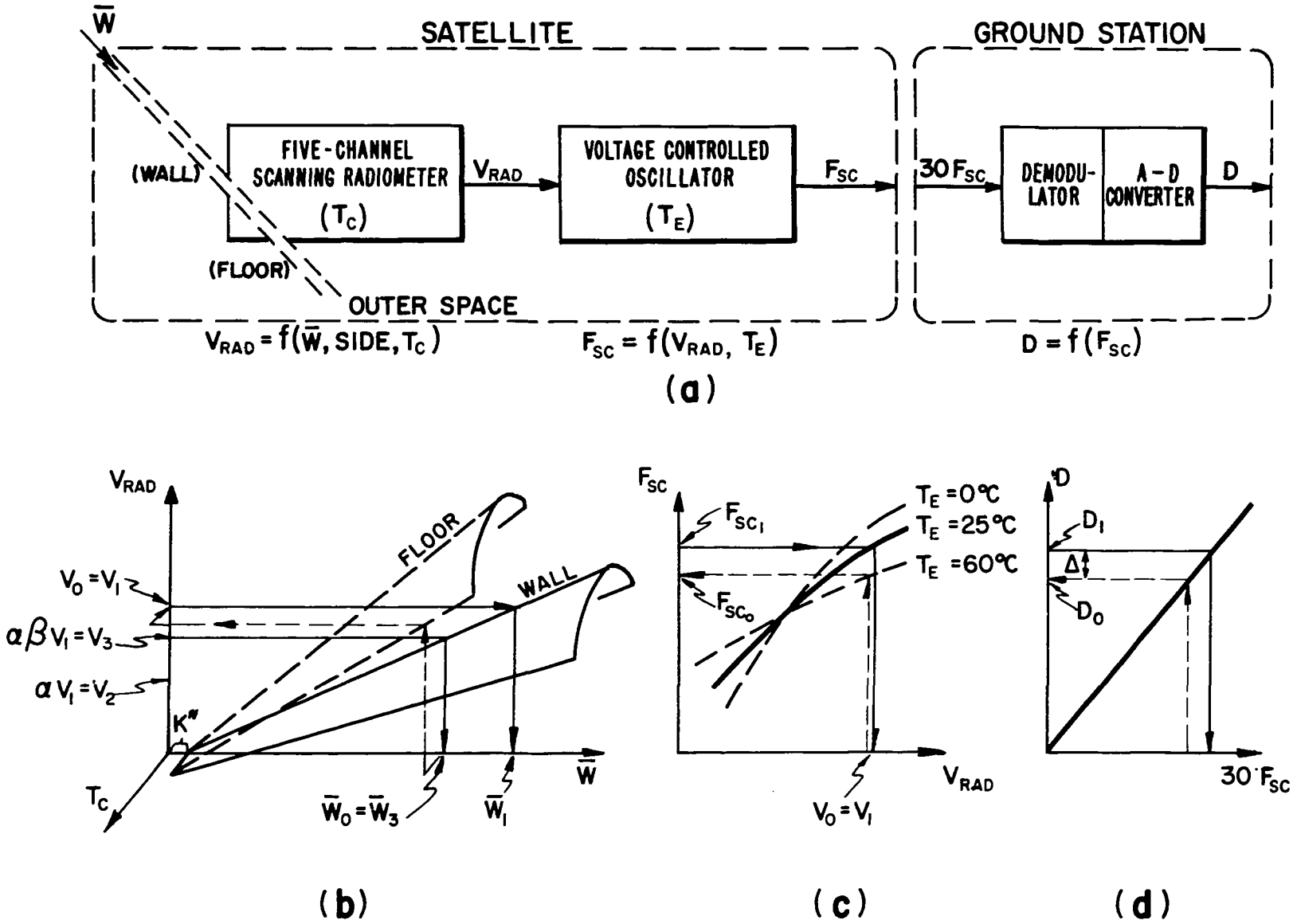

Figure 10—(a) Schematic representation of transfer functions associated with instrumentation in the satellite and at the ground station. *(b)* Three-dimensional representation of the response of the five-channel scanning radiometer. *(c)* The response of the voltage controlled oscillator shown as a parametric function of the electronics temperature T_E. *(d)* The method of introducing an electronics temperature correction Δ.

[1] $\Delta = f(D_0, T_E)$

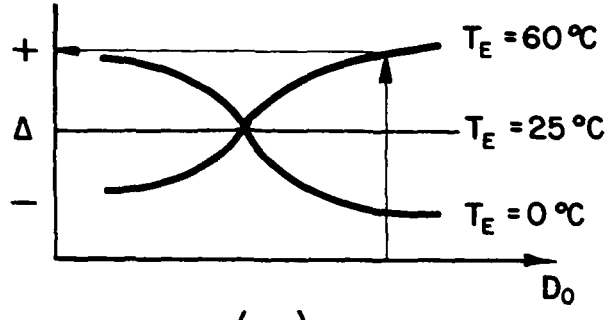

(a)

[2] $D_1 = D_0 + \Delta$

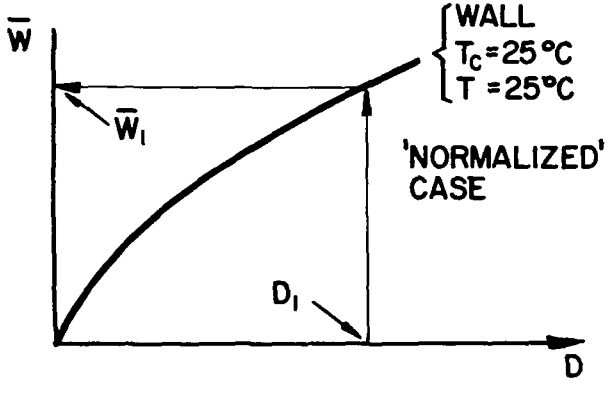

[3] $\bar{W}_1 = f(D_1)$: CORRECTED FOR T_E BUT NOT FOR T_C OR SIDE

(b)

[4] $V_0 = V_1 = V_{RAD}$(____ SIDE, T_C = X °C)

[5] $V_2 = V_{RAD}$(WALL SIDE, T_C = X °C)

[6] $V_3 = V_{RAD}$(WALL SIDE, T_C = 25 °C)

$V_{RAD} = f(\bar{W})$ CAN BE EXPRESSED LINEARLY BY

[7] $V_{RAD} = K'(\bar{W} - K'')$

BALANCE:

[8] $\alpha(\text{SIDE}, T_C) = \frac{V_2}{V_1}$

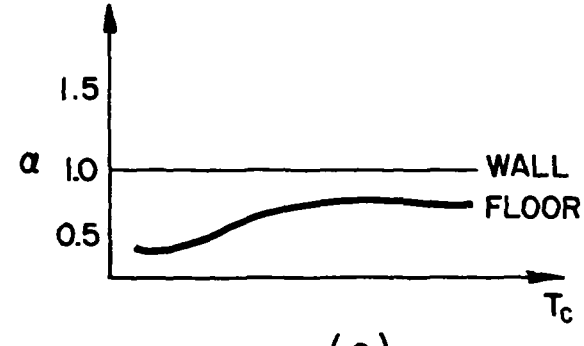

(c)

Figure 11—*(a)* Digital number correction increment Δ versus uncorrected digital number D_0 as a parametric function of the electronics temperature T_E. *(b)* Application of the Δ correction to obtain an effective radiant emittance corrected for T_E only. *(c)* Definition of the balance correction factor α.

TEMPERATURE STABILITY:

$$\beta(T_c) = \frac{V_3}{V_2}$$

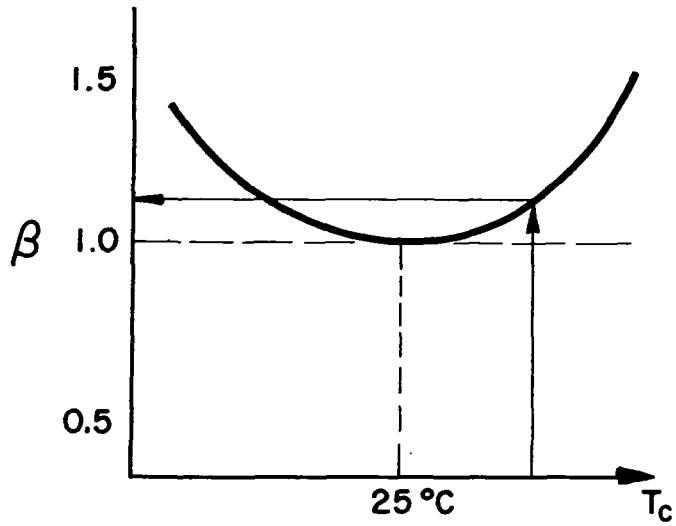

(a)

FROM [8] AND [9]

[10] $V_2 = \alpha V_1$

[11] $V_3 = \alpha \beta V_1$

FROM [7] AND [11]

[12] $V_3 = \alpha \beta K'(\bar{W}_1 - K'') = K'(\bar{W}_3 - K'')$

[13] $\boxed{\bar{W}_3 = \alpha \beta (\bar{W}_1 - K'') + K''}$

(b)

Figure 12—(a) Definition of the temperature stability factor β. *(b)* Derivation of the formula used in obtaining the final corrected effective radiant emittance.

THERMAL CHANNELS 1, 2, AND 4

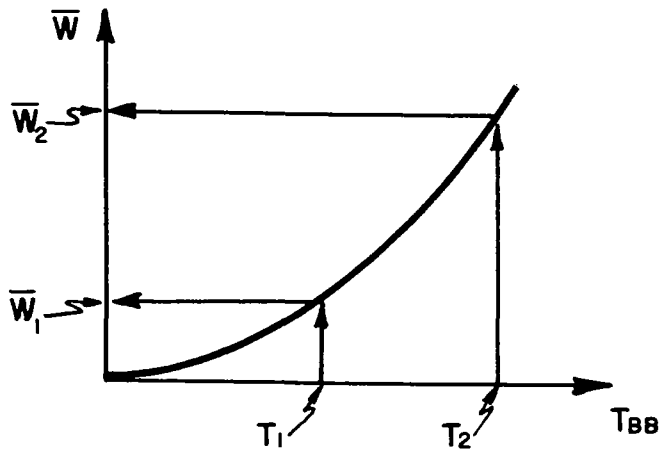

REFERENCE TARGET AT TEMPERATURE T_1
"HOT" TARGET AT TEMPERATURE T_2

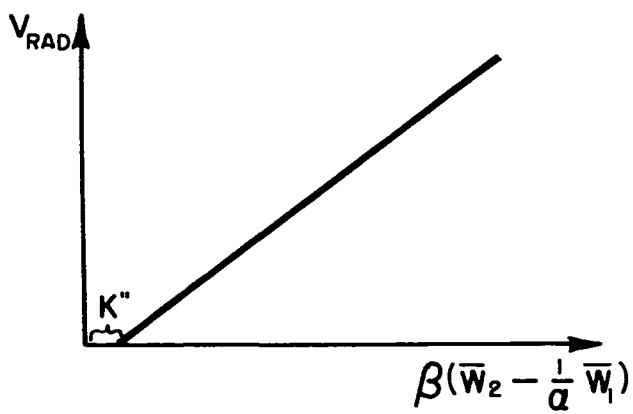

(a)

VISIBLE CHANNELS 3 AND 5

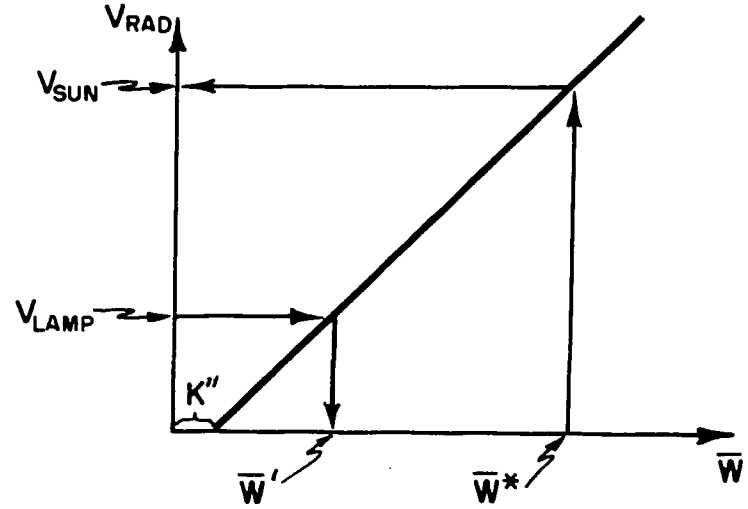

DIFFUSE SOURCE:

$$\overline{W}' = \frac{\cos\delta}{R^2}\int_0^\infty J_\lambda \phi_\lambda r_\lambda \, d\lambda$$

SUN AT NORMAL INCIDENCE ON ALBEDO 1.0 SURFACE:

$$\overline{W}^* = \frac{\Omega}{\pi}\int_0^\infty W_\lambda \, (T = 5800°K) \, \phi_\lambda \, d\lambda$$

$$V_{SUN} = \frac{\overline{W}^* - K''}{\overline{W}' - K''} V_{LAMP}$$

(b)

Figure 13—(a) Calibration of the thermal channels 1, 2, and 4. *(b)* Calibration of the visible channels 3 and 5.

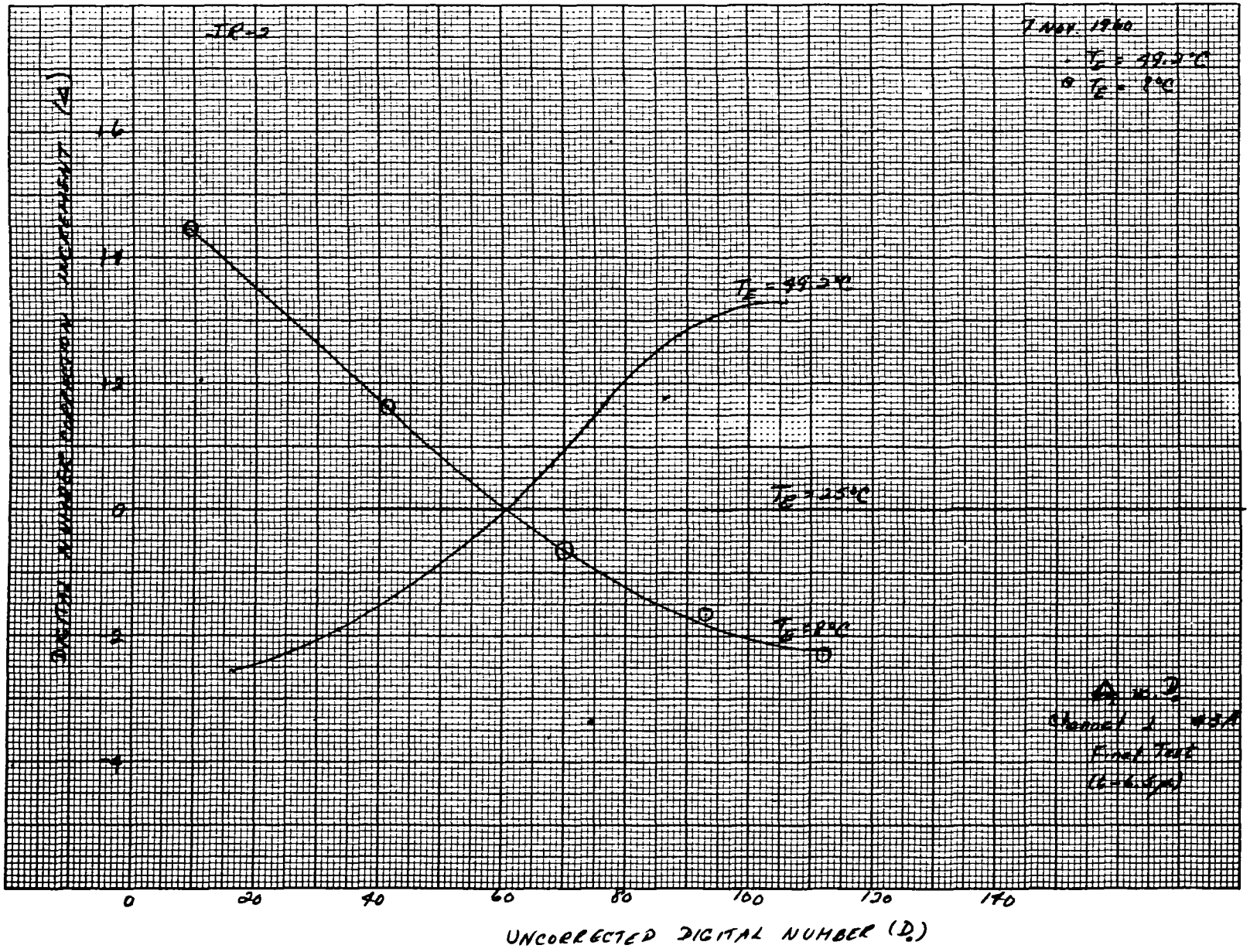

Figure 14—Digital number correction increment versus uncorrected digital number with electronics temperature as a parameter for channel 1.

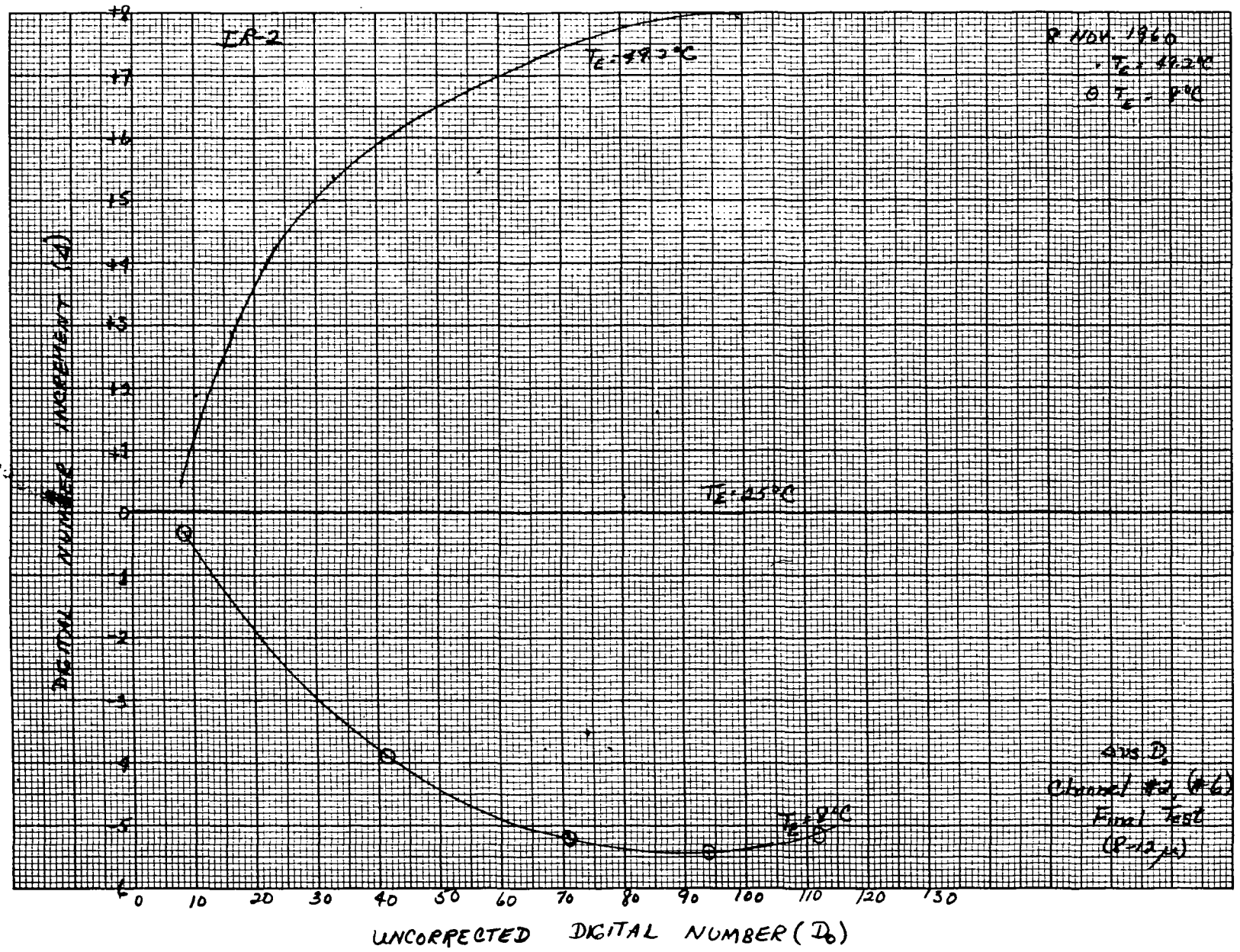

Figure 15—Digital number correction increment versus uncorrected digital number for channel 2.

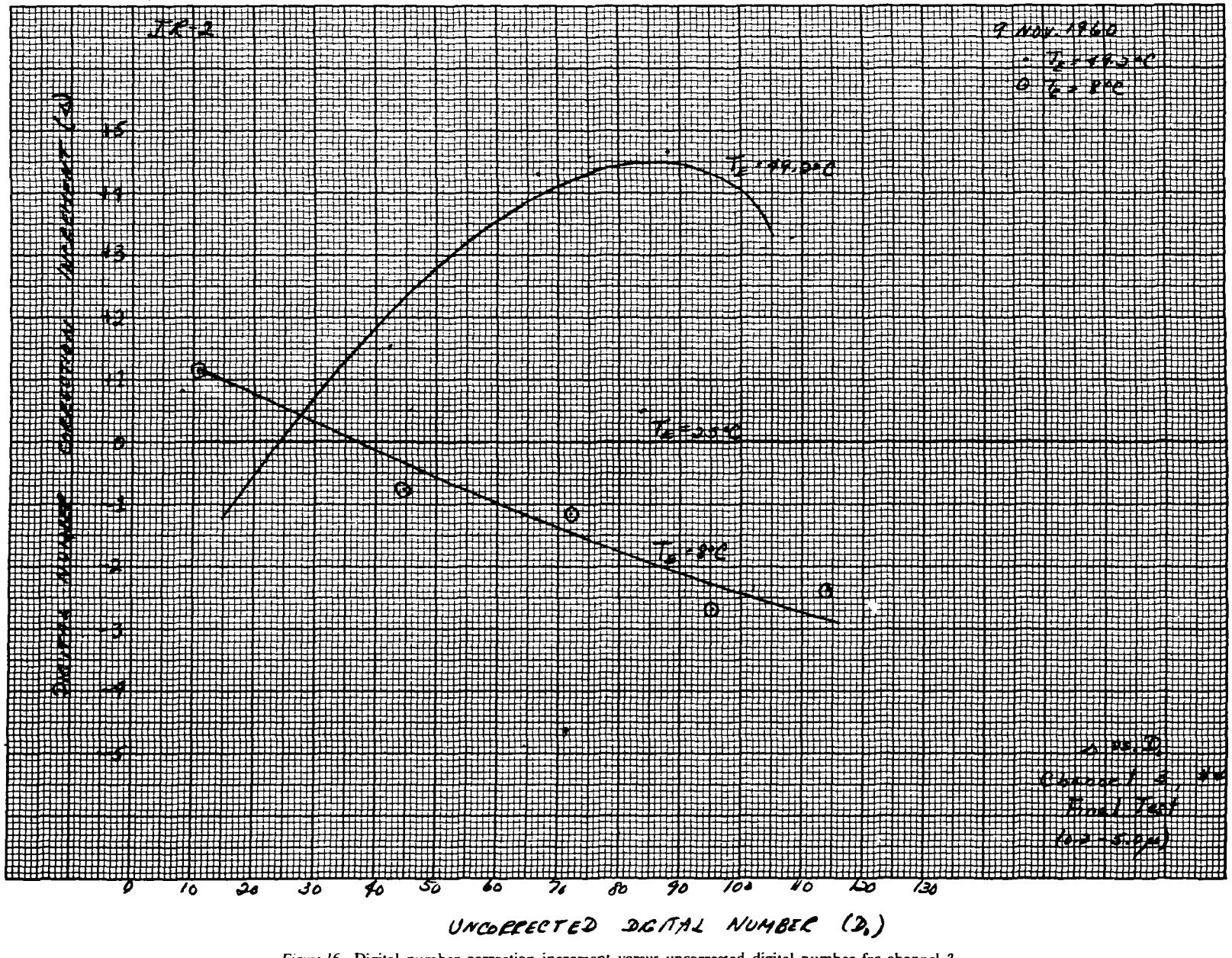

Figure 16—Digital number correction increment versus uncorrected digital number for channel 3.

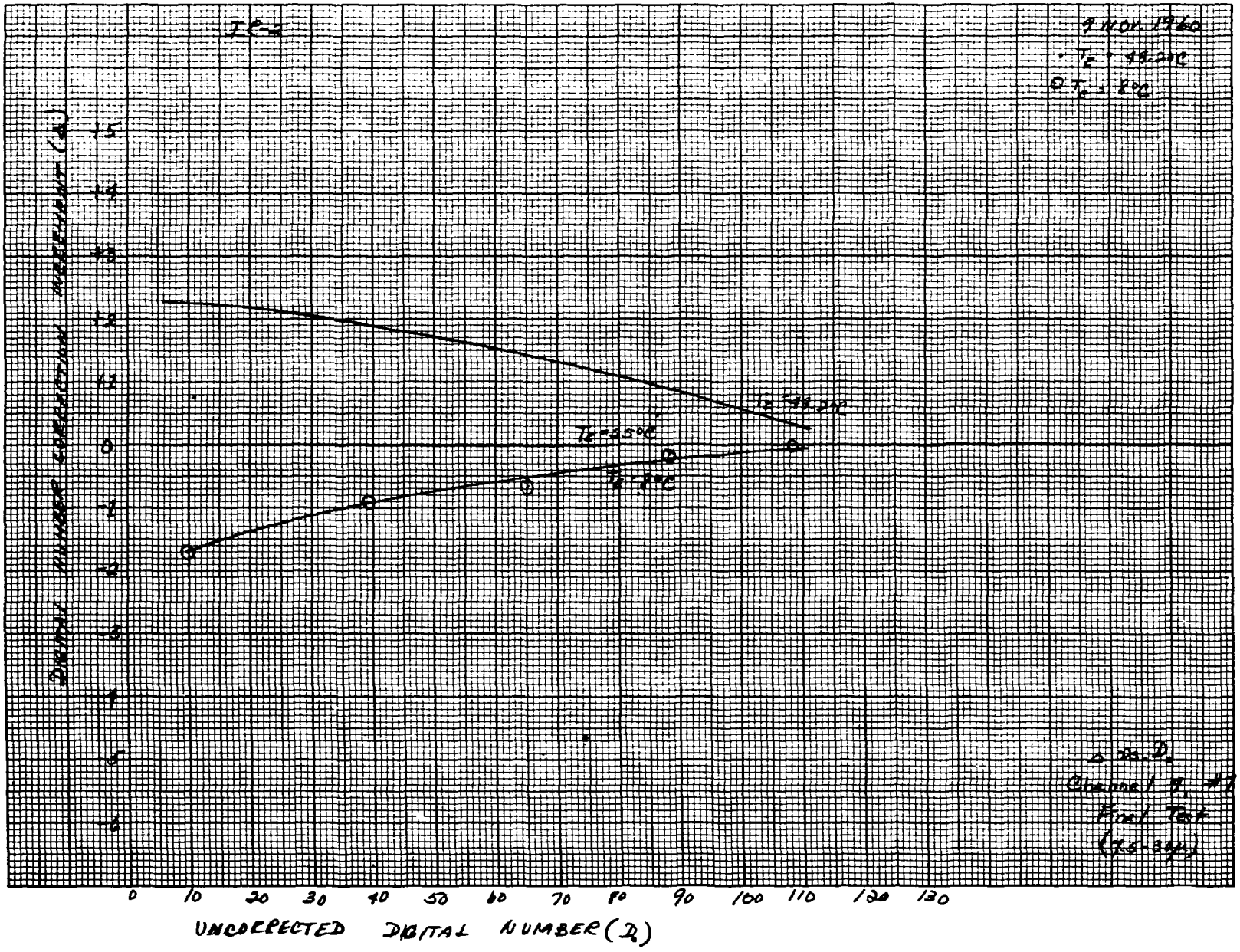

Figure 17—Digital number correction increment versus uncorrected digital number for channel 4.

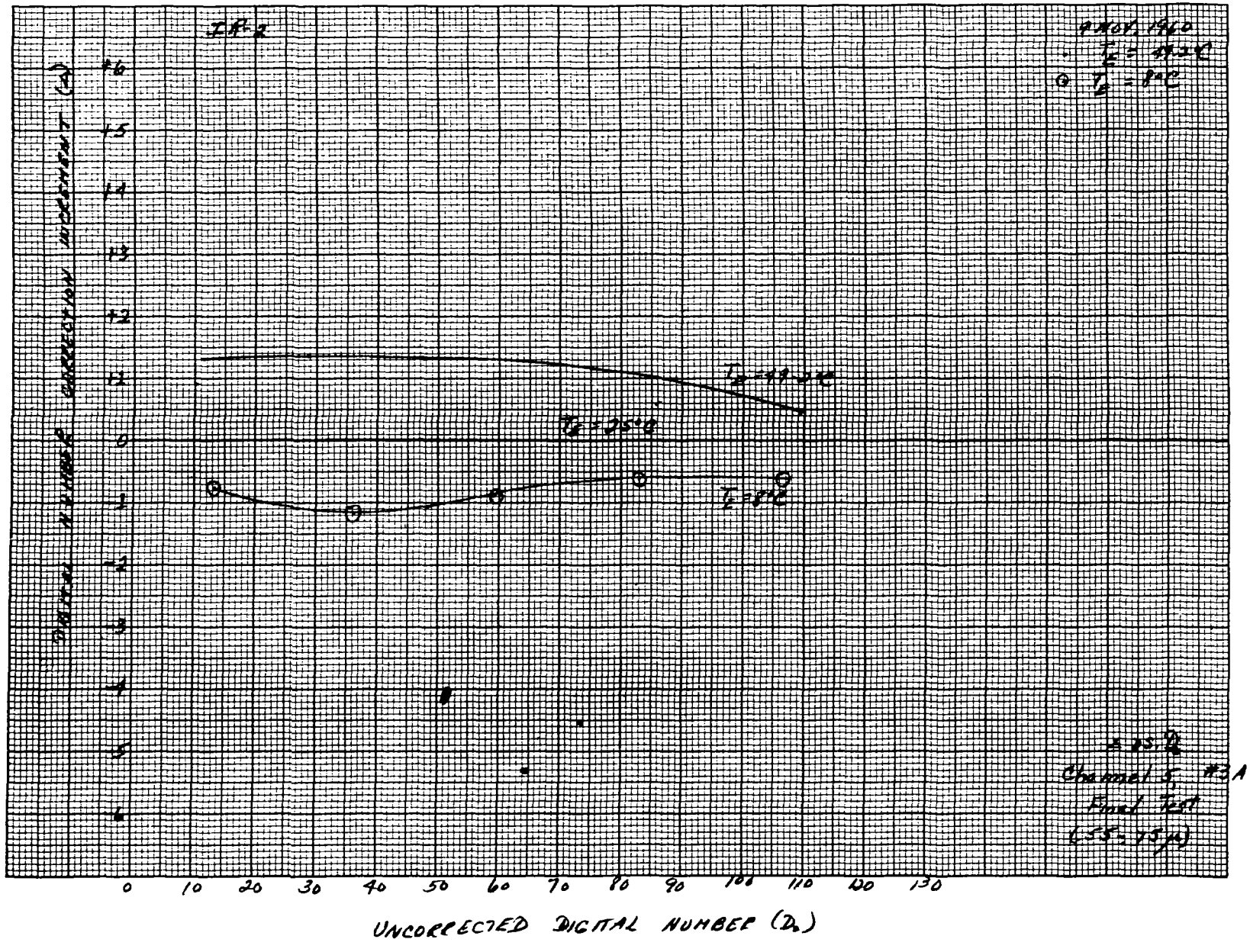

Figure 18—Digital number correction increment versus uncorrected digital number for channel 5.

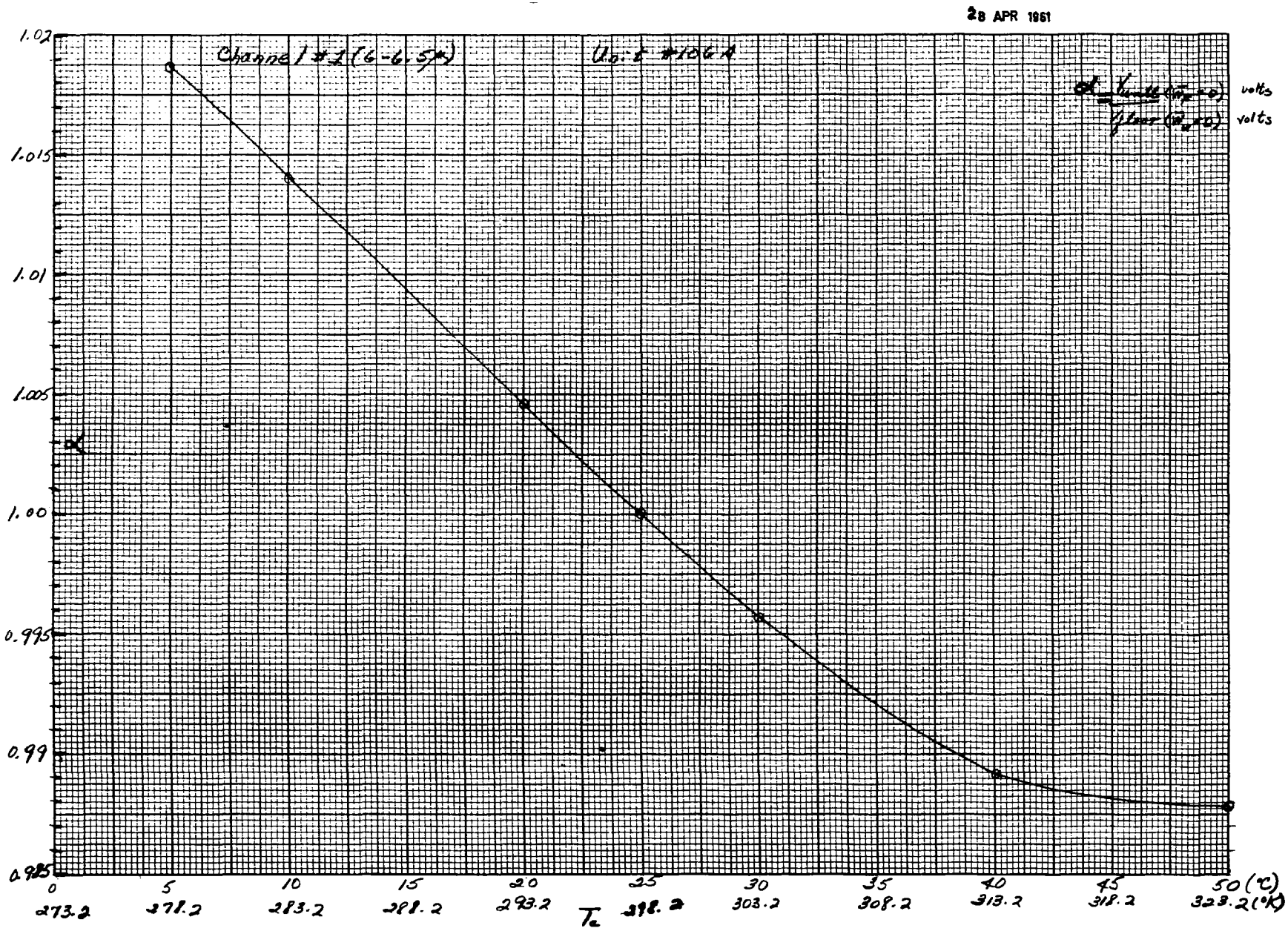

Figure 19—Balance correction factor versus radiometer housing temperature for channel 1.

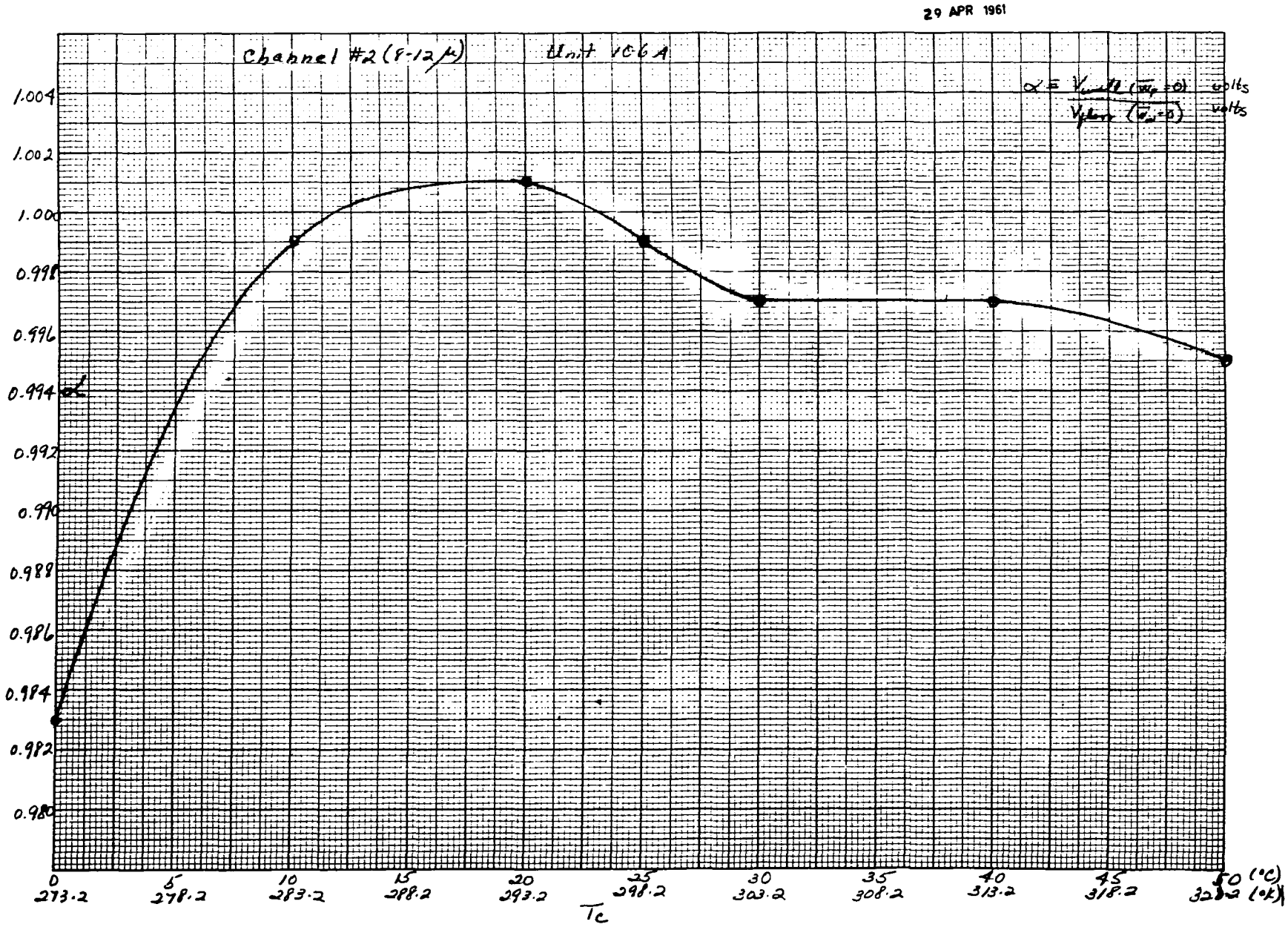

Figure 20—Balance correction factor versus radiometer housing temperature for channel 2.

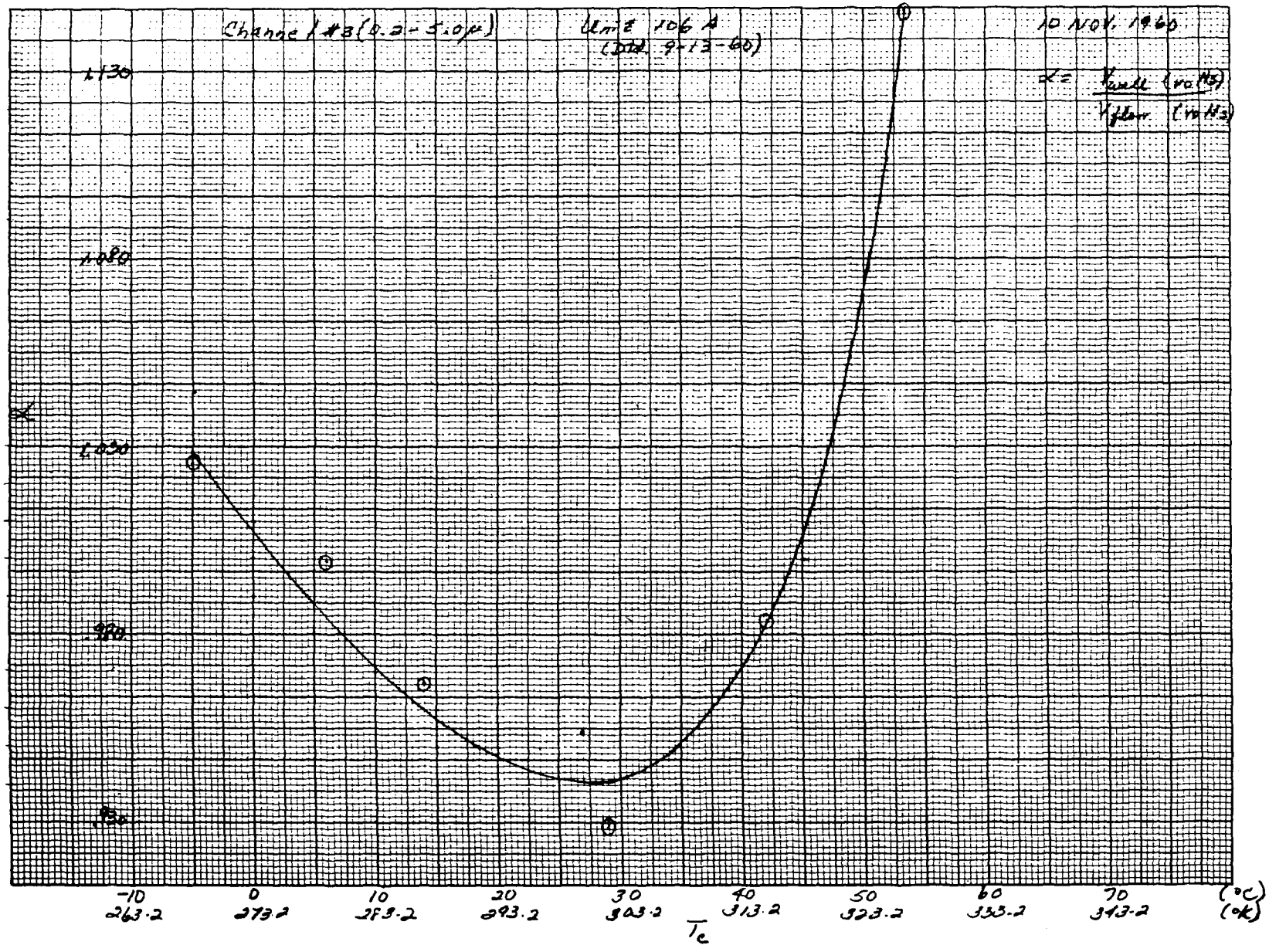

Figure 21—Balance correction factor versus radiometer housing temperature for channel 3.

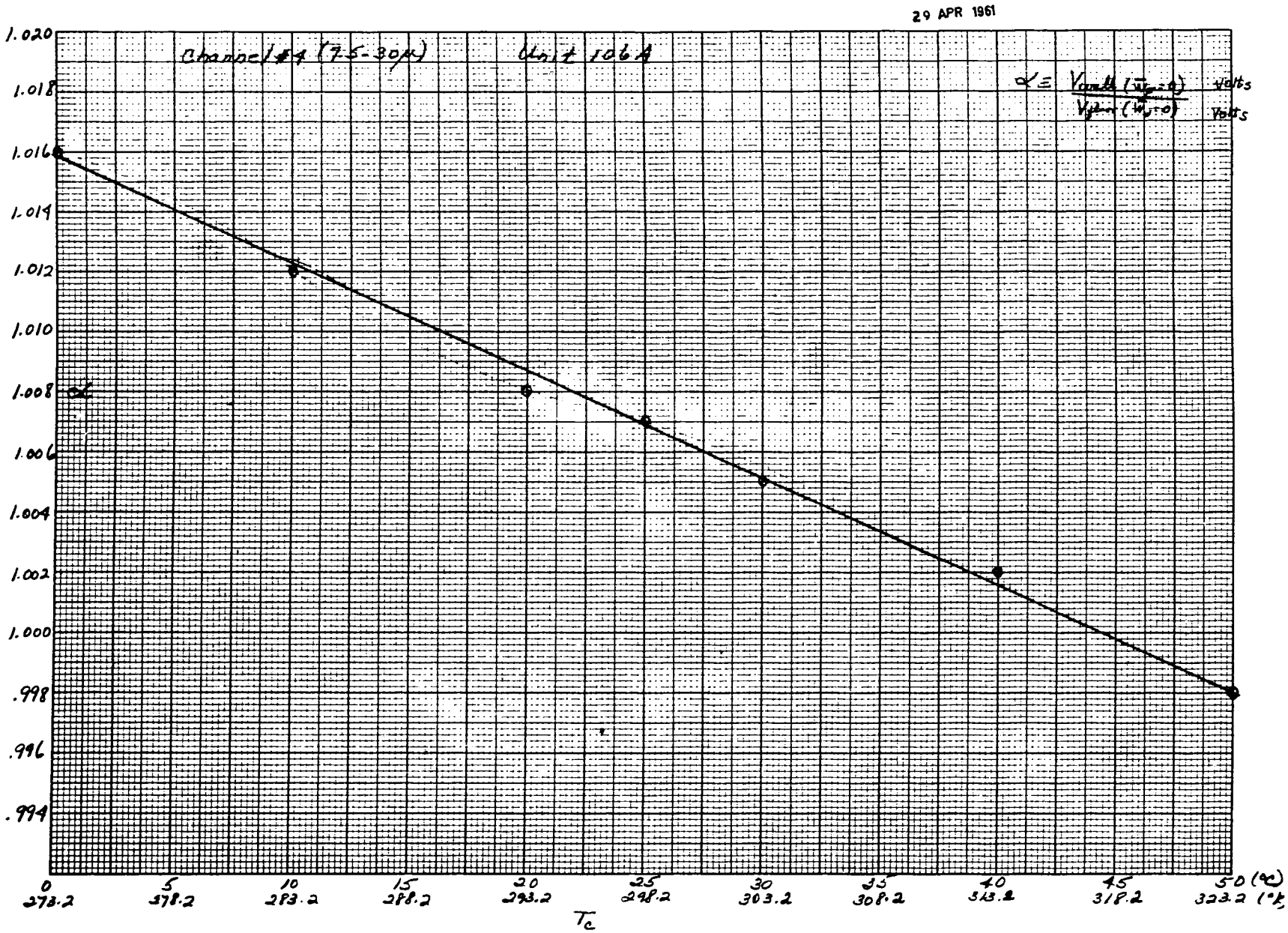

Figure 22—Balance correction factor versus radiometer housing temperature for channel 4.

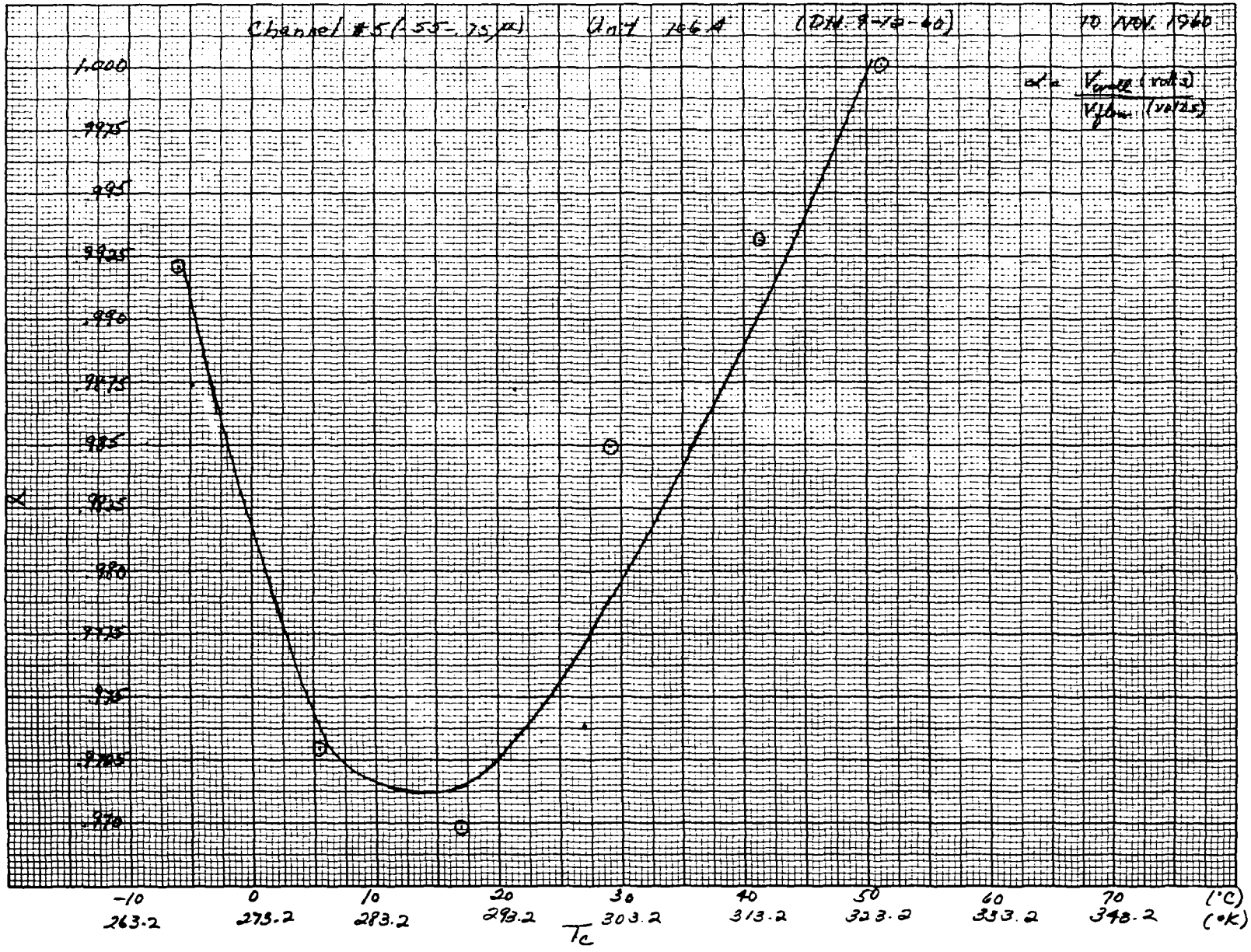

Figure 23—Balance correction factor versus radiometer housing temperature for channel 5.

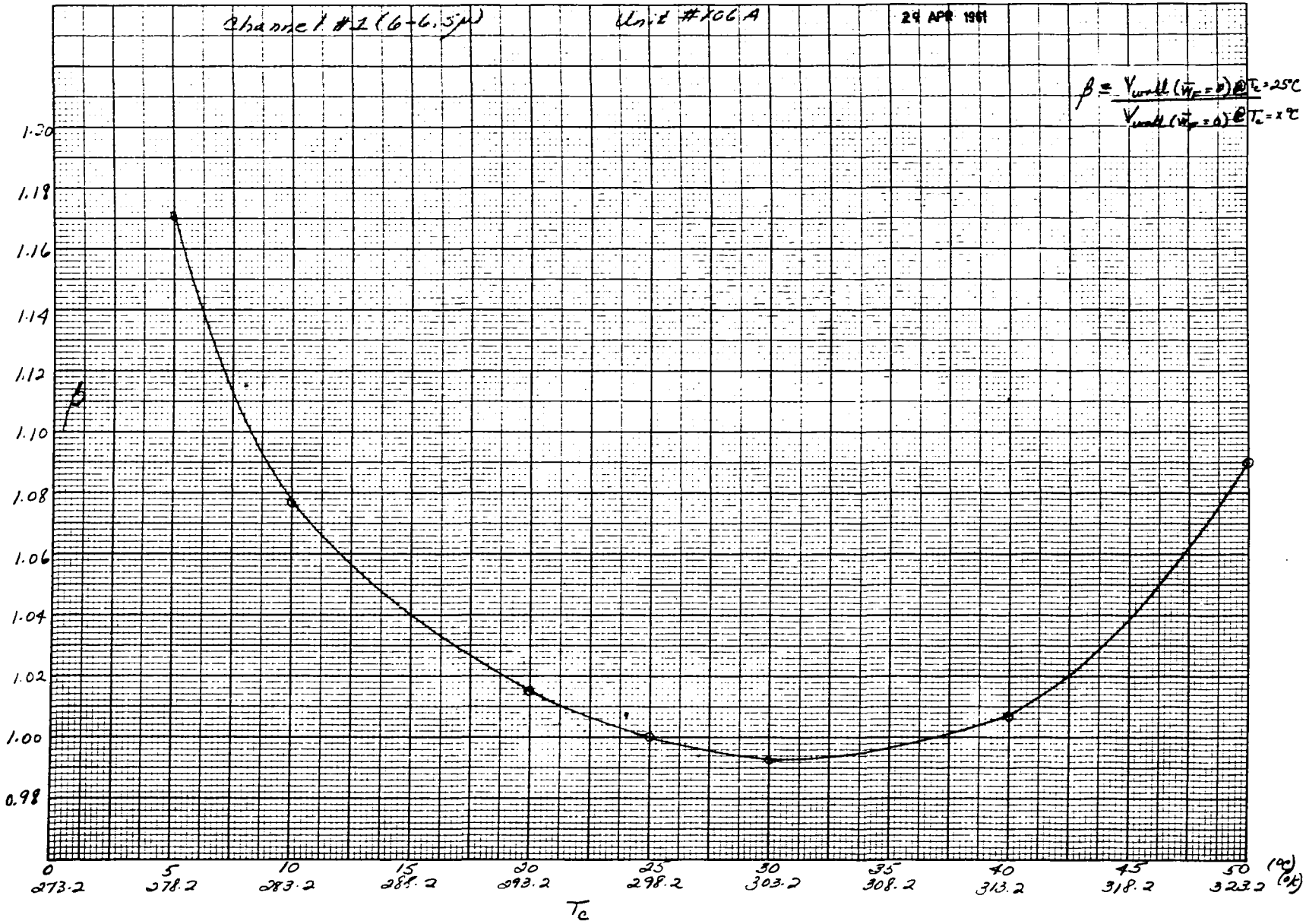

Figure 24—Thermal stability correction factor versus radiometer housing temperature, channel 1.

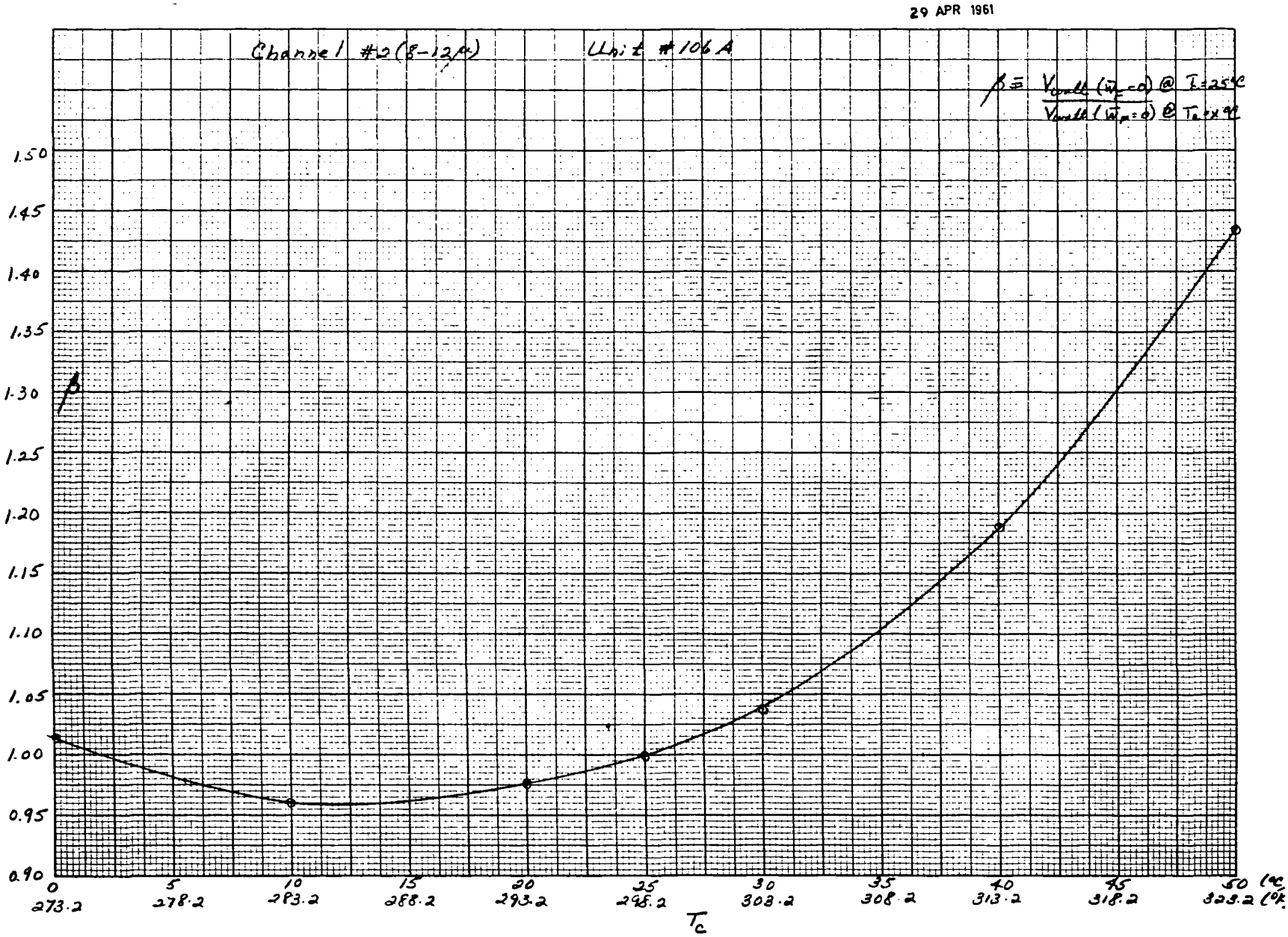

Figure 25—Thermal stability correction factor versus radiometer housing temperature, channel 2.

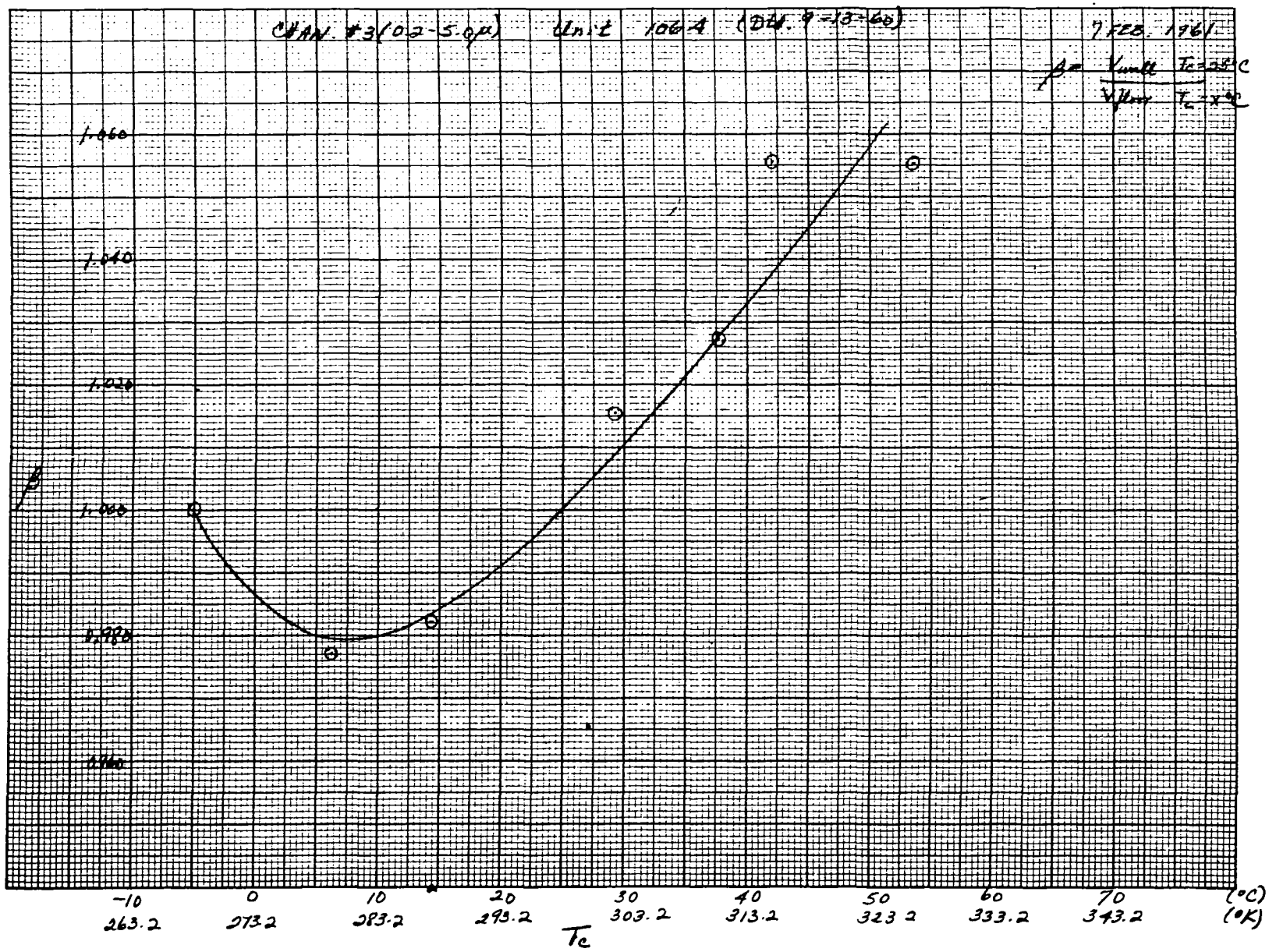

Figure 26—Thermal stability correction factor versus radiometer housing temperature, channel 3.

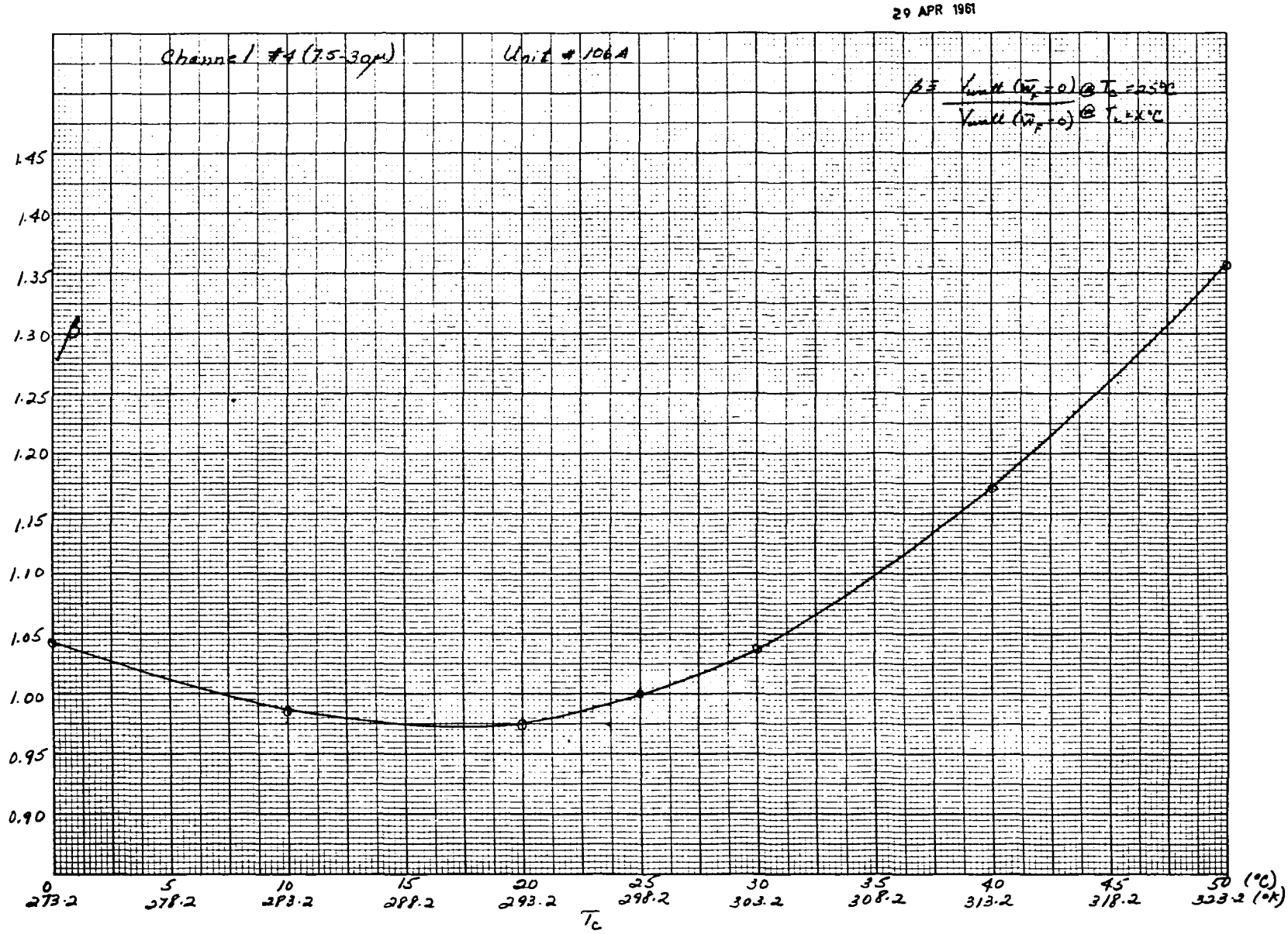

Figure 27—Thermal stability correction factor versus radiometer housing temperature, channel 4.

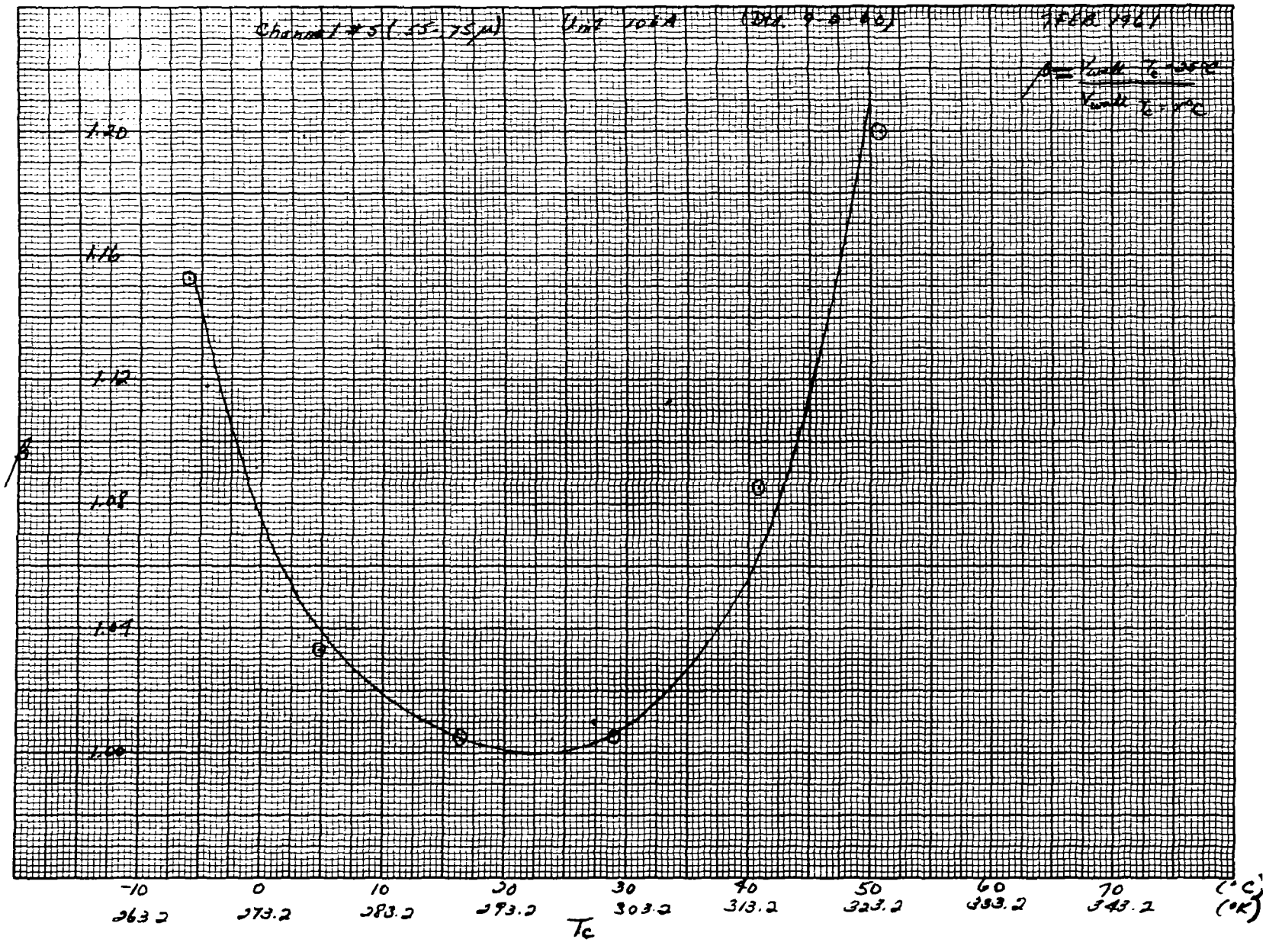

Figure 28—Thermal stability correction factor versus radiometer housing temperature, channel 5.

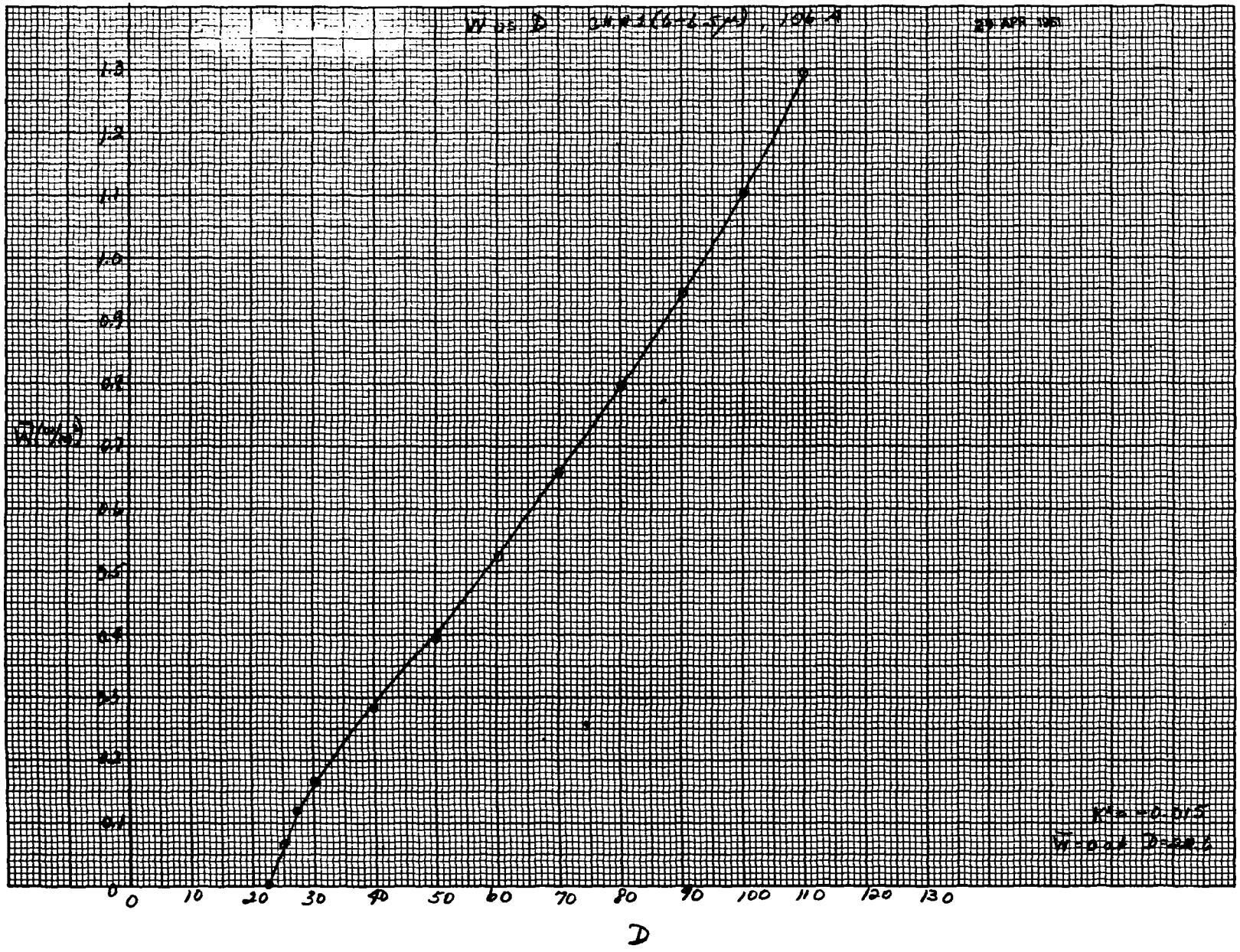

Figure 29—Effective radiant emittance versus digital number for the "normalized case" (wall side, $T_C=25°$ C, $T_E=25°$ C), channel 1.

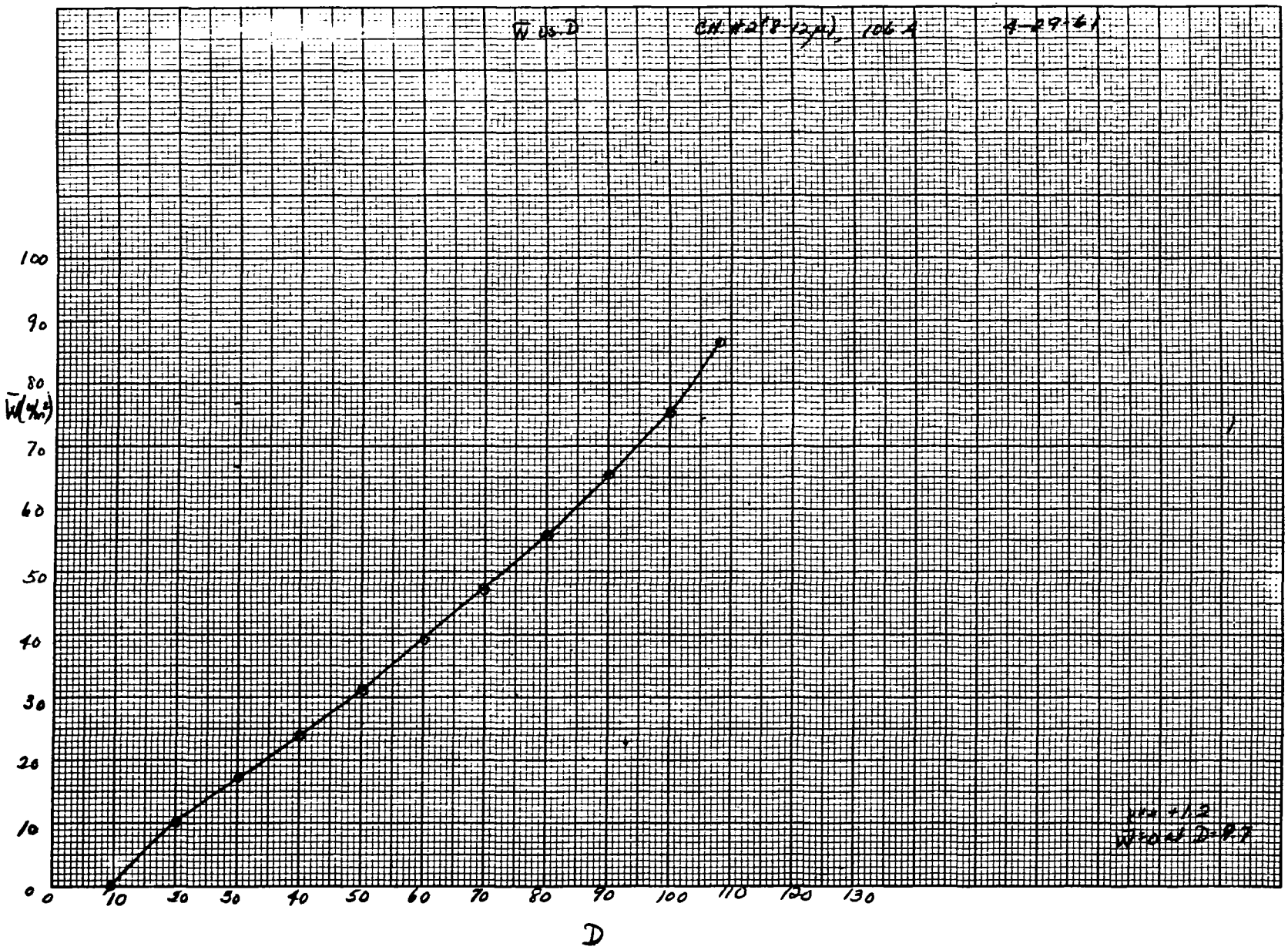

Figure 30—Effective radiant emittance versus digital number for the "normalized case," channel 2.

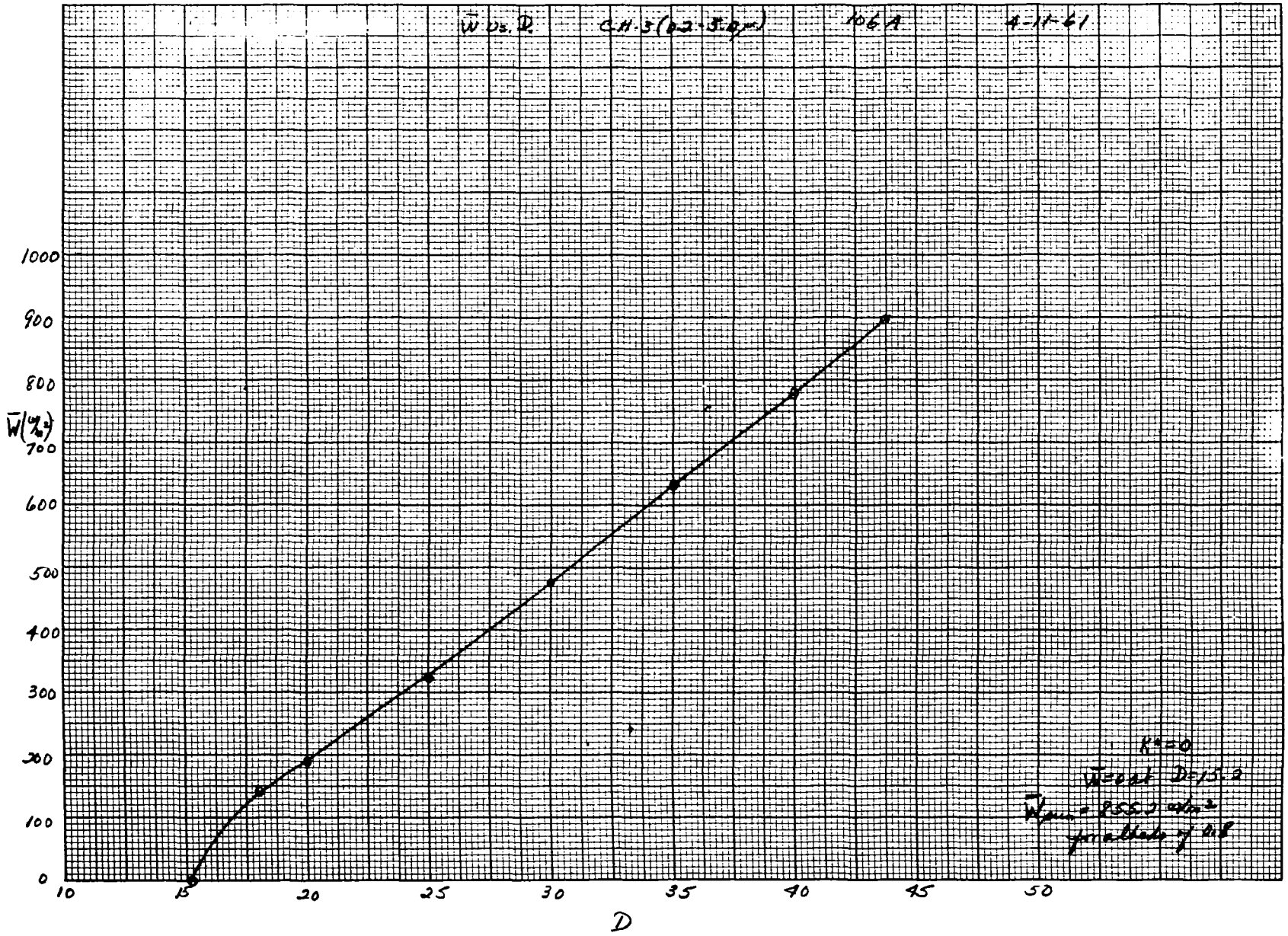

Figure 31—Effective radiant emittance versus digital number for the "normalized case," channel 3.

29 APR 1961

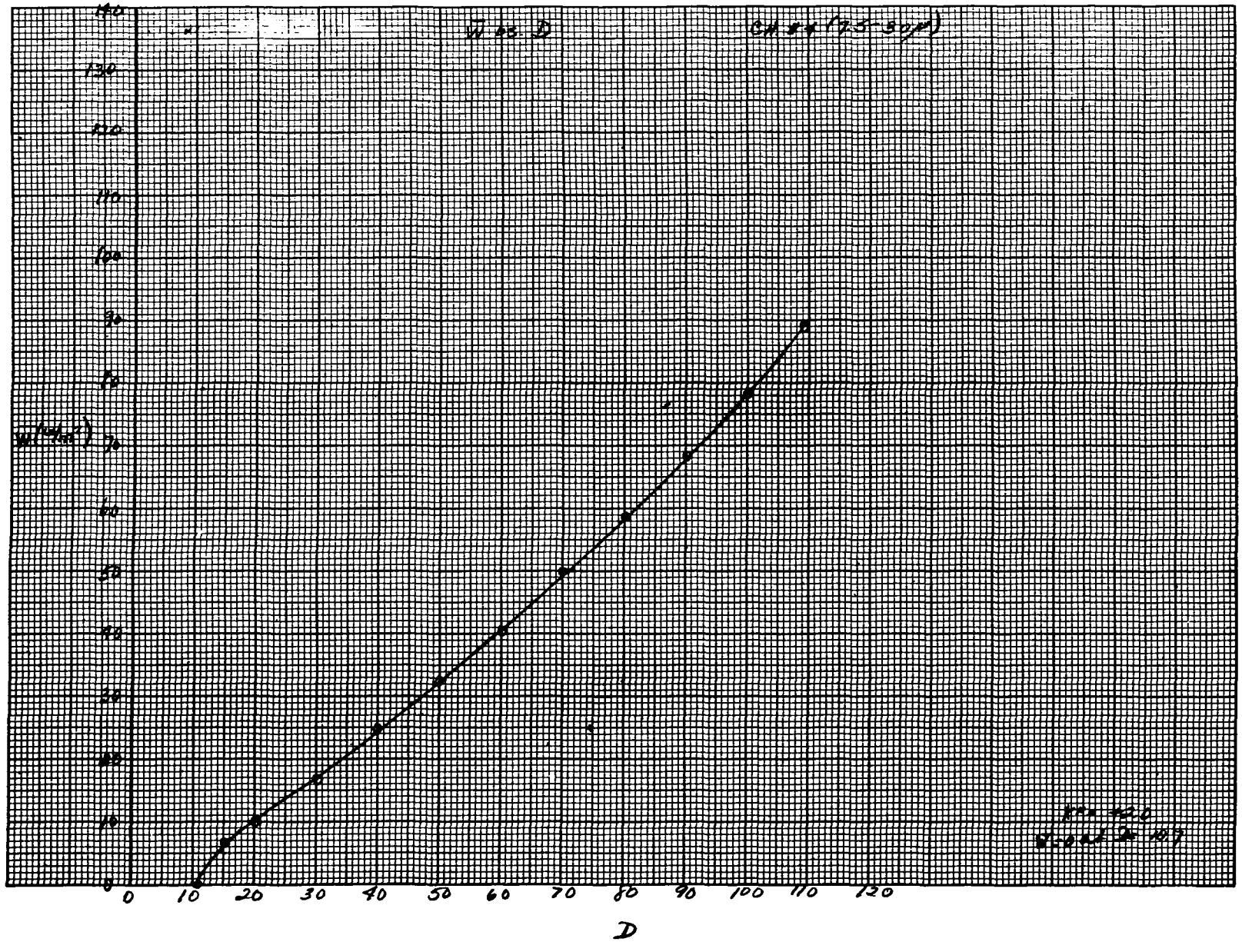

Figure 32—Effective radiant emittance versus digital number for the "normalized case," channel 4.

605807 O - 61 - 4

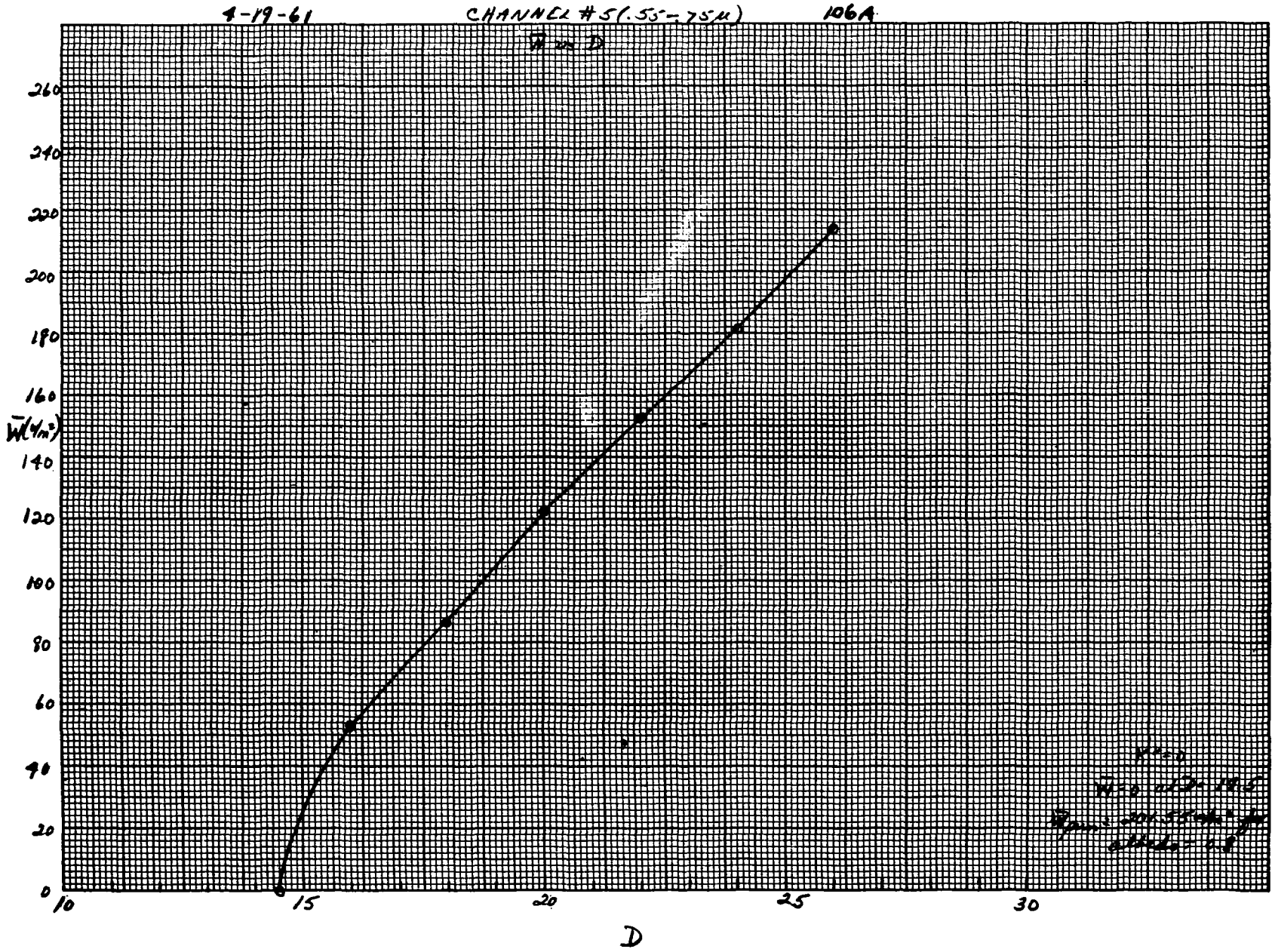

Figure 33—Effective radiant emittance versus digital number for the "normalized case," channel 5.

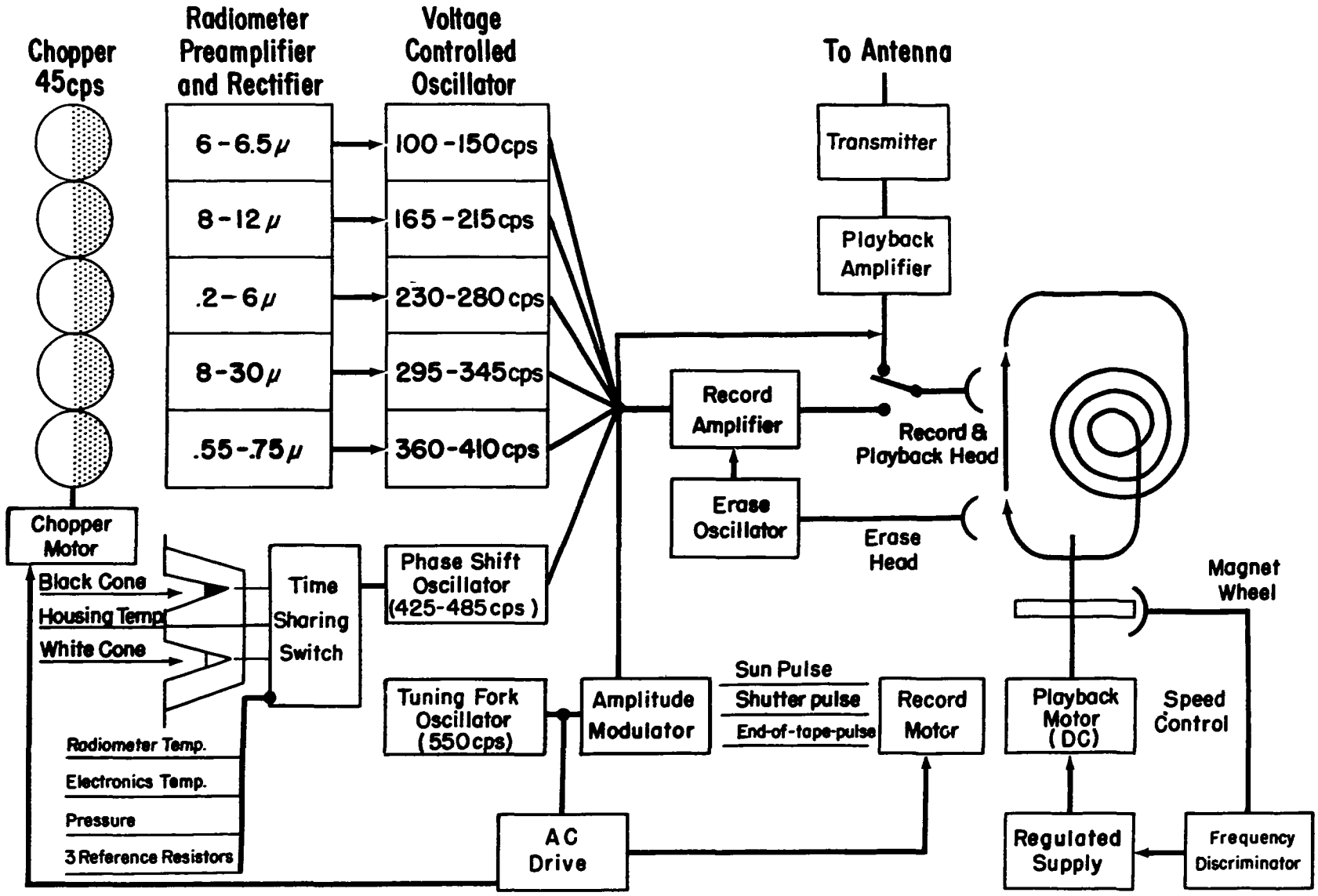

Figure 34—Block diagram of the radiation experiment in the satellite.

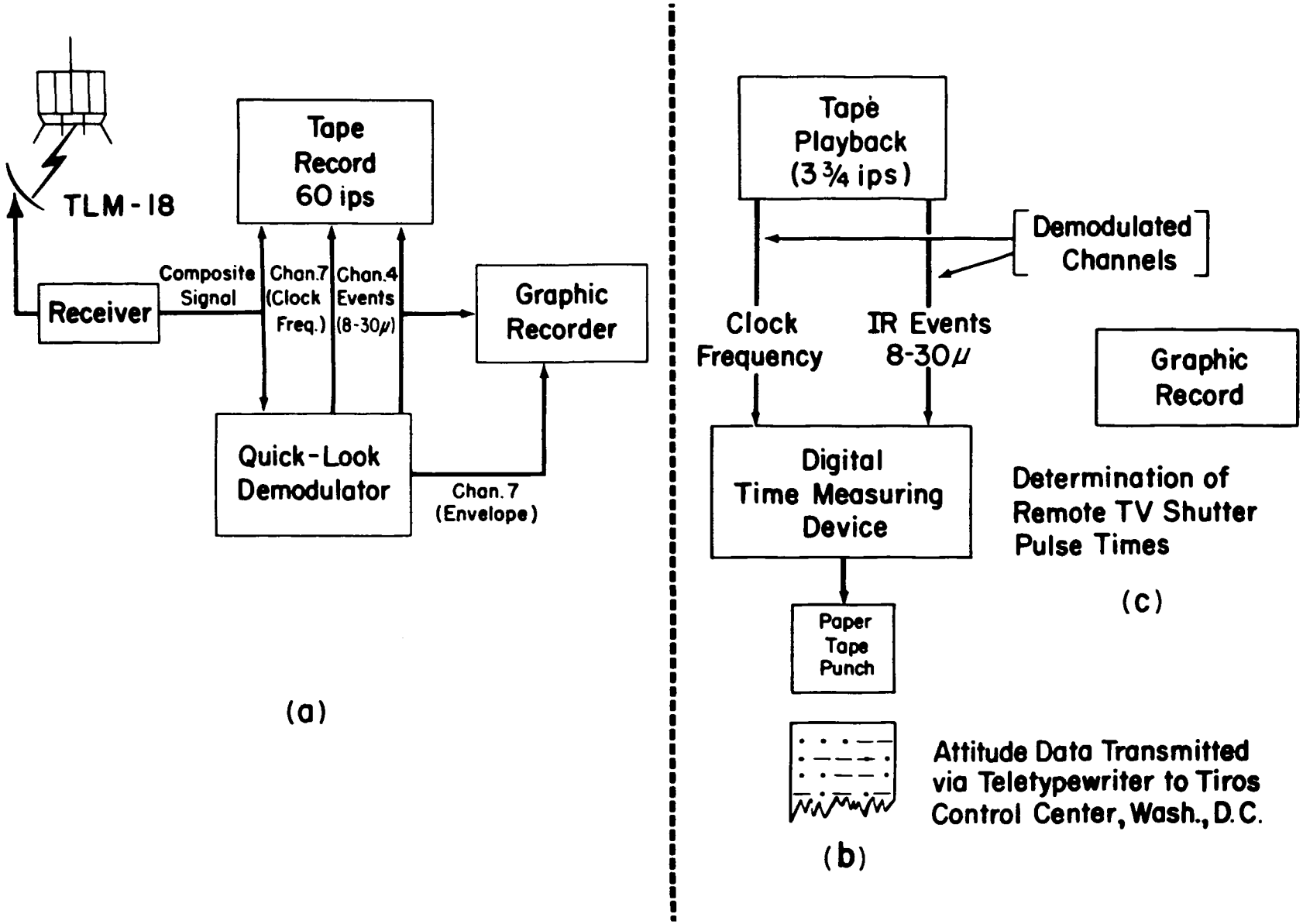

Figure 35 – Block diagram of information flow at a data acquisition station including auxiliary uses of the radiation data.

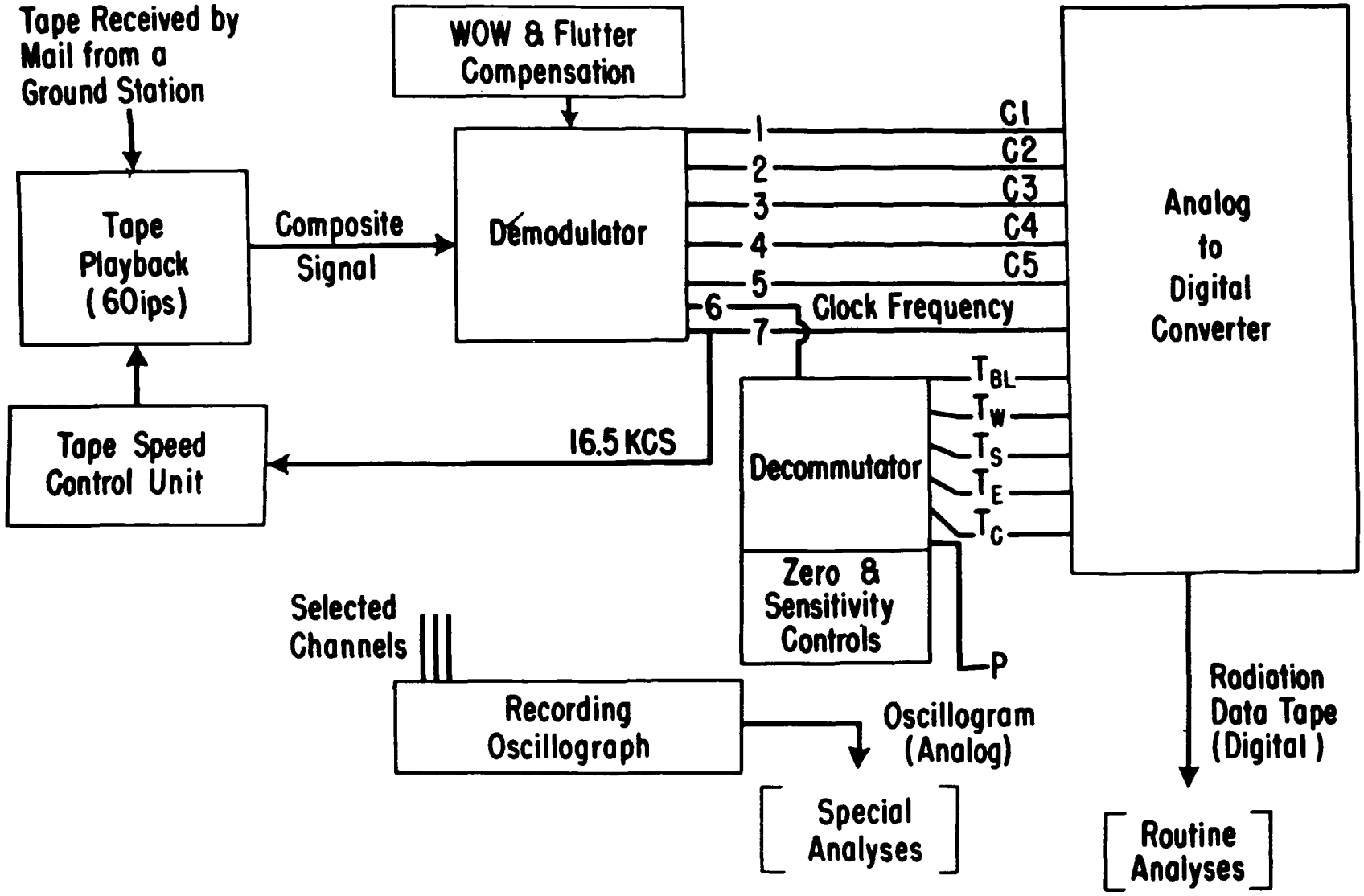

Figure 36—Block diagram of information flow at the data reduction center in producing a digital magnetic tape for computer input.

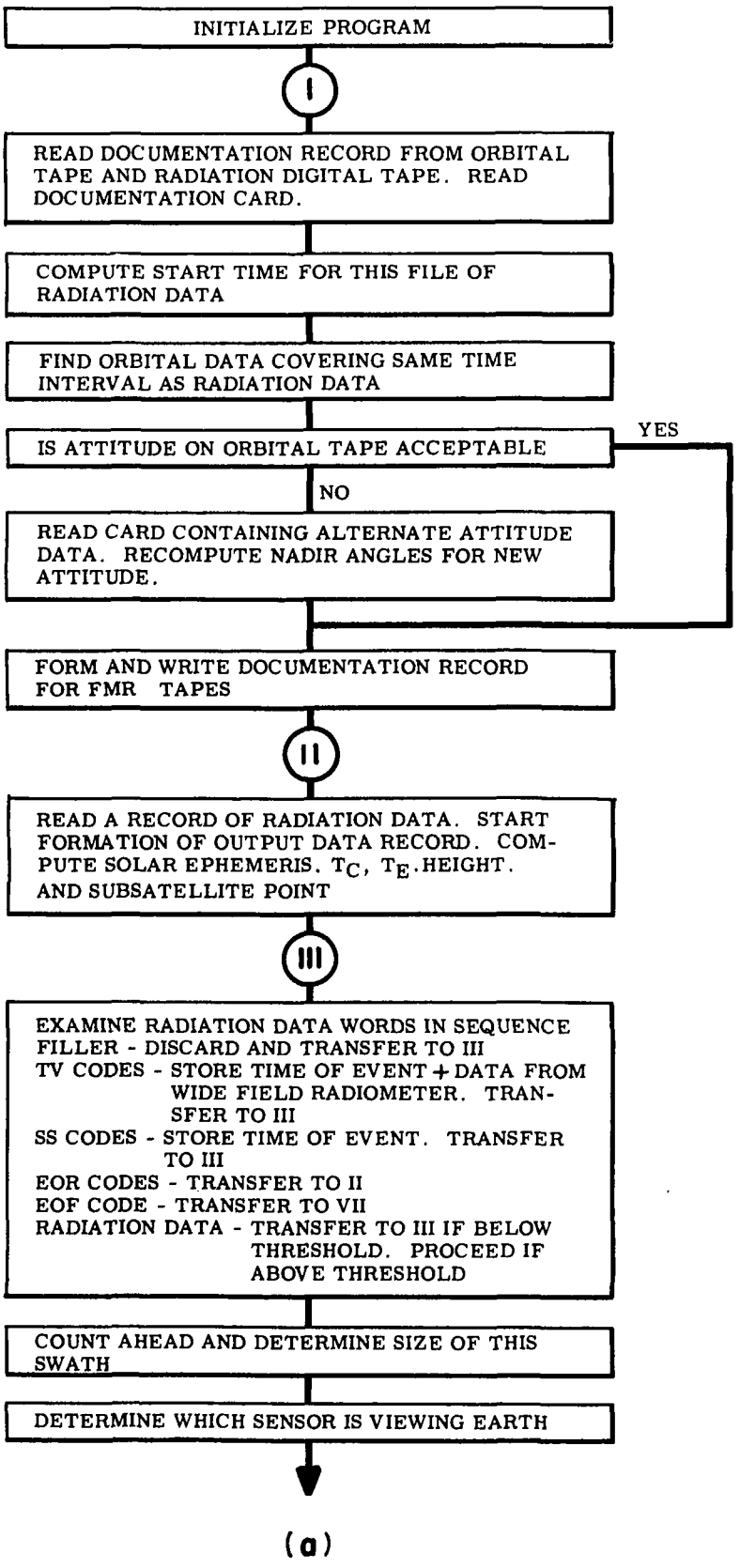

Figure 37—(a, b, and c) Flow diagram for the IBM-7090 computer program used in reducing the radiation data.

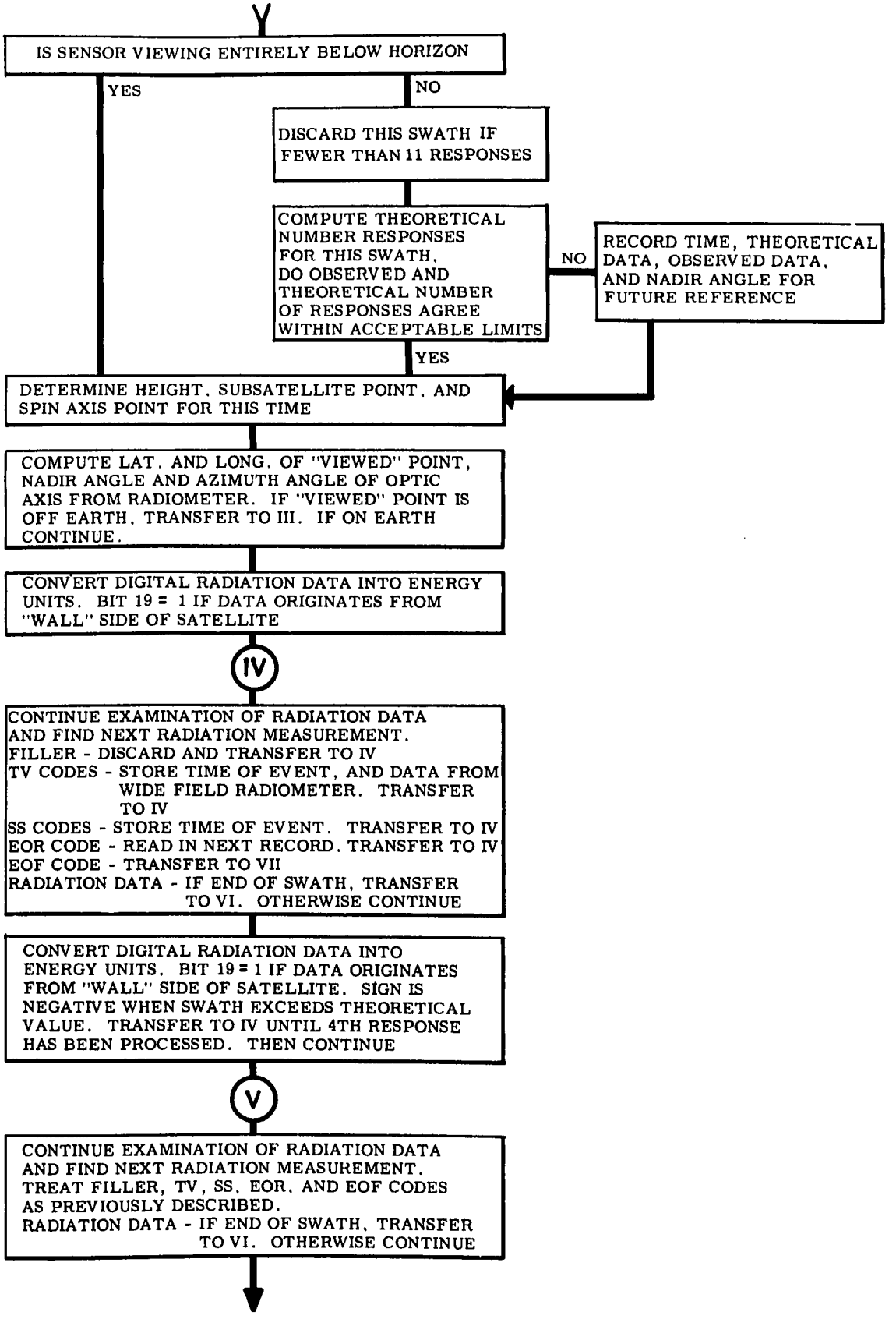
IS SENSOR VIEWING ENTIRELY BELOW HORIZON
YES
NO
DISCARD THIS SWATH IF FEWER THAN 11 RESPONSES
COMPUTE THEORETICAL NUMBER RESPONSES FOR THIS SWATH. DO OBSERVED AND THEORETICAL NUMBER OF RESPONSES AGREE WITHIN ACCEPTABLE LIMITS
NO
RECORD TIME, THEORETICAL DATA, OBSERVED DATA, AND NADIR ANGLE FOR FUTURE REFERENCE
YES
DETERMINE HEIGHT, SUBSATELLITE POINT, AND SPIN AXIS POINT FOR THIS TIME
COMPUTE LAT. AND LONG. OF "VIEWED" POINT, NADIR ANGLE AND AZIMUTH ANGLE OF OPTIC AXIS FROM RADIOMETER. IF "VIEWED" POINT IS OFF EARTH, TRANSFER TO III. IF ON EARTH CONTINUE.
CONVERT DIGITAL RADIATION DATA INTO ENERGY UNITS. BIT 19 = 1 IF DATA ORIGINATES FROM "WALL" SIDE OF SATELLITE
IV
CONTINUE EXAMINATION OF RADIATION DATA AND FIND NEXT RADIATION MEASUREMENT.
FILLER - DISCARD AND TRANSFER TO IV
TV CODES - STORE TIME OF EVENT, AND DATA FROM WIDE FIELD RADIOMETER. TRANSFER TO IV
SS CODES - STORE TIME OF EVENT. TRANSFER TO IV
EOR CODE - READ IN NEXT RECORD. TRANSFER TO IV
EOF CODE - TRANSFER TO VII
RADIATION DATA - IF END OF SWATH, TRANSFER TO VI. OTHERWISE CONTINUE
CONVERT DIGITAL RADIATION DATA INTO ENERGY UNITS. BIT 19 = 1 IF DATA ORIGINATES FROM "WALL" SIDE OF SATELLITE. SIGN IS NEGATIVE WHEN SWATH EXCEEDS THEORETICAL VALUE. TRANSFER TO IV UNTIL 4TH RESPONSE HAS BEEN PROCESSED. THEN CONTINUE
V
CONTINUE EXAMINATION OF RADIATION DATA AND FIND NEXT RADIATION MEASUREMENT.
TREAT FILLER, TV, SS, EOR, AND EOF CODES AS PREVIOUSLY DESCRIBED.
RADIATION DATA - IF END OF SWATH, TRANSFER TO VI. OTHERWISE CONTINUE

(b)

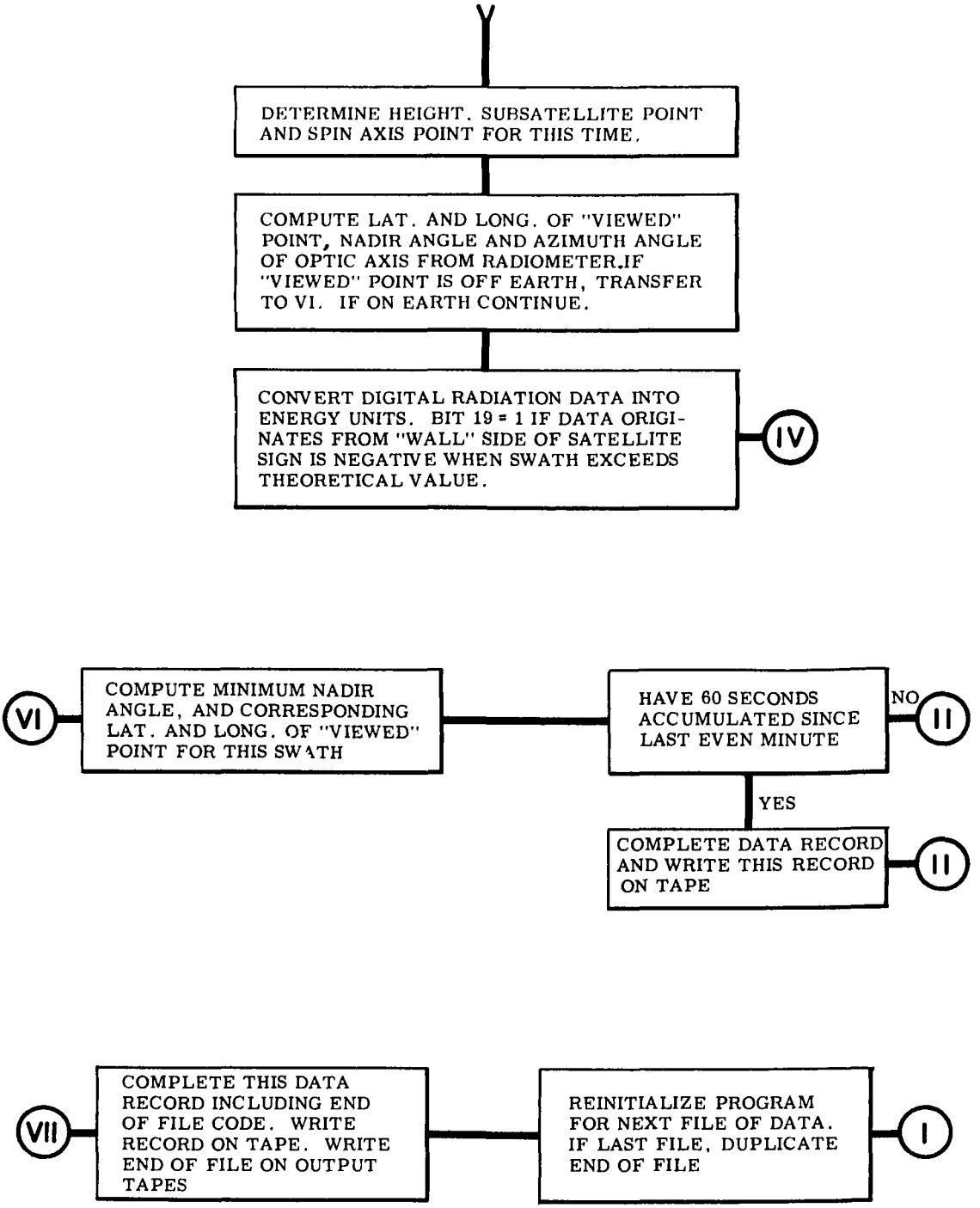
DETERMINE HEIGHT, SUBSATELLITE POINT AND SPIN AXIS POINT FOR THIS TIME.
COMPUTE LAT. AND LONG. OF "VIEWED" POINT, NADIR ANGLE AND AZIMUTH ANGLE OF OPTIC AXIS FROM RADIOMETER.IF "VIEWED" POINT IS OFF EARTH, TRANSFER TO VI. IF ON EARTH CONTINUE.
CONVERT DIGITAL RADIATION DATA INTO ENERGY UNITS. BIT 19 = 1 IF DATA ORIGINATES FROM "WALL" SIDE OF SATELLITE SIGN IS NEGATIVE WHEN SWATH EXCEEDS THEORETICAL VALUE.
IV
VI
COMPUTE MINIMUM NADIR ANGLE, AND CORRESPONDING LAT. AND LONG. OF "VIEWED" POINT FOR THIS SWATH
HAVE 60 SECONDS ACCUMULATED SINCE LAST EVEN MINUTE
NO
II
YES
COMPLETE DATA RECORD AND WRITE THIS RECORD ON TAPE
II
VII
COMPLETE THIS DATA RECORD INCLUDING END OF FILE CODE. WRITE RECORD ON TAPE. WRITE END OF FILE ON OUTPUT TAPES
REINITIALIZE PROGRAM FOR NEXT FILE OF DATA. IF LAST FILE, DUPLICATE END OF FILE
I

(c)

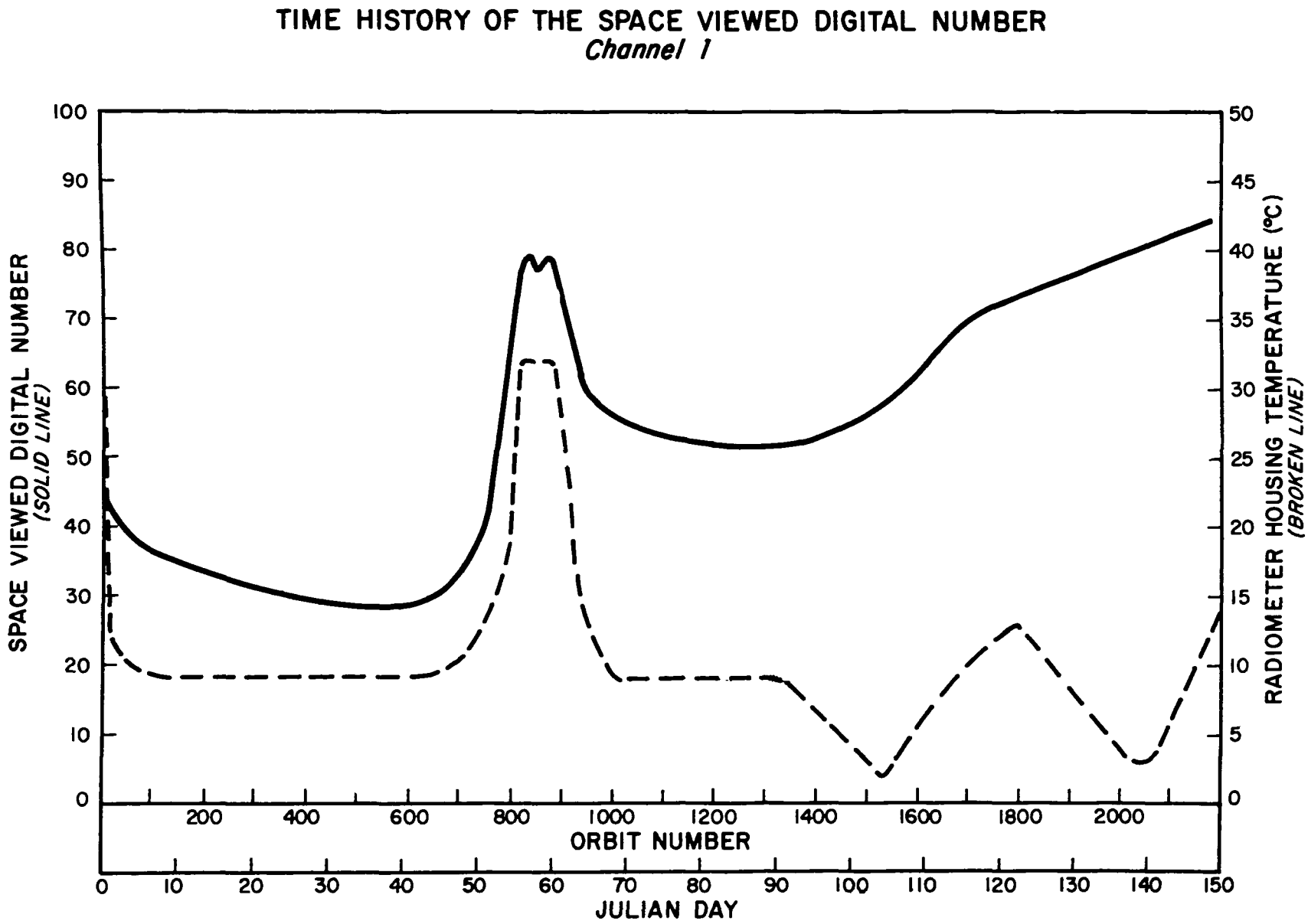

Figure 38—The time history of the channel 1 space viewed digital number (both radiometer optics viewing outer space simultaneously) shown as a solid line. The radiometer housing temperature time history is shown for comparison as a broken line.

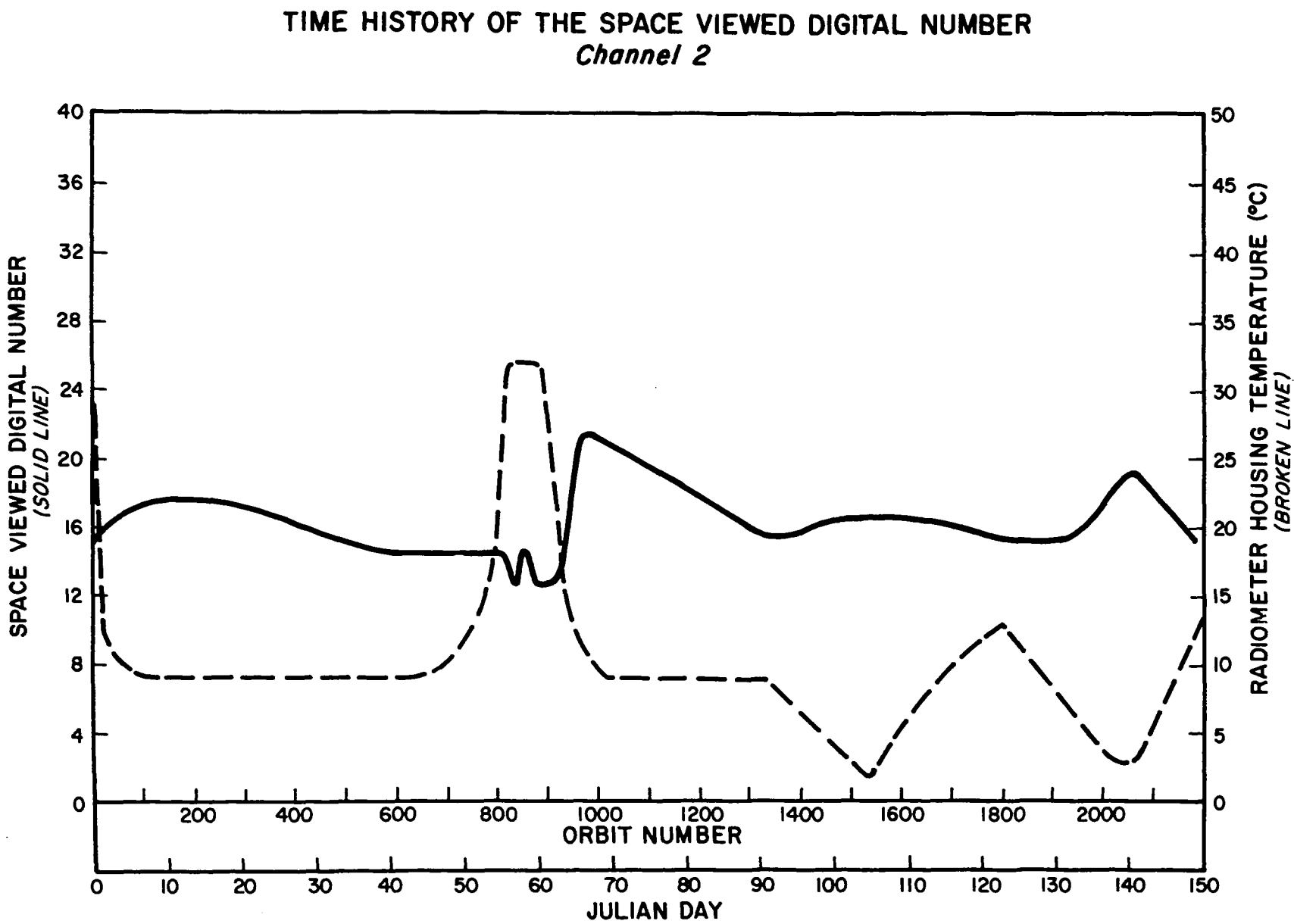

Figure 39—The time history of the channel 2 space viewed digital number shown as a solid line. The radiometer housing temperature time history is shown as a broken line.

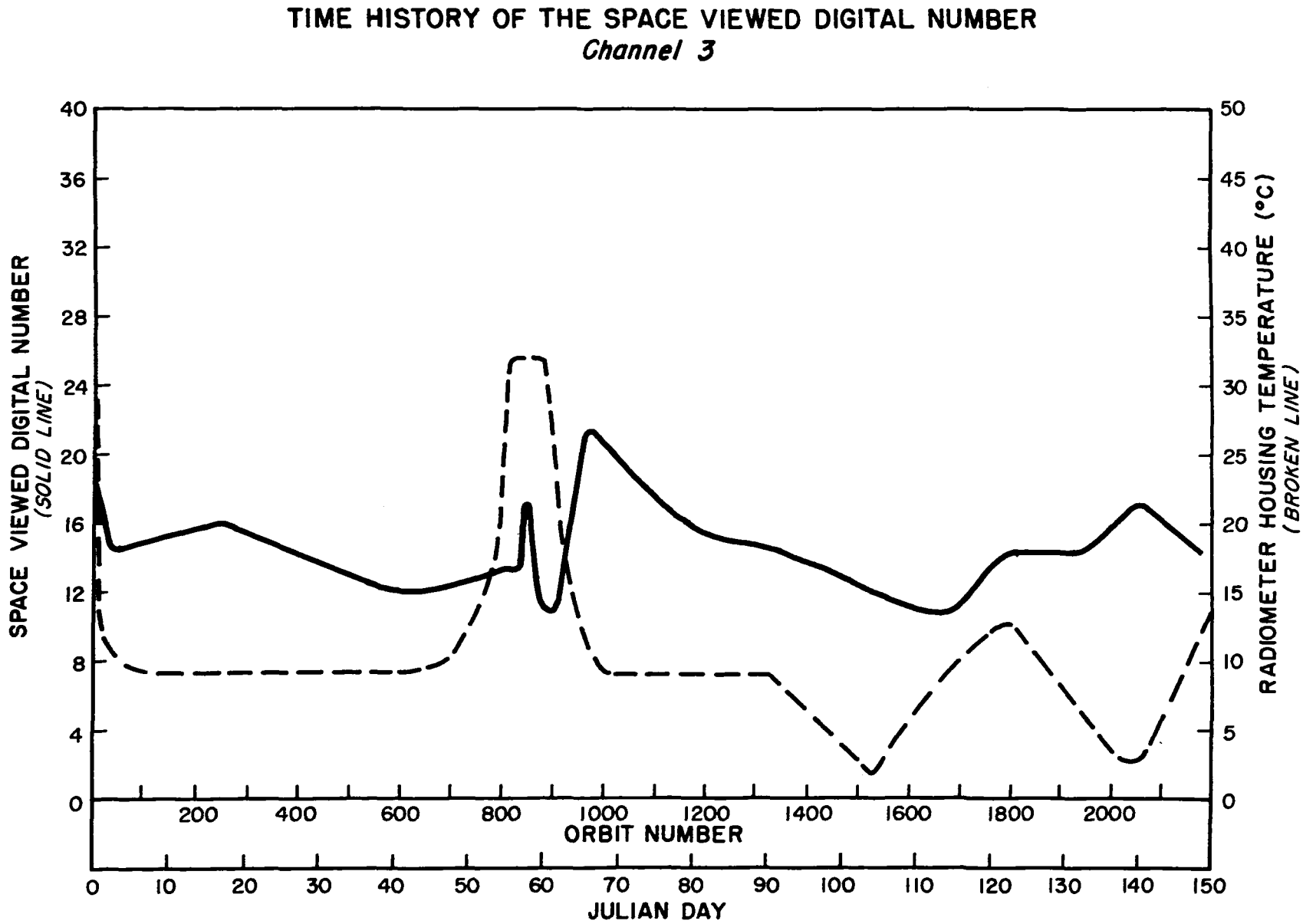

Figure 40—Time history of the channel 3 space viewed digital number shown as a solid line. The radiometer housing temperature time history is shown as a broken line.

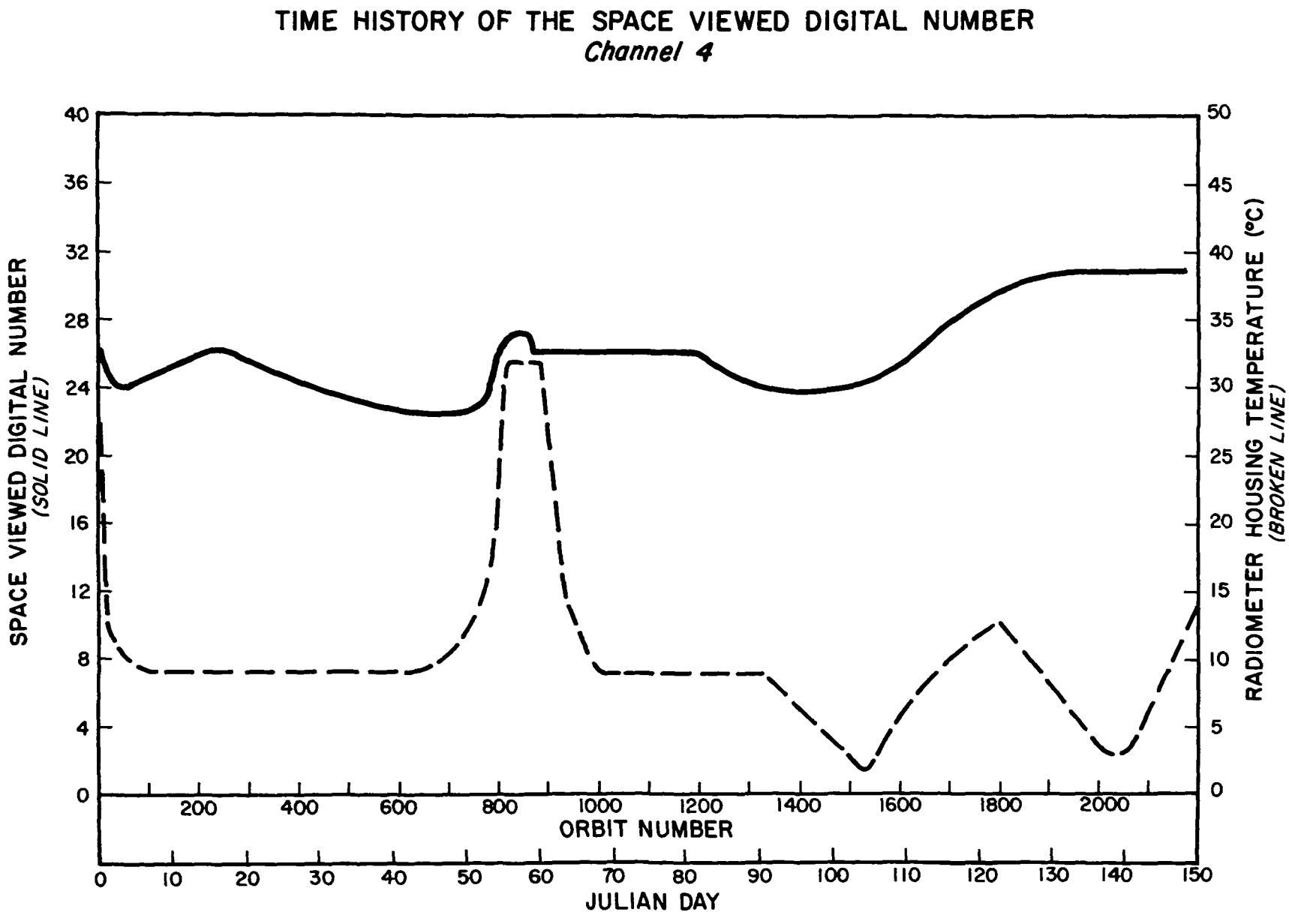

Figure 41—Time history of the channel 4 space viewed digital number shown as a solid line. The radiometer housing temperature time history is shown as a broken line.

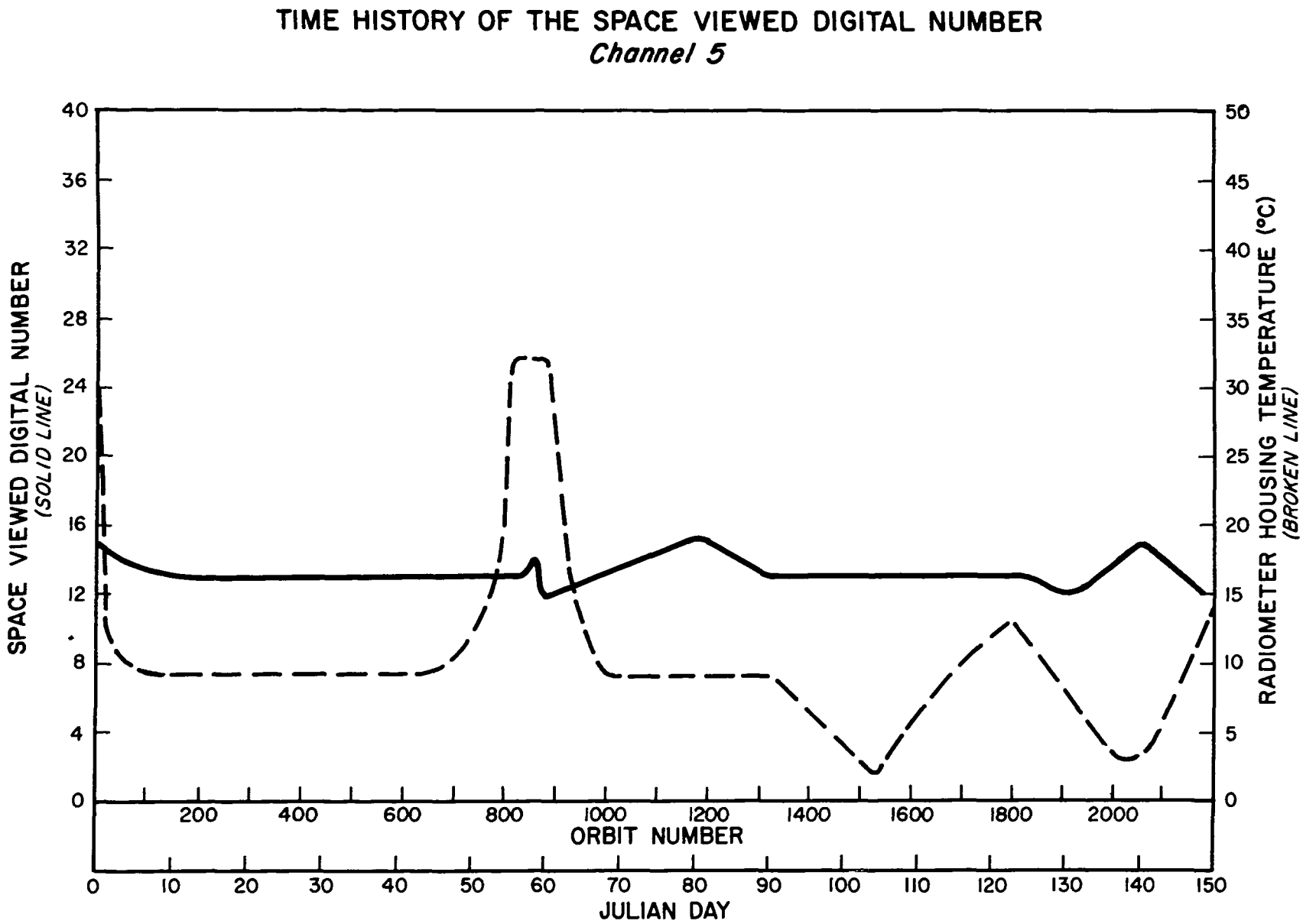

Figure 42—Time history of the channel 5 space viewed digital number shown as a solid line. The radiometer housing temperature time history is shown as a broken line.

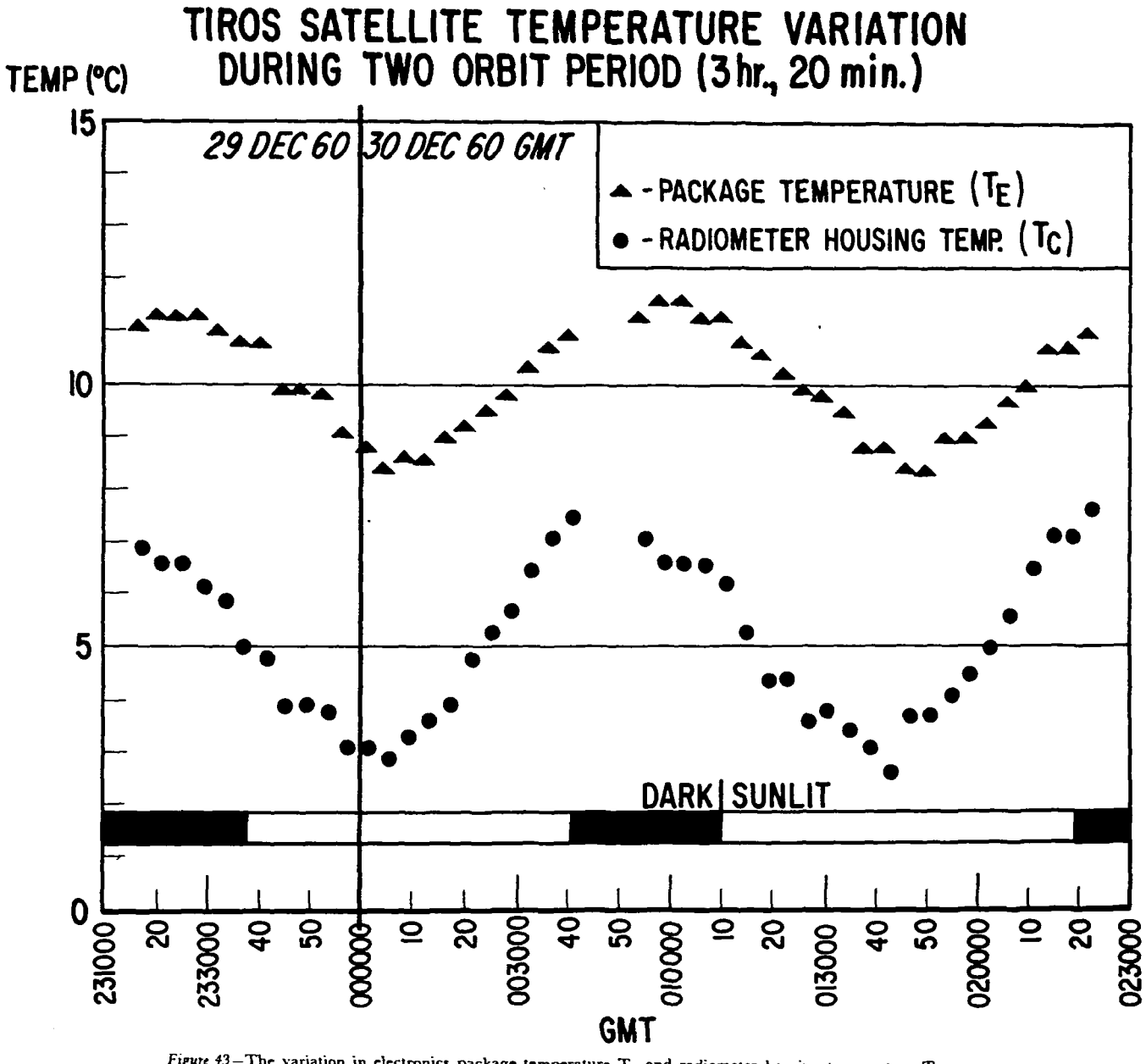

Figure 43—The variation in electronics package temperature T_E and radiometer housing temperature T_C over a two-orbit period. The dark and sunlit portions of the orbits are indicated. Due to the small variations, values of T_E and T_C averaged over an orbit were incorporated in the data reduction.

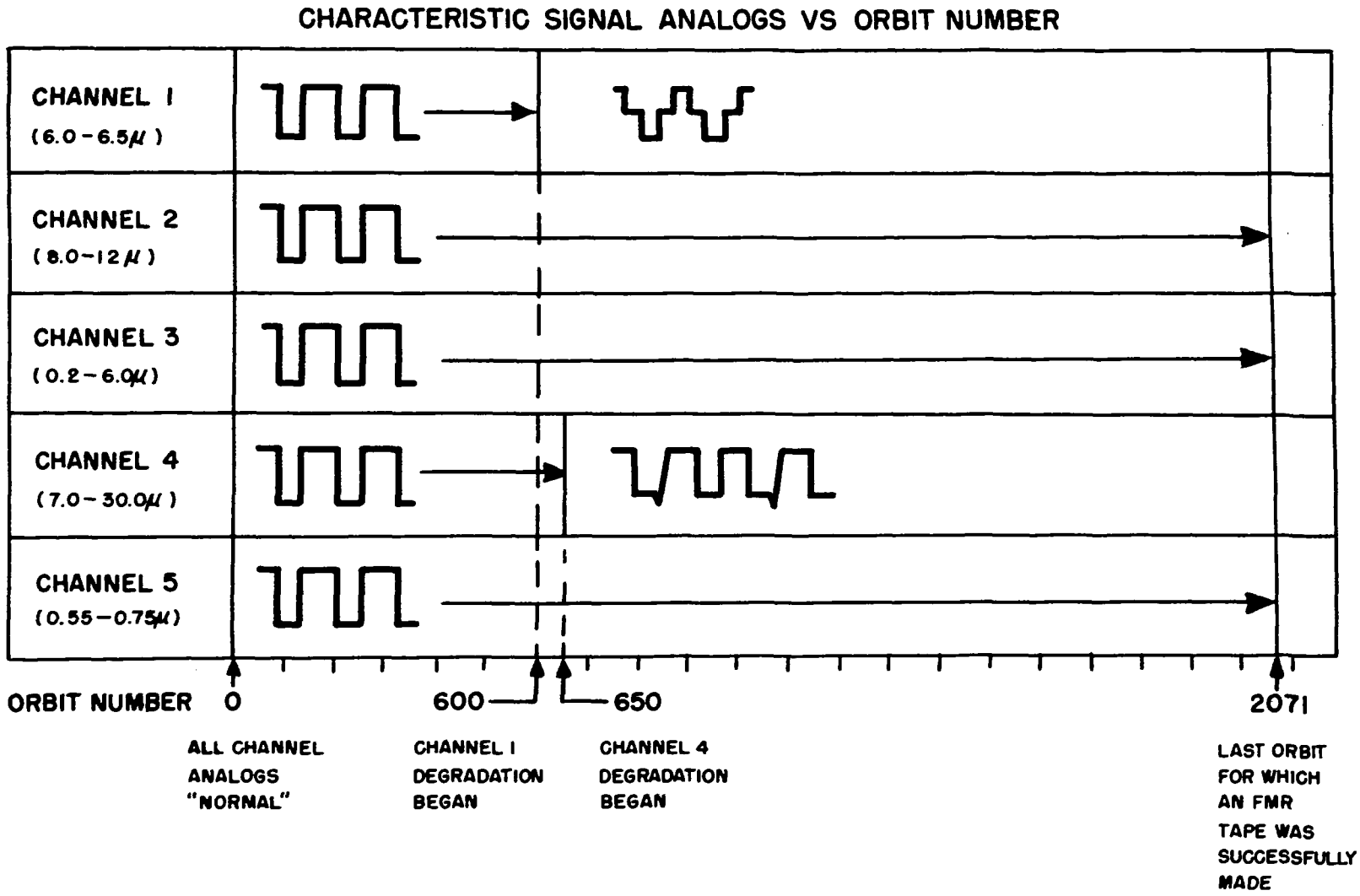

Figure 44—Time history of the characteristic analog signals of each channel as they appeared on oscillographic records. Degradation of channels 1 and 4 became pronounced after orbits 600 and 650 respectively.

U.S. GOVERNMENT PRINTING OFFICE: 1961 O - 605807